COMPUTATIONAL AND EXPERIMENTAL EVALUATION OF PEM FUEL CELL PERFORMANCE USING SERPENTINE FLOW FIELDS

A Dissertation
Submitted in partial fulfillment of the requirements for
the award of Degree of

DOCTOR OF PHILOSOPHY

in

MECHANICAL ENGINEERING

by

Venkateswarlu Velisala
(Roll No.: 701416)

Supervisor:

Dr. G. Naga Srinivasulu
Associate Professor

DEPARTEMENT OF MECHANICAL ENGINEERING
NATIONAL INSTITUTE OF TECHNOLOGY,
WARANGAL (TS), INDIA,
JUNE 2018

APPROVAL SHEET

This Thesis entitled "**COMPUTATIONAL AND EXPERIMENTAL EVALUATION OF PEM FUEL CELL PERFORMANCE USING SERPENTINE FLOW FIELDS"** by **Venkateswarlu Velisala** is approved for the Degree of Doctor Philosophy

Examiners

Supervisor

Dr. G. Naga Srinivasulu

(Asso. Prof., MED)

Chairman

Prof. P. Bangaru Babu,
MED, NIT WARANGAL

DEPARTEMENT OF MECHANICAL ENGINEERING

NATIONAL INSTITUTE OF TECHNOLOGY,

WARANGAL, TS, INDIA – 506004

CERTIFICATE

This is to certify that the dissertation work entitled **— COMPUTATIONAL AND EXPERIMENTAL EVALUATION OF PEM FUEL CELL PERFORMANCE USING SERPENTINE FLOW FIELDS**, which is being submitted by **Mr. Venkateswarlu Velisala** (Roll No. 701416), is a bonafide work submitted to the Department of Mechanical Engineering, National Institute of Technology, Warangal in partial fulfillment of the requirement for the award of the degree of **Doctor of Philosophy in Mechanical Engineering.**

To the best of our knowledge, the work incorporated in this thesis has not been submitted elsewhere for the award of any degree.

Dr. G. Naga Srinivasulu
Supervisor
Department of Mechanical Engineering
National Institute of Technology
Warangal- 506004

Prof. P. Bangaru Babu
Head,
Department of Mechanical Engineering
National Institute of Technology
Warangal-506004

DECLARATION

This is to certify that the work presented in the thesis entitled **"COMPUTATIONAL AND EXPERIMENTAL EVALUATION OF PEM FUEL CELL PERFORMANCE USING SERPENTINE FLOW FIELDS"** is a bonafide work done by me under the supervision of Dr. G. Naga Srinivasulu, and was not submitted elsewhere for the award of any degree. I declare that this written submission represents my ideas in my own words and where others' ideas or words have been included, I adequately cited and referenced the original sources. I also declare that I have adhered to all principles of academic honesty and integrity and have not misrepresented or fabricated or falsified any idea / data / fact / source in my submission. I understand that any violation of the above will be a cause for disciplinary action by the Institute and can also evoke penal action from the sources which have thus not been properly cited or from whom proper permission has not been taken when needed.

(Venkateswarlu Velisala)

(Roll No.: 701416)

Date:

Dedicated

to

- **My beloved father late Sri Panduranga Rao**
- **All my teachers**

ACKNOWLEDGMENT

Afterwards, I would like to express my sincere thanks and gratitude for my supervisors, Dr. G. Naga Srinivasulu, Mechanical Engineering Department, National Institute of Technology, Warangal, for his continuous guidance, support, enthusiasm and motivation in my PhD research work.

I am grateful to Prof. N.V. Ramana Rao, Director-NIT Warangal who has been constant source of inspiration for me. I thank Prof. P. Bangaru Babu, Head of the Department of Mechanical Engineering for his help and continuous encouragement to complete this work. I would like to express my sincere thanks to Prof. K. Madhu Murthy and Prof. G. Amba Prasad Rao (Mechanical Engineering Department), and Dr. P. V. Suresh (Chemical Engineering Department), learned members of my Doctoral Scrutiny Committee for being helpful and generous during the entire course of this work.

My sincere thanks also go to Prof. L. Krishnanad, Prof. C.S.P Rao and Prof. S. Srinivasa Rao, former HODs, Mechanical Engineering Department, National Institute of Technology, Warangal, for their encouragement, for providing access to the laboratory and research facilities. Without their precious support it would not be possible to conduct this research.

I would like to thank my family: my wife Manasa, my children, my parents (Sri Panduranga Rao and Smt. Eswaramma), my brothers (Atchaiah and Srinivasa Rao) and sister (Atchamma) for supporting me throughout writing this thesis and my life in general.

Last but not the least, I sincerely express my deepest gratitude to my fellow scholars for their help and exciting discussions in the last four years.

Venkateswarlu Velisala

(Roll No.: 701416)

Research Scholar

Department of Mechanical Engineering

National Institute of Technology Warangal- 506004

ABSTRACT

Fuel cell is a electro-chemical energy conversion system, which converts the chemical energy of fuel, directly into electrical energy. The ever increase in energy demand, non-polluting energy generation, and other environmental issues have persuaded many researchers to look for new efficient energy conversion technologies. Proton exchange membrane (PEM) fuel cells have many unique features compared with other types of fuel cell, such as relatively low operating temperature (around 80 ^{o}C), high power density, quick start, rapid response, and high modularity which makes them as the most promising system in the applications such as automotive, distributed power generation and portable electronic devices.

The aim of the present work is on evaluation of PEM fuel cell performance using serpentine flow fields with round corner by numerical modeling and experimentation. Three dimensional PEM fuel cell cell models of size 7x7, 7x12 and 7x17 cm are developed. Three types of flow field designs such as single, double and triple serpentine were considered for the supply of reactants. Computational fluid dynamics (CFD) based simulations were carriedout to analyse the pressure drop, distribution of reactants (H_2 and O_2), liquid water activity in the flow channels, current flux density and water content in the membrane. Further the effect of flow field design on the performance of PEM fuel cells were examined. Single, double and triple serpentine flow field plates were fabricated and experiments were conducted to validate the simulation results. Based on simulation and experimental results, it is observed that triple serpentine flow field performance is better than single and double serpentine flow field as it offer less pressure drop and uniform distribution of reactants.

The experimental tests were conducted by incorporating triple serpentine flow field in fuel cells to investigate the influence of cell design parameters such as membrane thickness and catalyst loading. The available membrane thicknesses are taken as 50, 51 and 175 µm. Similarly, the catalyst loadings are considered as 0.6, 0.8 and 1.0 mg/cm^2. The results revealed that the cells performance is increased with decreasing membrane thickness and increasing the catalyst (Pt) loading. Peak powers were obtained with a thin membrane (50 µm thickness) having 1.0 mg/cm^2 platinum loading.

Further, the experimental tests were conducted by incorporating triple serpentine flow field and 50 µm thickness membrane with 1.0 mg/cm^2 Pt loading to investigate the influence of cell operating parameters such as cell temperature (40, 50, 60, 70 and 80^{o}C), reactants humidification temperatures (40, 50, 60, 70 and 80^{o}C), and reactants flow rate on the performance of PEM fuel cells. The cell operating temperatures, reactants humidification

temperature are same for three active area PEMFCs and the reactants flow rates are different for three areas of PEMFC.

The fuel cell of active area 49 cm^2 with 50 µm membrane thickness and 1.0 mg/cm^2 platinum loading produced a peak power density of 418 mW/ cm^2 at 0.5 V when the cell was operated at 70^oC cell temperature, 70^oC anode humidification temperature, 60^oC cathode humidification temperature, 400 ccm H_2 flow rate and 800 ccm O_2 flow rate. In the same way, the cell of active areas 84 cm^2 and 119 cm^2 produced a peak powers of 395 mW/cm^2 and 374 mW/cm^2 respectively at 0.5 V. From this analysis it is observed that the power density of smaller active area (49 cm^2) cell is higher than the larger active area (84 and 119 cm^2) fuel cells. From this investigation, it is concluded that instead of going for larger active area cell one can choose smaller active area cell with more number (i.e stack) of cells.

CONTENTS

NOMENCLATURE

$\emptyset_e$	phase potential at the electrolyte
$\emptyset_s$	phase potential of solid
A_{cha}	cathode channel cross-sectional area
C_{H_2}	hydrogen concentration ($molm^{-3}$).
$C_{H_2O,a}^{MEM}$	membrane water concentration at anode ($Jmol^{-1}\ K^{-1}$)
$C_{H_2O,c}^{MEM}$	membrane water concentration at cathode ($Jmol^{-1}\ K^{-1}$)
C_{O_2}	oxygen concentration ($molm^{-3}$).
D_{ij}	binary diffusion coefficient (m^2s^{-1})
D_w	water diffusivity
N_w	net water flux across the membrane ($kg\ m^{-2}s^{-1}$)
P_s	water saturation pressure (Pa)
W_{cell}	cell power density (Wcm^{-2})
W_{net}	net power density (Wcm^{-2})
c_w	number of water molecules per sulfonic acid group
i_a	anode transfer current density (Am^{-2})
i_c	cathode transfer current density (Am^{-2})
k_e	ionic conductivity of the membrane (Sm^{-1})
k_p	permeability of GDL (m^2)
k_s^{eff}	ionic conductivity of solid phase (Sm^{-1})
n_d	electro-osmotic drag coefficient
w_i	species mass fraction *i* in the mixture
α_a	anode transfer coefficient
α_c	cathode transfer coefficient
η_a	anode potential difference
η_c	cathode potential difference
eff	effective

Greek Symbols

MEA	membrane electrode assembly
MEM	membrane
ref	reference

Subscripts/ Superscripts

T	cell operating temperature (K)
λ	water content in membrane
p	pressure (N m^{-2})
u	velocity (ms^{-1})
η	dynamic viscosity (kg $m^{-1}s^{-1}$)
ρ	density (kg m^{-3})

LIST OF FIGURES

LIST OF TABLES

CHAPTER 1

1. INTRODUCTION

Fuel cell (FC) is an electro-chemical energy conversion device, which converts chemical energy of fuel directly into electrical energy. The ever increase in energy demand, pollution-free energy generation, and other ecological issues have persuaded many researchers to look for new efficient energy conversion technologies [1]. Within such perception FC systems may consider as promising alternative due to practical advantages such as high-energy density, less harm to the environment, good dynamic response, and lightweight. Depending on type of electrolyte material used FCs are categorized as polymer membrane, alkaline, phosphoric acid, molten carbonate, and solid oxide fuel cells [2]. Proton exchange membrane (PEM) fuel cell has unique features such as relatively low operating temperature (around 80^{o}C), high power density, quick start, rapid response, and high modularity make them as the most promising system for power generation in the applications such as automotive, distributed power generation and portable electronic devices [3,4].

1.1 History of Fuel Cell

For the first time in 1839, Sir William Grove introduced the basic operating principle of FCs to the scientific community. Later in 1842, Grove produced a 50-cell stack and named as "gaseous voltaic battery". After Grove's invention, it took almost a century to re-introduce the FCs to the scientific community. In 1937, F.T. Bacon began to work on practical FC and he successfully built a 6 kW output stack by the end of the 1950s. In the early 1960s Grubb and Niedrach built a fuel cell using solid ion-exchange membrane electrolyte. Primarily, sulfonated polystyrene based membranes were employed as the electrolytes, then and there after Nafion membranes were substituted these sulfonated polystyrene based membranes. The Nafion has evidenced to be greater in performance and durability, and yet the most common membrane in use. This type of FC is generally called as polymer electrolyte membrane fuel cell or the proton exchange membrane fuel cell.

In the early 1960s, PEM fuel cell (PEMFC) was first used in the Gemini space program, that FC was developed by General Electric based on the work of Grubb and Niedrach. Following the Gemini Program the FC was also used in the Apollo program, to produce electricity for life support and communications. These FCs were made by Pratt and Whitney based on the Bacon's patents.

Due to their high cost, use of FC systems were limited in space applications and in some special applications. In 1990, Ballard Power systems started development of PEMFC systems. The strategy of Ballard was to reduce the cost of the fuel cell by using low cost materials and fabrication techniques, that FC turn out to be a real option for many applications. In 1993, Ballard Power Systems manifested fuel cell powered buses.

In 1993, Energy Partners demonstrated the first passenger car operating on PEMFCs. At the end of the century, almost all car manufacturers picked up on this activity and had built and manifested a fuel cell-powered vehicle. The timeline of FC development history is shown in Figure 1.1.

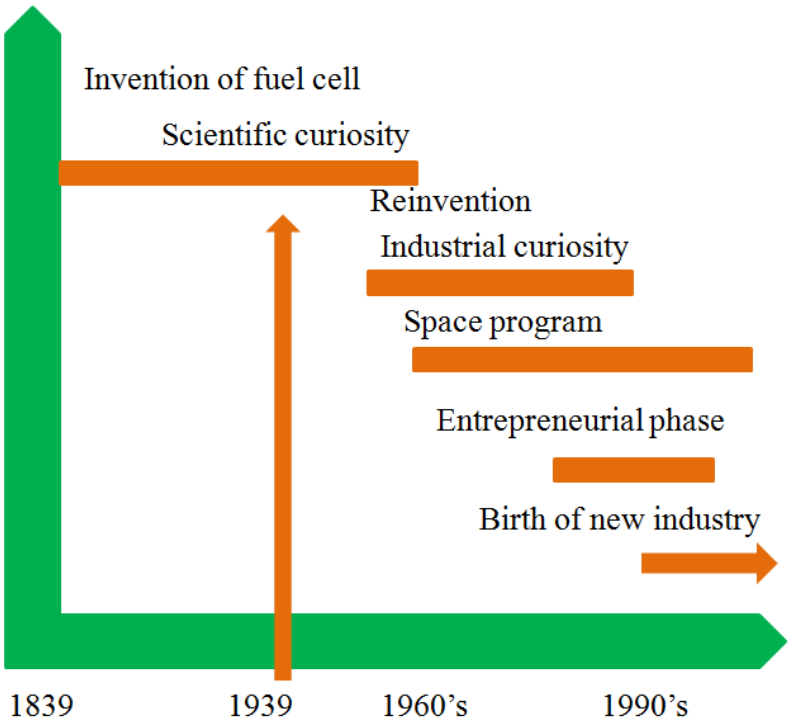

Figure 1.1 History of fuel cells

1.2 Principle of operation of PEM fuel cell and its components

Figure 1.2 illustrates the schematic of a PEMFC. Hydrogen (H_2) comes into the anode flow channel and disperses into the anode gas diffusion layer (GDL) whereas oxygen (O_2) enters into the cathode flow channel and disperses into the cathode gas diffusion layer (GDL). The membrane comprises catalyst usually platinum, on both sides and it is made from a material that only permits the hydrogen ions and offer resistance to the flow of electrons. When hydrogen and oxygen reaches the catalyst layers (CLs) through GDLs on the PEM, the following reaction takes place.

$$\text{Anode: } H_2 \rightarrow 2H^+ + 2e^- \qquad (1.1)$$

$$\text{Cathode: } ½\ O_2 + 2e^- + 2H^+ \rightarrow H_2O \qquad (1.2)$$

At anode catalyst layer hydrogen splits into hydrogen ions and electrons. Hydrogen ions pass from anode side to cathode side, through the membrane and electrons flow out of the cell through an electrical circuit. At the cathode CL oxygen reacts with hydrogen ions and electrons flow into the cathode, completing an electrical circuit. The overall reaction in a hydrogen and oxygen fuel cell is given in Equation 1.3.

$$\text{Overall: } H_2 + 1/2\ O_2 \rightarrow H_2O \qquad (1.3)$$

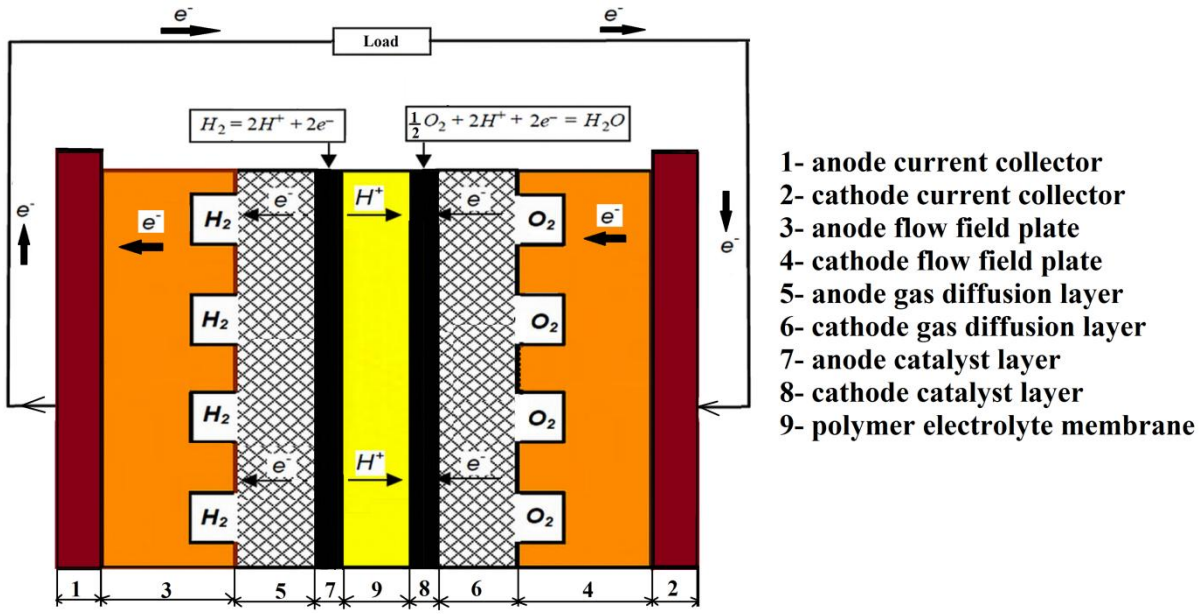

Figure 1.2 Schematic of a PEM fuel cell along with parts

1.2.1 *Membrane (PEM)*

The membrane is considered as the heart of the PEMFC, in which hydrogen ions transport from the anode CL to the cathode CL. The membrane function is to separate the fuel (H_2) and oxygen (O_2). The hydrogen ions/protons transfer from anode to cathode through the membrane, the membrane need to possess relatively high proton conductivity. Also the membrane should be chemically and mechanically stable in the fuel cell environment. Perfluorocarbon-sulfonic acid ionomer (PSA) membrane is usually used in PEMFCs. Dupont developed the membranes based on a sulfonated tetrafluoroethylene-based fluoropolymer-copolymer (Nafion family) and are considered as the best material for the membrane. A fully humidified membrane conducts the protons effectively, therefore it is essential to keep

membrane hydrated. Sometimes the water produced in the electrochemical reactions is inadequate to keep the enough humidification level in the membrane. Also, use of dry reactant gases and the electro-osmotic drag results in an under-humidified state. Therefore, it is desirable to humidify the inlet reactant gases before enter into the cell to achieve the required humidification level in the membrane [5].

1.2.2 Catalyst Layers (CLs)

In a PEMFC, there are two CLs on both sides of the membrane. These CLs are placed between the membrane and GDLs at the anode and the cathode sides respectively. All the electrochemical reactions take place at the catalyst layer. The catalyst layer must have high intrinsic activity, larger active surface area, high ionic and electric conductivity, high porosity for reactants entry as well as product removal. Usually Platinum (Pt) is preferred as the catalyst in PEMFCs because of its great stability and reactivity. Sometimes Pt alloys also can be preferred as catalyst to further improve kinetic activity, stability, and tolerance to impurities when reformate gas is used on the anode side. Pt is generally in the form of tiny particles and these small Pt particles are reinforced on the carbon particles to offer a high surface area. A catalyst layer showing with Pt supported on carbon is depicted in Figure 1.3.

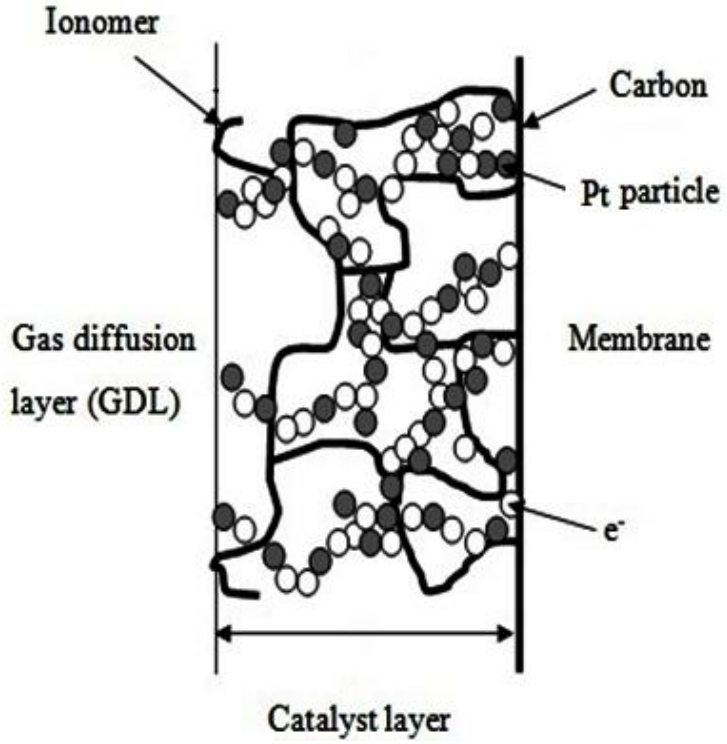

Figure 1.3 Catalyst layer [6]

1.2.3 Gas Diffusion Layers (GDLs)

There are two GDLs bonded to anode and cathode catalyst layers. Usually hydrophobic carbon fiber paper or cloth is used as GDL and it is called the substrate. A microporous layer (MPL) with hydrophobic property is applied to the catalyst side of the substrate. The hydrophobicity is usually attained through application of Poly Tetra Fluoro Ethylene (PTFE). The SEM images of carbon fiber paper and cloth are shown in Figure 1.4. The following are some key functions of GDL

- It works as a passageway for transport of the reactants from the flow channels to the reaction site.
- It works as a passageway for evacuation of product (water) from the reaction site to the flow channels.
- It works as a heat conductor.
- It conducts the electrons from CL to the current collector via bipolar plate.

The membrane electrode assembly (MEA) is the combination of membrane, CLs and GDLs.

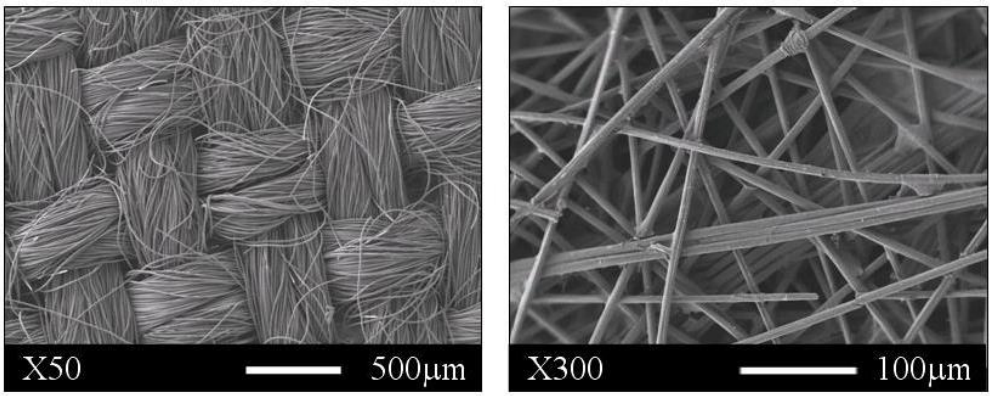

Figure 1.4 GDL material: carbon cloth (left) and carbon paper (right) [7]

1.2.4 Flow Field Plates (FFP)

Every single PEM fuel cell has two flow field plates (FFP) and MEA is kept in between these two flow fields and assembled with the help of bolts and nuts. These FFPs are in direct contact with GDLs. These flow field plates are generally made out of graphite material or metals. The key purposes of the FFPs are:

 To distribute the reactants to the GDLs, and evacuate the unused gases and water from the cell.

 To transfer electrons and heat.

 To give mechanical strength.

To serve these purposes the FFPs need to be chemically stable, electrically and thermally conductive, mechanically strong and contamination free. Figure 1.5 shows the commonly used flow field designs in PEM fuel cells.

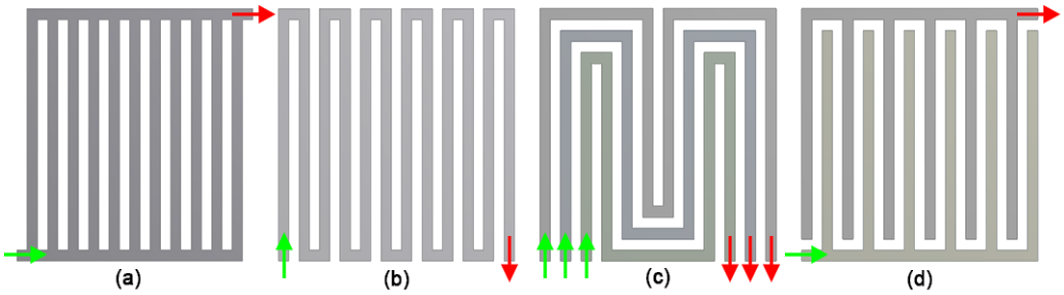

Figure 1.5 Common flow-fields: (a) Parallel (b) 1-pass serpentine (c) 3-pass serpentine and (d) Interdigitated [8].

With the help of above, described components a complete fuel cell can be assembled with the help of bolts & nuts and the exploded view of a complete PEM fuel cell can be seen in Figure 1.6.

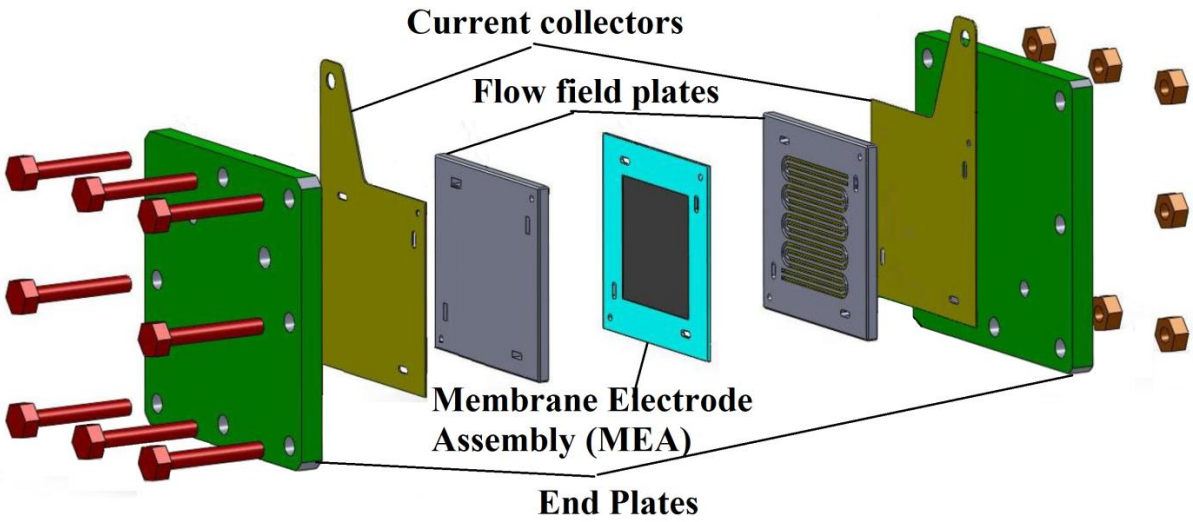

Figure 1.6 Exploded view of a PEM fuel cell

1.3 Performance of PEMFC

The performance of the PEM fuel cell can be summarized with a graph of its current-voltage characteristics. This graph shown in Figure 1.7 is called *i*–V curve (solid line), displays the voltage output of the FC for a given current output. An ideal FC will generate any quantity of current at a constant voltage when there is enough supply of reactant gases. In practice, the real output voltage of a fuel cell is less than the ideal thermodynamically predicted voltage. Besides that, a further increase in the current drawn results drop in FC output voltage and limits the total power output. The power (*P*) output of a fuel cell is given by the product of current and voltage

$$P = V * \mathrm{I} \qquad \textbf{(1.4)}$$

Power density curve of a fuel cell can be drawn from the data obtained from fuel cell *i*-V curve, which gives the power output of a FC. Power density curves (dotted line) is shown in Figure 1.7. FC voltage is given on the primary *y*-axis (left), while power density is given on the secendary *y*-axis (right).

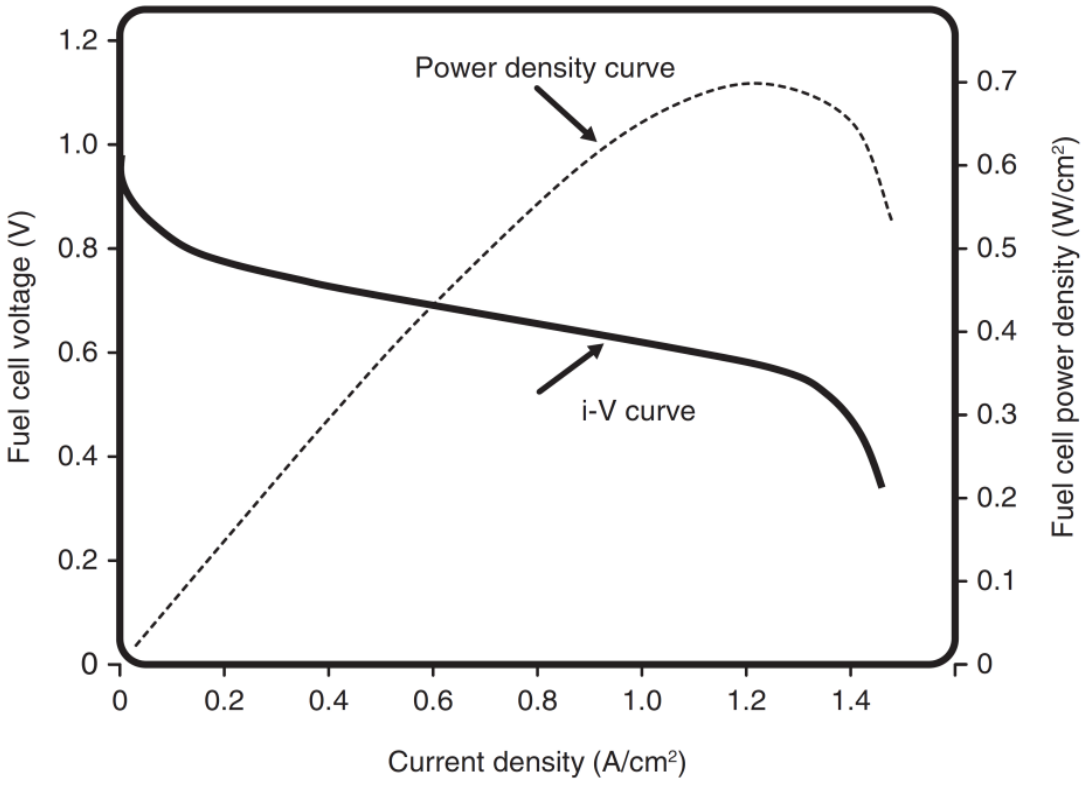

Figure 1.7 polarization and performance characteristics of a fuel cell [9]

The current generated in a FC is directly proportional to the quantity of fuel consumed. It is difficult to keep the fuel cell at a high voltage under the current load. Due to irreversible losses the output voltage of a practical fuel cell is lower the thermodynamically predicted output voltage. These irreversible losses are greater while more current is drawn from the FC. Three foremost types of FC losses given below are shown in the *i–V* curve of a FC and its characteristic shape.

1. Activation losses

2. Ohmic losses

3. Concentration losses

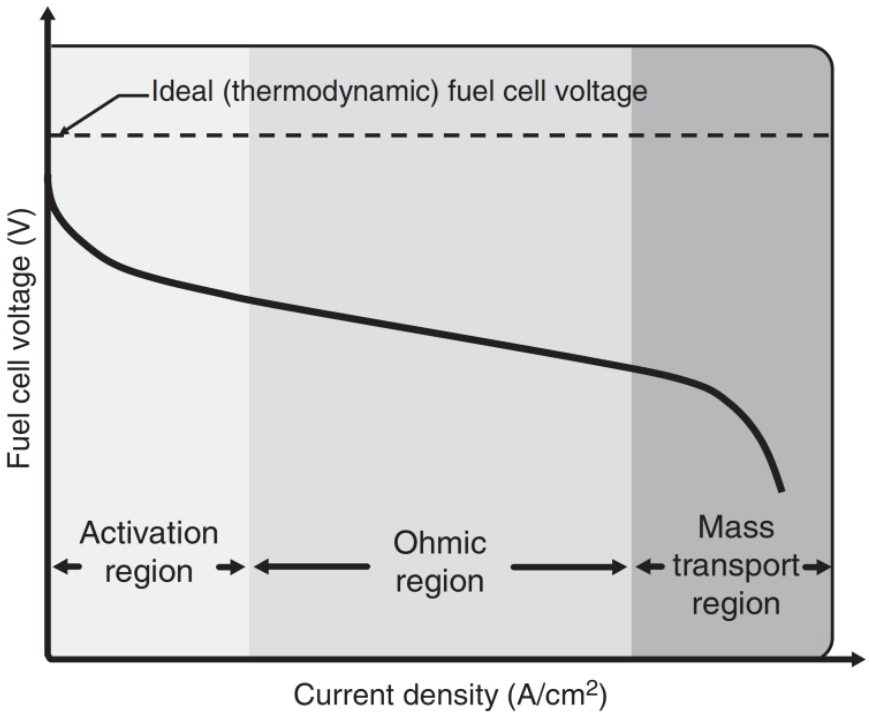

Figure 1.8 Polarization curve with irreversible losses of a fuel cell

The actual output voltage of a FC can be composed by beginning with the thermodynamically predicted voltage output and then deducting the voltage drops due to three losses mentioned above:

$$V_{cell} = E_r - \eta_{act} - \eta_{ohmic} - \eta_{conc} \qquad (\mathbf{1.5})$$

$$E_{nernst} = 1.229 - 0.85 * 10^{-3}(T - 298.15) + 4.3085 * 10^{-5}\, T[\ln(P_{H_2}) + \ln 0.5\,(P_{O_2}) \qquad (\mathbf{1.6})$$

Where V_{cell} is cell output voltage, E_r is reversible cell voltage, η_{act} is activation losses, η_{ohmic} is ohmic losses, η_{conc} is concentration losses.

These three irreversible losses each add to the characteristic shape of the fuel cell *i–V* curve. As illustrated in Figure 1.8, the activation losses majorly influence the first part of the curve, the ohmic losses are most ostensible in the middle part of the curve, and the concentration losses are most significant in the tail of the *i–V* curve. Equation 1.5 helps to characterize and model the performance of practical fuel cells.

Activation losses

Activation loss is associated to the energy barrier that need to be overcome to start a chemical reaction. At low current density, the electron transfer rate is sluggish and a bit of the cell voltage is lost to be able to compensate for having less electro-catalytic activity. The activation voltage drop can be described as

$$V_{act} = \frac{RT}{\alpha nF}\, ln\left(\frac{i}{i_0}\right) \qquad \textbf{(1.7)}$$

Where T is Fuel cell operating temperature (kelvin), R is Universal gas constant,α is the transfer constant, n is number of electrons participated in the reaction, F is Faraday's constant, *i* is cell current density, and i_0 is the exchange current density.

Ohmic losses

Every material comes with an inherent amount of resistance to charge flow. The materials usual resistance to charge-flow triggers ohmic polarization, which in turn causes drop in FC voltage. The resistive losses take place in the electrolyte (ionic), electrodes (electronic and ionic), and terminal connections of the cell (electronic). The ohmic losses (ohmic voltage drop) can be described as

$$V_{ohmic} = i * R_{ohmic} \qquad \textbf{(1.8)}$$

Where *i* is the current density and R_{ohmic} resistivity of membrane. The cell resistance relies upon membrane water content λ_{mem} and cell temperature. On the other hand, the cell resistance is proportional to thickness of the membrane (t_{mem}) and inversely proportional to the conductivity of the membrane (σ_{mem}). Thus resistivity of membrane can be described as follows

$$R_{ohmic} = \frac{t_{mem}}{\sigma_{mem}} \quad \textbf{(1.9)}$$

The membrane conductivity greatly depends on membrane water content λ_{mem} and cell temperature T_c. The membrane conductivity can be determined using the following formula

$$\sigma_{mem} = (0.005139 * \lambda_{mem} - 0.00326) exp\left[1268 * \left(\frac{1}{303} - \frac{1}{T_c}\right)\right] \quad \textbf{(1.10)}$$

Concentration losses

Concentration losses are associated with mass transport limitations (reactants / products)**.** In this region, the reactants turn out to be consumed at higher rates than the supplied rate whereas the product amasses at a larger rate than it could be cleared. Eventually, this will influence the reaction completely and the FC voltage drops to zero

$$V_{conc} = i(\beta_1 * \frac{i}{i_{max}})^{\beta_2} \quad \textbf{(1.11)}$$

Where β_1 , β_2 are constants depends on cell temperature and partial pressure of reactants. β_2 can be taken as 2, and β_1 is defined by Pukrushpan et al.[10] as follows

$$\beta_1 = \begin{cases} (7.16 * 10^{-4} * T_c - 0.622)\left(\frac{P_{O_2}}{0.1173} + P_{sat}\right) + (-1.45 * 10^{-3} * T_c + 1.68) \\ if \ \frac{P_{O_2}}{0.1173} P_{sat} \leq 2 \ atm \\ else \\ \left(8.66 * 10^{-5} * T_{fc} - 0.068\right)\left(\frac{P_{O_2}}{0.1173} + P_{sat}\right) + \left(-1.6 * 10^{-3} * T_{fc} + 0.54\right) \\ if \ \frac{P_{O_2}}{0.1173} P_{sat} \geq 2 \ atm \end{cases} \quad \textbf{(1.12)}$$

Where P_{sat} is water saturation pressure, P_{O_2} is Partial pressure of oxygen and T_{fc} cell temperature.

1.4 Organization of Thesis

The thesis comprises of 5 chapters, chapter 1 outline a short introduction of PEMFC. The literature review on PEMFC is provided in chapter 2. The gaps observed from the literature review and thesis objectives also presented in chapter 2. Both experimental methodology and computational methodology for PEMFC have been presented in chapter 3. In this chapter the fundamental concepts behind the electrochemistry modeling, current and mass conservation, liquid water formation and transport phenomena have been offered. The results of PEM fuel

cell validation have been achieved through the CFD modelling is provided in chapter 4. Other results in consort with research objectives are also presented in chapter 4. Finally, the overall conclusions are drawn out of this research and some recommendations for the future research are given in chapter 5. Appendix covers research output in the form of peer-reviewed journal and conference papers.

CHAPTER 2

2. LITERATURE REVIEW

Significant amounts of theoretical and experimental studies have been carried out by many researchers on PEM fuel cells (PEMFCs). Experimental tests are commonly used approaches for understanding and predicting PEMFC performance. Some empirical and mathematical models also proposed in the literature to comprehend and analyze performance of PEMFCs. These models usually acceptable with the experimental data by means of a single equation but they are less precise and trustworthy in envisaging the fuel cell performance. To understand basic transport processes, more fundamental models were developed to simulate the performance of PEMFCs. The objective of the current literature review is to overview the PEM fuel cells development.

For the first time in 1839, Sir William Grove demonstrated the principle of a fuel cell (FC). After his demonstration, it took almost one decade to re-introduce the FC to the scientific community. Being enthralled with Grove's invention, Bacon began working on FCs in 1939 and successfully constructed a FC stack of 6 kW output power 1959 [11]. Later FCs have been used in the U.S. Space Program for the first time. Furthermore, the FCs were used in the Apollo Space Program to produce power for life support and communications. Based on Bacon's patents, Pratt and Whitney made the fuel cells. General Motors made trials with a FC operated van by the mid-1960s, in the meantime the U.S. Space Program has continued to effectively make use of FCs up to today. In the 1960s many industries recognised that the FCs can be used in different applications, but because of their high manufacturing cost and technical difficulties, FCs were not have the capacity to monetarily focused with other energy conversion devices. In the 1980s, the Canadian Government sponsored the preliminary development work of FCs which was supported by Ballard Power Systems. Later in 1989, the company decided to concentrate on FC systems for transportation and stationary applications.

2.1 Studies on 1-D and 2-D PEMFC models

Gurau et al.[12] presented a mathematical model of a PEMFC and obtained strenuous analytical results of the model. Their modeling domain comprises of cathode flow channel, gas diffusion layer (GDL), catalyst layer (CL), and the membrane. Beginning with oxygen transport equations and Ohm's law for proton movement, expressions for the oxygen distribution in the flow channel, GDL, CL, current density in the CL and membrane

phasepotential have been derived. Bernardi & Verbrugge [13] presented a mathematical model of the solid polymer electrolyte FC to (i) examine causes which are limiting the FC performance and (ii) explain the mechanism of species transport in the intricate network of gas, liquid, and solid phases of the FC. Parthasarathy et al. [14] examined the temperature dependency on the kinetics of the reduction of oxygen kinetics at the platinum/Nafion interface of PEM fuel cell and they derived empirical relationships between the exchange current densities and the transfer coefficients as a function of temperature. Amphlett et al. [15] presented a generalized steady-state electrochemical model of the PEMFC and investigated the polarization curve empirically. The empirical relationship permits the prediction of cell voltage, so that it is possible to avoid complicated numerical computations in the estimation of activation and ohmic overpotentials. However, the empirical model is inadequate in capturing the internal resistance of the membrane and the proportion of water in the cathode catalyst layer, since the latter is a function of the temperature and the results calculated by using Amphlett's model are valid only for the isothermal situation.

Kim et al. [16] presented an empirical model which fits into the entire polarization curve of the PEMFC. The authors found that addition of an exponential term be responsible for compensation for the mass-transport region at high current densities. Kazim et al. [17] presented a 2-D steady state PEMFC model with conventional and interdigitated flow fields. The outcomes of this model uncovered that limiting current density of interdigitated flow field fuel cell is about 3 times the limiting current density of the conventional flow field fuel cell. Mann et al.[18] developed a generalised steady-state electrochemical model (GSSEM) which is more extensive in pertinence than the previous steady state electrochemical models (SSEM) of Amphlett et al. [15]. It now holds the ability to deal with PEMFCs of any active area and Nafion membrane thickness. Fowler et al.[19] modified the genaralised steady-state electrochemical model (GSSEM) of Mann et al.[18] with incorporation of voltage degradation term to estimate the durability of fuel cells and named this model as generalised steady-state electrochemical degradation model (GSSEDM). Wang et al.[20] developed a spherical flooded-agglomerate model for the cathode CL of a PEMFC. This model incorporates the kinetics of oxygen reduction at the interface of catalyst-membrane, proton transportation through the membrane, the oxygen diffusion through pores, and the dissolved oxygen diffusion through membrane. The studies (1-D and 2-D models) presented so far require number of simplifications due to limitations of the numerical techniques.

2.2 Studies on 3-D PEMFC models

Dutta et al. [21] developed a first true three-dimensional (3-D) numerical model based on the commercial CFD software ANSYS-FLUENT to aid in understanding of gas flow, species transport, and electrochemical aspects of a fuel cell. Berning et al. [22] developed a nonisothermal 3-D, single-phase model using the CFD program CFX-4.3 (AEA Technology). This model consist of the gas flow channels, GDLs, and membrane; the CLs were treated as interfaces. Kumar & Reddy [23] developed a computational 3-D half-cell PEMFC model to study the impact of different channels sizes and shapes in the flow-field. Their channel study results showed that high fuel consumptions (≈80%) were obtained with optimum channel depth and width as well as land width were close to values of 1.5, 0.5 and 1.5 mm, respectively. The channel shapes study results revealed that channel cross-section in triangular and hemispherical shape caused an improvement in hydrogen consumption around 9% at the anode.

Berning & Djilali [24] developed a 3-D single-phase model of a PEMFC and studied the influence of cell operational and material parameters on the cell performance. Nguyen et al.[25] presented a 3-D computational fluid dynamics model of a PEMFC with serpentine flow field channels using the CFD program CFX-4.3. A distinctive feature of this model is the implementation of VTC (voltage-to-current) algorithm, which allows for a far more accurate three-dimensional variation of the electrochemical kinetics. Furthermore, the 3-D activity of the catalyst layer is also considered in this model. Lum & McGuirk [26] build up a steady-state, 3-D model of a complete PEMFC and carried out some parametric studies, such as variation of electrode thickness, shoulder width, degree of permeability and oxidant concentration on cell performance. Lin & Beale [27] developed a 3-D full model and a hybrid model for an industrial PEM fuel cell to predict water transport distribution within the cell and also the impact of oversaturation and dehydration on either side of the membrane, on the overall cell performance. Yan et al.[28] proposed a 3-D PEMFC model with a novel straight channel tapered in height or width to increase the fuel utilization efficiency. The results revealed that the tapered channel designs enhance fuel velocity, fuel transport through porous layers, fuel utilization, and the liquid water removal capability.

Yan et al. [29] build up 3-D PEMFC models to investigate the performance with various flow field designs such as parallel flow field, parallel flow field with baffles, Z-type flow field, Z-type flow field with baffles and serpentine flow field. The authors reported that parallel flow

field with baffles offers less pressure drop and best performance. Liu et al. [30] presented an isothermal, steady-state, 3-D multicomponent transport model for PEMFC with straight gas channels and their findings revealed that the distribution patterns are moderately uniform at low current densities and are non-uniform at high current densities because of the mass transfer limitation. Jang et al. [31] developed a 3-D numerical PEMFC models with parallel flow field, Z-type flow field, and serpentine flow fields to investigate the performance as well as transport phenomena of the PEMFCs. The authors reported that the PEMFC with serpentine flow field offered best performance, followed by Z-type flow field and then parallel flow field. Sadiq Al-Baghdadi [32] also developed a full 3-D, non-isothermal CFD model of a tubular in shape PEMFC to study the transport phenomena. Wang et al.[33] developed a 3-D numerical PEMFC model and investigated the local transport phenomena and performance of the cell using parallel and interdigitated flow fields. The results of the studies shown that the performance of PEMFC with interdigitated flow field is superior over the PEMFC with parallel flow field.

Weng et al.[34] presented a 3-D PEMFC model with contracted outlet flow channels to analyze the performance of the FC and the local transport phenomena. The authors reported that the contracted channel design ameliorate the reactant velocities, which enhances liquid water evacuation and increases reactant utilization. Rismanchi & Akbar [35] also presented a 3-D PEMFC model with square cross section straight flow channels to study the flow structure, species concentrations and current distribution inside the cell. Wang et al.[36] presented a full 3-D, two-phase transport model for PEMFCs based on the two-fluid method to examine the influence of gas channel aspect ratio on the performance of FCs with one pass and three pass serpentine flow field. The results revealed that enhancement in the cell performance can be obtained with decrease in the aspect ratio and the aspect ratio has less influence on the performance for the three-pass serpentine flow field PEMFC than one pass serpentine flow field PEMFC because of the weaker under-rib convection. Manso et al. [37] presented a 3-D CFD model for PEMFC with serpentine flow field to examine the influence of the flow channel's aspect ratios, varying between 0.07 and 15. The study concluded that the channel with high aspect ratio displayed more uniform current distributions, moderate temperature distribution gradients, and higher water content in the membrane than channel with low aspect ratio.

Robles et al. [38] developed a single phase 3-D PEMFC model with a flow field path in the shape of 1, 2, 3, 4, 6, and 8 concentric spirals. The authors found that model with 4 spirals is best geometry due to the more uniform current density distribution, a uniform water distribution, and relatively small pressure drop. Choi et al.[39] presented a 3-D PEMFC with serpentine flow field having five flow passes to examine the influence of flow channel height and width on pressure drop and liquid water removal. The authors noticed reduction in the pressure drop with increase in channel height and width. The authors also noticed that the increase in the channel width caused quicker liquid water removal than when the channel height increases. Khazaee & Ghazikhani [40] built a duct-shaped PEMFC numerical model and investigated the influence of number of connections between bipolar plate (BP) and GDL on the cell performance and species distribution. The study concluded that increase in the number of connections between BP and GDL caused increase in the cell performance, utilization of hydrogen, oxygen and water generation

Sierra et al. [41] conducted a 3-D numerical analysis on a PEMFC model using serpentine, interdigitated and straight channels adapted to tubular plates. The authors compared the numerical results with literature data described for analogous designs and the results reveal that the conventional flow channel designs have several benefits (uniform pressure and current density distributions) over the rectangular designs. Performance and flow characteristics of bigger-size PEMFC (cell active area 300 cm^2) having branch channel were studied by Han et al. [42] through simulation and experiments. The branch channel (f=0.5) performance is compared with serpentine channel performance and found that the performance of branch channel was analogous to serpentine channel performance. Also found that the pressure drop in the branch channel is less by 52.5% than serpentine channel. Limjeerajarus & Amornkitt [43] numerically studied the effect of six flow field designs namely 1-S, 3-S, 5-S, parallel, 3-PIS and 5-PIS as well as number of channels on performance of a small PEMFC (5 cm^2 active area). The authors reported that: i) 1-S flow field gave the highest performance and uniformity whereas the parallel flow field gave the least performance, ii) with the same number of channels, the parallel in series (PIS) flow fields performance is superior than the multi-channel serpentine flow field. Rostami et al.[44] developed a single phase model of PEMFC with serpentine flow field and studied the effect of bend size (from 0.8 mm to 1.2 mm) on the cell performance. The study concluded that bend size of 1.2 mm has an improved performance when matched with the other bend sizes.

Paulino et al.[45] presented a CFD based 3-D PEMFC model with single channel and studied the effect of channel cross section (rectangular, trapezoidal and hybrid stepped geometries) on performance and water management of the cell. The results revealed that the performance of rectangular channel FC was slightly higher than stepped and trapezoidal channel FCs while water management behavior of stepped and trapezoidal channel FCs was superior than the rectangular channel FC.

2.3 Studies on PEMFC flow field designs

Nguyen [46] developed a non-conventional flow channel to enhance the mass-transport of the reactants from the flow channels to the porous electrodes and to decrease the cathode electrode water flooding**.** Kazim et al.[17] presented a simple 2-D PEMFC model to explore the influence of conventional and interdigitated flow fields on cell performance. The outcomes demonstrate that limiting current density of interdigitated flow field PEMFC is 3 times the limiting current density of conventional flow field PEMFC. Dutta et al. [21] developed a first true 3-D PEMFC with straight channel and studied the gas flow, species transport, and electrochemical aspects of the cell. The authors also studied the performance of the cell with and without inclusion of GDL. The results indicated that addition of gas diffusion layer (GDL) generates a lower and more uniform current density compared to case without GDL. Kazim et al.[47] inspected the effect of cathode operating conditions on the performance of PEMFC with an interdigitated flow field. The operating conditions include cathode porosity, inlet oxygen mole fraction, operating temperature and pressure. The results demonstrate that increasing the porosity of the GDL as well as mole fraction, operating pressure or temperature of the oxygen increase the overall performance of the fuel cell.

Kumar & Reddy [48] studied the effect of different flow field designs, viz. (1) serpentine; (2) parallel; (3) multi-parallel; and (4) discontinuous on the steady state and transient state performance of PEMFC through simulations. The study concluded that multi-parallel design steady state and transient state performance was better than other three designs. Yan et al.[28] proposed a novel flow channel design having varying cross-section for PEMFCs and studied the influence of the taper ratio of channel height and width. The results revealed that the flow area variation along the flow channel contributes to observable influence on the reactants velocity in flow channel, liquid water removal capability, the reactants transportation and consumption, and the cell performance. The best performance was achieved at the height taper ratio of 0.5 and the width taper ratio of 1.8 among the taper ratios studied.

Yan et al. [29] developed 3-D PEMFC models to investigate the performance with several flow channel designs viz. parallel flow field, parallel flow field with baffles, Z-type flow field, Z-type flow field with baffles and serpentine flow field. The results revealed that parallel flow field with baffles offered less pressure drop and best performance. Sun et al. [49] presented a 3-D numerical PEMFC model with trapezoidal cross-sectional shaped single 3-pass serpentine flow field to study the pressure distribution and flow cross-over through GDL. The results revealed that increase in channel size ratio (R=B/A), increases the flow cross-over through GDL and this increase in the flow cross-over decrease the pressure drop across the channel. Shimpalee et al.[50] developed a 200 cm^2 active area PEM fuel cell 3-D numerical models with (a) 3-channel serpentine, (b) 6-channel serpentine, (c) 13-channel serpentine, (d) 26-channel serpentine, and (e) 26-channel complex serpentine flow fields to study the impact of channel path length on species distribution and performance of the cell. The model results concluded that with smaller path lengths or more number of channels helps to achieve more uniform local temperature, water content, and current density distribution.

Su et al. [51] developed a 25 cm^2 active area 3-D PEMFC model with straight and serpentine flow field plates to study the influence of step depth on pressure drop and mass transfer phenomena. The authors observed i) an increase in the performance and pressure drop with the number of step-depths in the straight flow pattern, ii) no increase in the performance and pressure drop with the number of step-depths in the serpentine flow pattern. Hongthong et al. [52] developed a 3-D, single phase, compressible and isothermal PEMFC models of 5 cm^2 active area and examined the impact of the geometry and pattern of the flow channel on the performance of the FC. The results demonstrate that the change in channel geometry has no impact on the FC performance and interdigitated flow channel pattern offers a higher limiting current density and performance than the conventional flow channel pattern on the cathode side. Al-baghdadi & Al-janabi [53] developed a full 3-D, non-isothermal CFD model of a PEMFC with straight flow field channels to study species transport, heat transfer, electrochemical kinetics, and the water transport through the membrane. Ferng & Su [54] developed a 3-D CFD model of PEMFC with different types of flow field channels namely parallel and serpentine flow channels, single-path and multi-path flow channels, and uniform depth and step-wise depth flow channels to study their effect of cell performance. The results confirmed that the parallel flow channel with the step-wise depth design significantly promotes the cell performance.

Wang et al. [33] developed a 3-D numerical PEMFC model and investigated the local transport phenomena and cell performance using parallel and interdigitated flow fields. The results revealed that the performance of PEMFC with interdigitated flow field is superior over the PEMFC with parallel flow field. Yan et al. [55] presented a 3-D full PEMFC model with serpentine flow field to analyze the effects of the channel height and length contraction ratios on the cell performance. The authors concluded that i) when the power losses because of pressure drops are neglected, the performance of the cell having the contracted outlet channel keep on increase, ii) when the pressure losses are considered, the optimum performance is attained at a height contraction ratio of 0.4 and a length contraction ratio of 0.4.

Weng et al.[34] developed a 3-D PEMFC model with contracted outlet flow channels to analyze the performance and the local transport phenomena of the FC and the reaults indicated that the contracted channel design enhances the reactant velocities in the contracted area, which enhances liquid water removal and increases reactant utilization. Jeon et al. [56] conducted CFD based simulations for 10 cm^2 active area PEMFC with four types of serpentine channels namely single channel, double channel, cyclic-single channel, and symmetric-single channel to examine their influence on performance of the PEMFC. The simulation results revealed that double serpentine channel performs better at high humidity inlet conditions while at low humidity inlet conditions cyclic-single channel and symmetric-single channel flow-field performs better. Min [57] presented a 3-D model of PEMFC with stepped flow field channel and carried out simulations. The results reported that the stepped flow field increases the reactant concentration distribution, local current density distribution, water vapor concentration distribution and performance of the FC.

Wang et al. [36] presented a full 3-D, two-phase transport model for PEMFCs based on the two-fluid method to examine the influence of flow channel aspect ratio on the FC performance using single (1-S) and triple serpentine (3-S) flow field designs. The results revealed that for both designs, the performance of the FC increases with reducing the aspect ratio. Iranzo et al. [58] conducted experiments on a 50 cm^2 PEMFC under various operating conditions and with different flow field designs to study the performance. The authors reported that the PEMFC with serpentine flow field perform is superior than the PEMFC with parallel flow field and supply of pure oxygen and humidified reactant also improved the PEMFC performance. Carton & Olabi [59] conducted DOE study on a 14.45 cm^2 PEM fuel cell with serpentine, parallel and maze type flow plate designs under different operating

conditions (H_2 flow rate, O_2 flow rate and the inlet H_2 pressure). The results show that the serpentine flow plate design is more effective design than the maze or parallel flow design and the parallel flow design performed fairly well at high inlet pressures but over-all statically the serpentine flow plate achieved better performance.

Bansode et al. [60] carried out computational and experimental studies on a PEMFC using 3 types of flow fields (parallel, serpentine, and mixed). In addition, they studied the effect of flow rate and temperature on cell performance. The results indicated that the mixed flow field offered best electrochemical performance as well as moderate pressure drop compared with the parallel and serpentine flow-fields. Wang et al. [61] presented a 3-D, two-phase PEMFC model with serpentine flow field and studied the influence of cathode channel size on the FC performance. The numerical predictions revealed that smaller cross-sectional area channels enhanced the liquid water removal and optimal performance obtained with a 0.535x0.535 mm^2 cross-sectional area flow channel when pressure drop losses are considered.

Fontana et al.[62] developed a complete 3-D PEMFC model to investigate the effects of non-uniform cross-sectional area flow channels on the FC performance. The results reveal that an inclination of 0.75^o in the flow channel improves the current density by approximately 9.5% and the power density by 8% and the pressure drop in the flow channel increase by factors of about 2 and 3.5 for angles of 0.5^o and 0.75^o, respectively. Yan et al. [63] fabricated a 256 cm^2 active area PEMFC with serpentine flow field and conducted experiments with two membranes namely PRIMEA 5621 and PRIMEA 57. The authors found that the PRIMEA 57 membrane performance is better than the PRIMEA 5621 membrane. Suresh et al. [64] developed a flow field which is based on the enhancement of the local cross-flow conditions in a split serpentine flow field and concluded that split serpentine flow field enhances the cross flow, reduces the total pressure drop, increases the stoichiometric ratio and provides higher current as well as power.

Chiu et al. [65] presented a 3-D numerical PEMFC model with parallel, interdigitated and serpentine flow fields to examine performance and transport phenomena. The authors also examined the influence of channel geometry and size on the cell performance and water activity in the channels. The results revealed that decrease in channel height caused increase in water removal rate and decrease in cell performance and parallel flow channel width increase resulted drop in the cell performance due to low gas velocity with less water removal. Jang et al. [66] proposed spiral channels for PEM fuel cells and conducted both

simulations and experiments to evaluate the performance of PEMFC using spiral and serpentine flow channels. The authors compared the spiral and the serpentine channels results and found that cell with spiral channel performs better than cell with serpentine channel due increased heat and mass transfer and reduced pressure drop in the channels.

Sreenivasulu et al. [67] conducted experimental study on a PEMFC with three types of flow fields (4-Serpentine, interdigitated and dual inlet and single outlet flow channel) to explore the effect of back-pressures on FC performance. The results indicated that highest PEMFC performance can be obtained using 4-Serpentine flow channel and with and without back-pressure. Additionally, the performance of twin inlet and single outlet flow channel PEMFC is better than the interdigitated channel PEMFC at higher back pressures. Liu et al. [68] conducted experimental study on single cell PEMFC and PEMFC stack to examine the influence of different flow field designs on performance. The study found that PEMFC with serpentine flow fields exhibited paramount performance than other designs, while the PEMFC with spiral flow field design exhibited the poor performance. Khazaee [69] conducted numerical and experimental investigations on 25 cm^2 active area PEM fuel cell to study the effect of rectangular, triangular and elliptical channel geometries on cell performance. Both numerical and experimental results reveal that PEMFC with rectangular geometry channel performed better than the cells with triangular and elliptical geometry channel.

Torkavannejad et al. [70] developed circular, square and octagonal duct-shaped PEMFCs and analysed their performance numerically. The results indicated that the performance of square duct shaped PEMFC is better circular and octagonal duct shaped PEMFCs. Performance and flow characteristics of large-sized PEMFC (active area 300 cm^2) having branch channel were studied by Han et al. [42] through simulation and experiments. They compared the performance of branch channel (f=0.5) with serpentine channel and found that the performance of branch channel was similar to serpentine channel performance. In addition, they found that the pressure generated inside the branch channel is lower by 52.5% than serpentine channel.

Iranzo et al. [71] conducted experiments on a 50 cm^2 PEMFC with multi-pass serpentine flow field channels to examine the influence of orientation (horizontal and vertical) on liquid water distribution and cell performance. Their results reveal that the configuration with horizontal cathode flow field channels gives a better cell performance and prevents the blocking of flow channels with liquid water. Li et al. [72] proposed waved serpentine flow field (WSFF)

channels for PEM fuel cells and conducted both numerical as well as experimental studies. The results reveal that WSFF channel offered less pressure drop and better performance than conventional serpentine flow field (CSFF) channel. WSFF channel also enhanced the oxygen transport and liquid water removal.

2.4 Studies on PEMFC design and operating parameters

The performance of fuel cells is known to be affected by various cell operating and design parameters, for example, temperature, pressure, humidification of the reactant gases, cell components dimensions, shape. It is essential to be acquainted with the impacts of these parameters on cell operation to enhance cell performance. In this regard, it is useful to recognize the operating conditions that offer the maximum possible power output with respect to the chosen current density. With regards to the current density, the operating conditions to attain the maximum power are different, and thus it is useful to know the complete operation map of the PEMFC. Figure 2.1 shows the various design and operating parameters which affect the FC output.

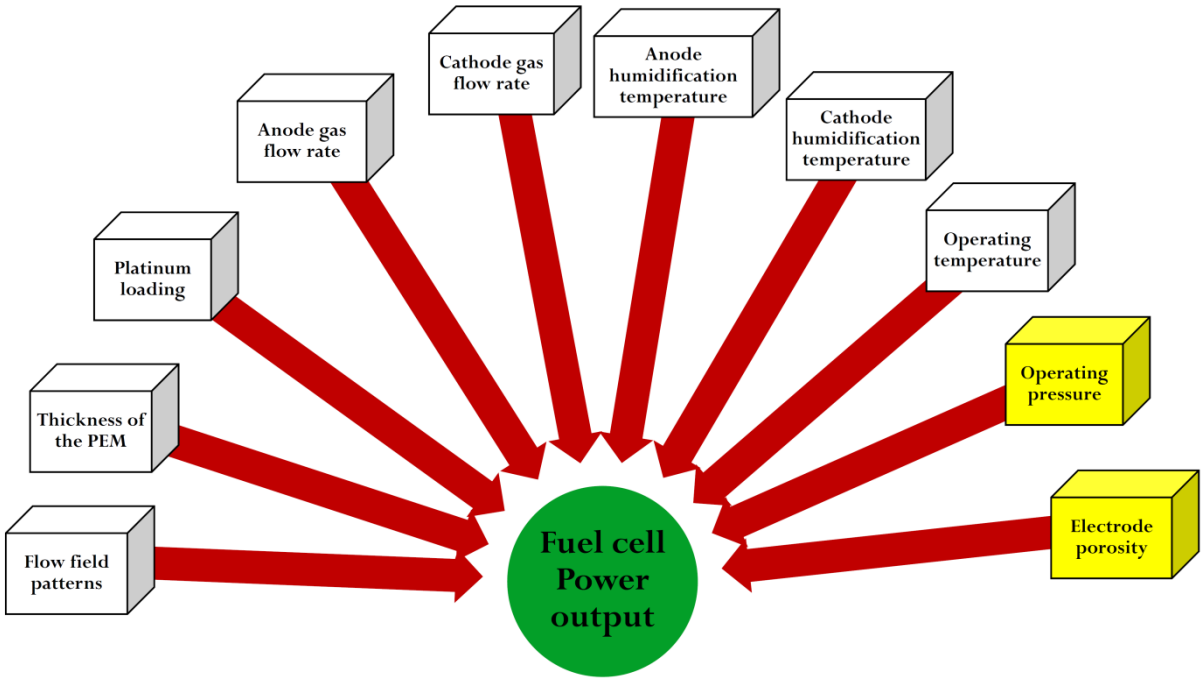

Figure 2.1 Factors affecting the fuel cell output

For safe and efficient operation of PEM fuel cells, the influence of operating parameters such cell temperature, gas humidification temperature, pressure, gas flow rate need to be study and optimize in addition to design parameters such as dimensions of flow channel, membrane, catalyst loading, and gas diffusion layers. It is well known that both membrane dehydration

and flooding can limit the performance of PEM fuel cells, and therefore it is very important to understand the water and thermal management of fuel cell and their effects on the cell's performance. Wang et al. [73] experimentally examined the influence of different cell operating temperatures, different cathode and anode humidification temperatures, different operating pressures on performance of 7.2x7.2 cm active area single PEM fuel cell. They concluded that the cell performance improves with the increase of cell operating temperature and pressure. The authors also concluded that anode humidification temperature has great impact on the FC performance at lower current densities and no effect at higher current densities. While the cathode humidification temperature impact is not significant on the FC performances, particularly at higher current densities.

Berning & Djilali [24] developed a 3-D single-phase model of a PEMFC and studied the influence of operating and cell material parameters on the fuel cell performance. The study found that both cell operating temperature and pressure has positive influence on cell performance. Kazim et al. [47] investigated the influence of cathode operating conditions viz cathode electrode porosity, inlet oxygen mole fraction, cell temperature and pressure on the performance of PEMFCs using an interdigitated flow field. The results demonstrate that increase in the porosity of the gas diffusion layer as well as mole fraction, temperature or pressure of the oxygen increase the overall performance of the FC.

Kumar & Reddy [23] developed a computational 3-D half-cell PEMFC model for predicting the effect of different channels dimensions and shapes in the flow-field plate. Their studies on effect of channel dimensions showed that high fuel consumptions (≈80%) were obtained with optimum channel width, land width and channel depth were close to values of 1.5, 0.5 and 1.5 mm, respectively. The investigations on the influence of channel shapes revealed that triangular and hemispherical shaped cross-sections increase in the hydrogen consumption by around 9%. Wang & Liu [74] conducted both experimental and numerical studies on a interdigitated flow field PEM fuel cell (50 cm^2) to investigate the influence of different cell temperatures, humidification temperatures, backpressures and mass flow rates on cell performance. The authors concluded that the increase in cell temperature showed positive influence on cell performance when sufficient humidification is provided and negative influence when sufficient humidification is not provided. The authors also concluded that with the increase in the anode and cathode humidification temperature, operation pressure and reactant flow rate, the cell performance improves.

Hsieh et al. [75] experimentally examined the effect of different operating temperature and backpressure on a micro PEMFC performance with three different flow field configurations (interdigitated, mesh, and serpentine) and reported that increase in the temperature and backpressure caused increase in the cell performance. Yan et al. [76] conducted experimental studies on 198.1 cm^2 active area PEM fuel cell with different flow field designs to investigate the influence of flow channel dimensions and operating parameters on FC performance. The authors observed decrease in the cell performance with increase in the cell temperature (from 50 to 70◦C). The authors also observed that increase in the cathode humidification and cathode gas flow rate increase the FC performance.

Amirinejad et al. [77] conducted experiments on a 5 cm^2 active area PEMFC by varying operating conditions to study their influence on cell performance. The results iindicated that temperatures, pressures, and reactants humidity could drop the mass transport limitations and increase the performance of the FC. Yu et al. [78] carried out parametric analysis for a 25 cm^2 PEMFC performance using design of experiments (DOE). The study revealed that the operating pressure, the operating temperature, and the interaction between these two parameters have a noteworthy influence on the FC performance. Yan et al. [79] conducted experiments with Core 5621 and Core 57 MEAs for a 256 cm^2 PEMFC to study the influence of operating temperature on FC performance. The authors found that the FC performance improvement with an increase in cell temperature when the FC temperature is less than the humidification temperature. On the otherhand when the cell temperature is higher than the humidification temperature, the FC performance decreased with increase in cell temperature.

Tohidi et al. [80] developed a 1-D, steady state and isothermal PEMFC model to investigate the influence of different parameters such as relative humidity, temperature, pressure, membrane thickness, and stoichiometric flow ratio of anode and cathode on FC performance. The authors reported that the cell performance improves with increase of the operating pressure, temperature, anode and cathode stoichiometric flow ratio. While the performance of the FC can decrease by decreasing the relative humidity of inlet gases and increasing the membrane thickness. Ting et al. [81] build up a PEMFC using Au-coated Ni-foam as the bipolar plate and studied the influence of operating parameters on the cell performance. Among the operating parameters, the effect on the cell performance, from most significant to least, is as follows: cell operating temperature, cathode humidification temperature, cathode-gas stoichiometric ratio.

Platinum (Pt) is a rare and costly metal, therefore reducing its loading without losing performance has always been a main goal. Both the electron transfer coefficient and exchange current density are platinum loading dependent. Zahari & Aziz [82] studied the performance of PEMFC at different catalyst loadings (0.3, 0.35,0.40, 045 and 0.50 mg/cm^2). The authors obtained best fuel cell performance at 0.50 mg/cm^2 platinum loading in both anode and cathode. Okafor & Mogbo [83] also studied the performance of 50 cm^2 PEMFC at 0.5 mg/cm^2 and 1.0 mg/cm^2 Pt loadings. The authors found that MEAs with 1 mg/cm^2 Pt loading offered lower ohmic resistance, activation resistance, and total cell resistance than MEAs with of 0.5mg/cm^2 Pt loading. Meng et al. [84] studied the effect cathode platinum loading (0.1, 0.2 and 0.4 mg/cm^2) and backpressure (100, 150 and 200 kPa) on PEMFC performance. The results revealed that increase of Pt loading decreased the transport losses under the equivalent backpressure. They also reported that increase in the backpressure enhanced the cell performance, and this improvement in performance is more noticeable at a low Pt loading. Gazdzicki et al. [85] examined the impact of the Pt loading on the performance and degradation of a 19 cells PEMFC rainbow stack and varied the platinum in the range of 0.05–0.20 mg/cm^2 on the anode and 0.15–0.40 mg/cm^2 on the cathode. The study concluded that the cell performance is independent of the anodic Pt loading for current densities up to 1.4 A cm^2 and the performance drops significantly for cathodic Pt-loadings < 0.2–0.25 mg/cm^2 and for current densities ≥ 1.0 A/cm^2.

Chen et al. [86] numerically examined the effects of various bend angle and width of the flow channel for a 25 cm^2 active area PEMFC performance. The authors reported that flow channel with the combination of 60 deg and 120 deg, attains the peak performance due to the highest mass diffusion rate, especially at low operating voltage regime. Takalloo et al. [87] numerically and experimentally examined the effect of inlet gas humidification and inlet gas flow rate on the performance of PEMFC. The study concluded that increase in inlet gas humidity improve the performance because of drop in ionic resistance of the membrane and increase in inlet gas flow rates to a particular level will increase the diffusion possibility for gaseous forms and helps to improve the cell performance. Ozen et al. [88] experimentally investigated the effects of operation conditions on the performance of a 25 cm^2 PEM fuel cell and presented the results along with a detailed literature review on the allied topics. The results indicated that the FC performance could be ameliorated with enhancing the relative humidity (RH) and temperature of the inlet gases and the cell operating temperature.

2.5 Research gaps identified from the literature review

- Full 3-D modeling taking into account Round Corner Serpentine Flow Fields (RCSFFs), electrochemical reactions, and charge flow (electrons and protons) in all regions of single PEM fuel cells, with a detailed comparison of the simulation results with experimentation has not been studied comprehensively.
- The experimental studies on the effect of active area and catalyst loading on the performance of PEMFCs are relatively less.
- Experimental studies on the effects of operating parameters such as reactant flow rates, cell and gas temperatures, and gas humidification temperatures on performance of the larger active area PEMFCs are very less.

2.6 Objectives of the present research work

The objectives of the present work are

- To develop 3-D CFD model of PEM fuel cell having active area 49 cm^2 (7cm x 7cm), 84 cm^2 (7cm x 12cm) and 119 (7cm x 17cm) cm^2.
- To investigate the effect of single serpentine (1-S), double serpentine (2-S) and triple serpentine (3-S) flow fields on fuel cell performance using Ansys Fluent.
- To investigate the cell performance experimentally by incorporating 1-S, 2-S and 3-S flow fields for three active area fuel cells and validate the simulation results with experimental results.
- To analyze experimentally the effect of membrane thickness, cell active area and catalyst loading on cell performance.
- To experimentally investigate the influence of operating parameters namely cell temperature, reactants humidification temperature and reactants flow rate on the performance of FCs.

CHAPTER 3

3. METHODOLOGY

3.1 Computational methodology

Computational evaluation of PEM fuel cell performance includes three major steps. The first step is modeling the geometry of the PEMFC by means of computer-aided design software. The geometrical model forms the basis for creating a computational mesh. The second step involves generating the mesh from the geometry. In order to solve the numerous of equations associated with a fuel cell simulation, the entire cell is split into a finite number of discrete volume elements or computational cells. The relevant equations are then solved in each individual cell and integrated over the computational domain to give a solution for the entire domain. Generating a good mesh is one of the challenging steps. It needs a careful balance of generating adequate computational cells to capture the geometry without exceeding the available memory of the meshing computer. Many other factors must also be considered in order to create a computational mesh which delivers archetypal results when simulated.

The third and final step involves inputting the various physical and operating parameters of the simulation. Some of these include thermal and electrical properties of the various materials, operating temperatures and pressures, inlet gas flow rates, open circuit voltage, porosity, and humidification among many others. The flow chart of the computational methodology can be seen in Figure 3.1.

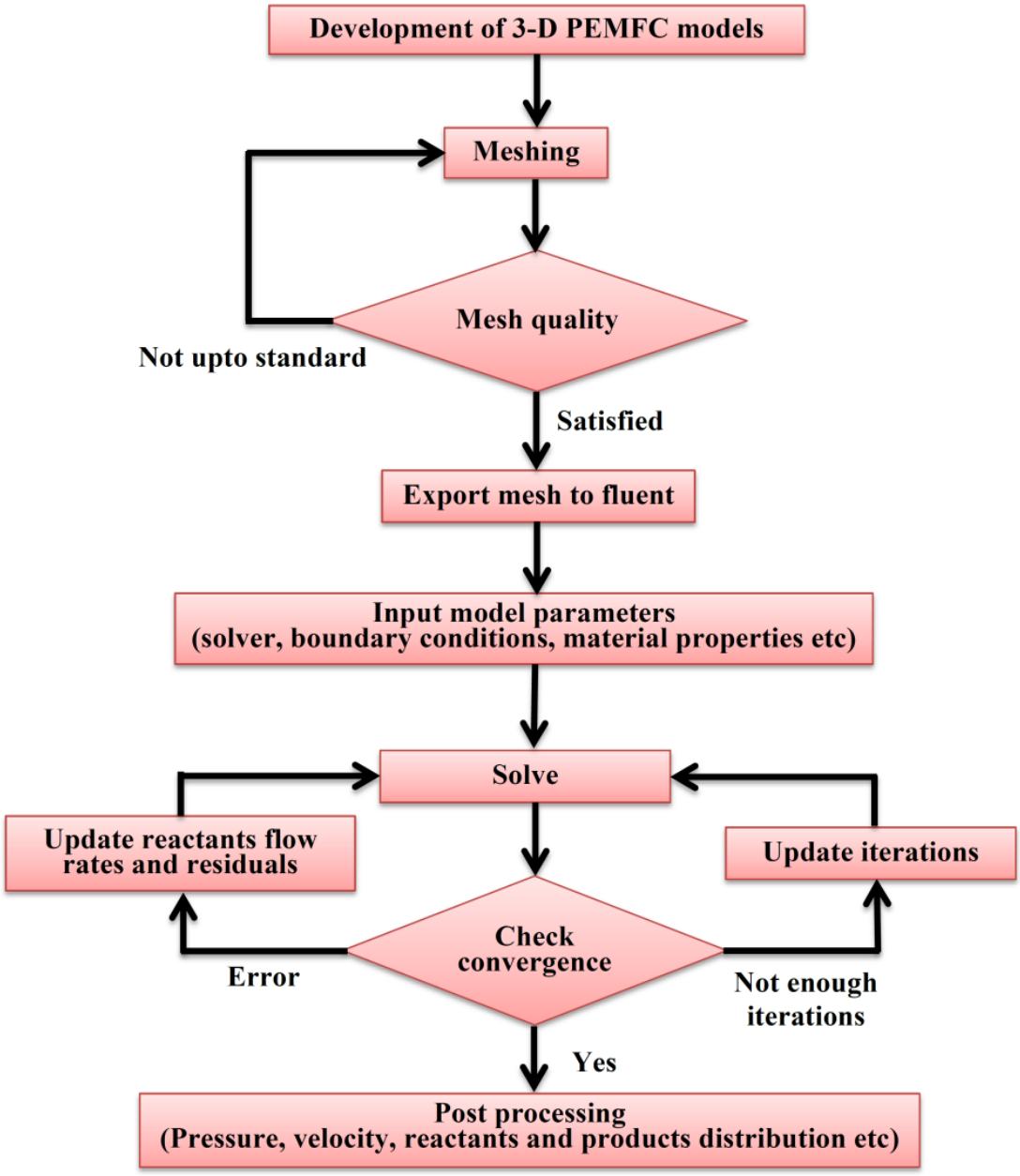

Figure 3.1 Flow chart of computational methodology

3.1.1 Modeling assumptions

The developed models were assumed as 3-D, steady and isothermal. The reactants at inlet to the channel assumed as perfect gases, the flow is laminar, incompressible and the porous layers assumed as isotropic and the thermo-physical properties assumed as constant [89].

3.1.2 Governing equations

Fundamental conservation equations such as conservation of mass, momentum and charge were used to develop a mathematical model for PEMFC. Conservation of energy equation

was not considered as the model was assumed as isothermal. The PEMFC was examined in four parts: flow channels, GDLs, CLs and the membrane.

Flow channel

Continuity equation for mass transport in a flow channel is

$$\rho(u.\nabla)u + \nabla p - \nabla.\eta(\nabla u + (\nabla u)^T) = 0 \qquad \textbf{(3.1)}$$

$$\nabla.(\rho u) = 0 \qquad \textbf{(3.2)}$$

Maxwell-Stefan relation describes the mass transport of the species

$$\nabla.\left[-\rho w_i \sum_j \left(D_{ij}\nabla x_j + \left(x_j - w_j\right)\frac{\nabla p}{p}\right) + \rho w_i u\right] = 0 \qquad \textbf{(3.3)}$$

Gas diffusion layer

The phenomena taking place in the GDL may be explained by Darcy's law. Continuity equation with generation term

$$\rho(u.\nabla)u + \nabla p - \nabla.\eta(\nabla u + (\nabla u)^T) = -\frac{\eta}{k_p}u \qquad \textbf{(3.4)}$$

A charge balance must be performed in the GDL

$$\nabla.\left(k_s^{eff}\nabla\emptyset_s\right) = 0 \qquad \textbf{(3.5)}$$

Catalyst layer

A simplified Butler-Volmer equation is adapted to calculate local current density at the anode and cathode.

$$i_a = i_a^{ex}\left(\left(\frac{C_{H_2}}{C_{H_2}^{ref}}\right)^{0.5}\left[\frac{\alpha_a+\alpha_c}{RT}F\eta_a\right]\right) = 0 \qquad \textbf{(3.6)}$$

$$i_c = i_c^{ex}\left(\left(\frac{C_{O_2}}{C_{O_2}^{ref}}\right)^{0.5}\left[exp\left(-\frac{\alpha_c F\eta_c}{RT}\right)\right]\right) = 0 \qquad \textbf{(3.7)}$$

Electrolyte

Charge balance of the electrolyte by neglecting crossover of gases

$$\nabla.(k_e\nabla\emptyset_e) = 0 \qquad \textbf{(3.8)}$$

Net water flux through the membrane

$$N_w = n_d M_{H_2O}\frac{i}{F} - \nabla.(\rho D_w \nabla c_w) \qquad \textbf{(3.9)}$$

The water diffusivity in the membrane

$$D_w = 1.3 * 10^{-10} exp\left[2416\left(\frac{1}{303} - \frac{1}{T}\right)\right] \qquad \textbf{(3.10)}$$

Water content inside the membrane is related to water vapor activity which affects the membrane protonic conductivity[90].

$$\lambda = 0.043 + 17.18a - 39.85a^2 + 36a^2 \qquad if\, a < 1 \qquad \textbf{(3.11)}$$

$$\lambda = 14 + 14(a-1) \quad if\ a > 1 \qquad \textbf{(3.12)}$$

$$a = \frac{a_a + a_c}{2} \qquad \textbf{(3.13)}$$

$$a_a = \frac{C_{H_2O,a}^{MEM} RT}{P_{sat}} \qquad \textbf{(3.14)}$$

$$a_c = \frac{C_{H_2O,c}^{MEM} RT}{P_{sat}} \qquad \textbf{(3.15)}$$

3.1.3 Development PEM fuel cell models

The first step in the development of FC model is modeling of individual parts of the three active area PEMFCs such as current collector, gas diffusion layer, catalyst layer (for anode and cathode) and a membrane (PEM) in SOLIDWORKS 2010. These parts have been assembled to get the complete fuel cell assembly. The geometric dimensions of these components have been given in Table 3.1. The exploded view of the PEMFC with proposed serpentine flow fields is shown in Figure. 3.2.

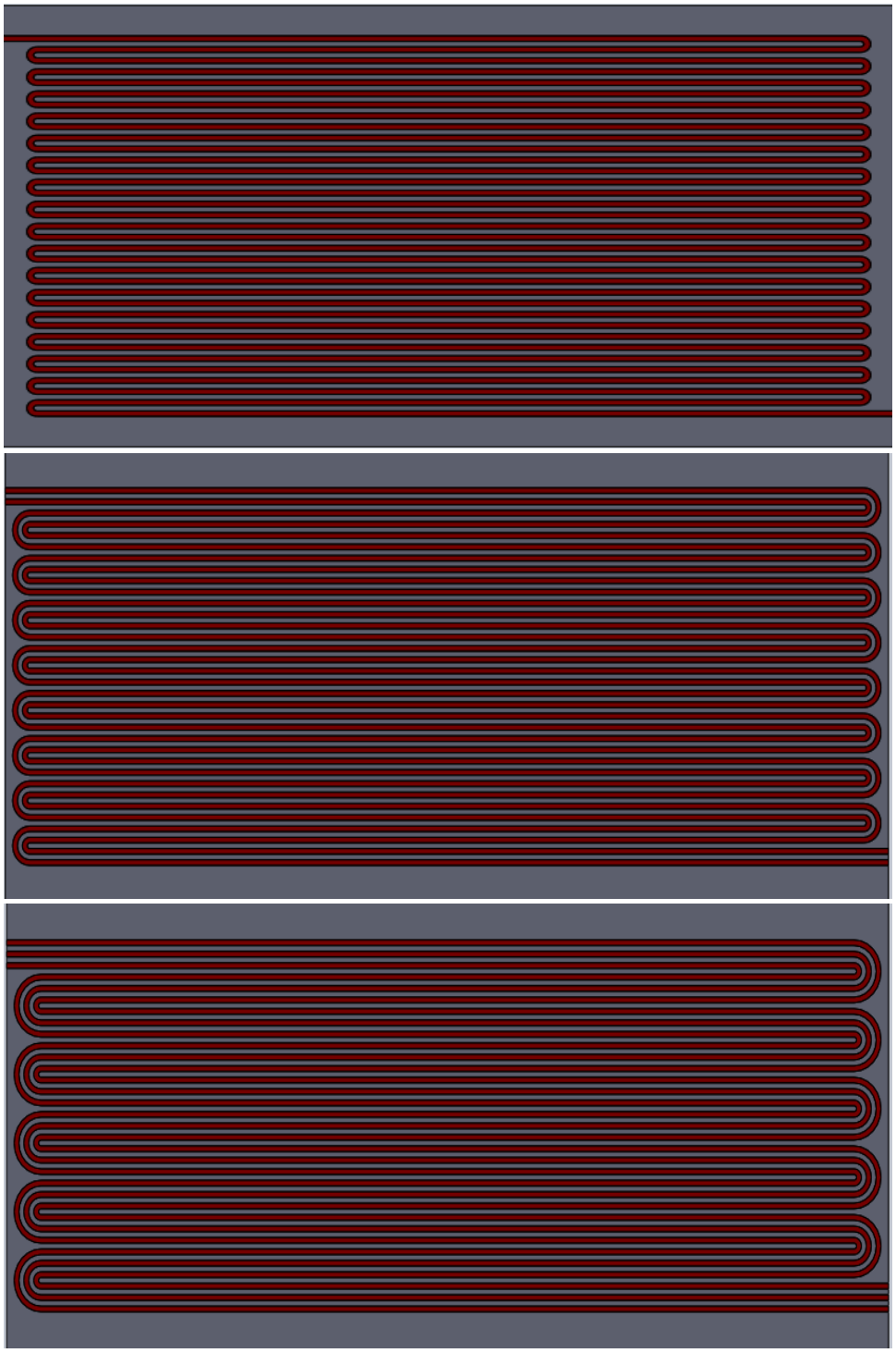

Figure 3.2 7 cm x 17 cm size single (top), double (middle) and triple (bottom) serpentine flow field designs

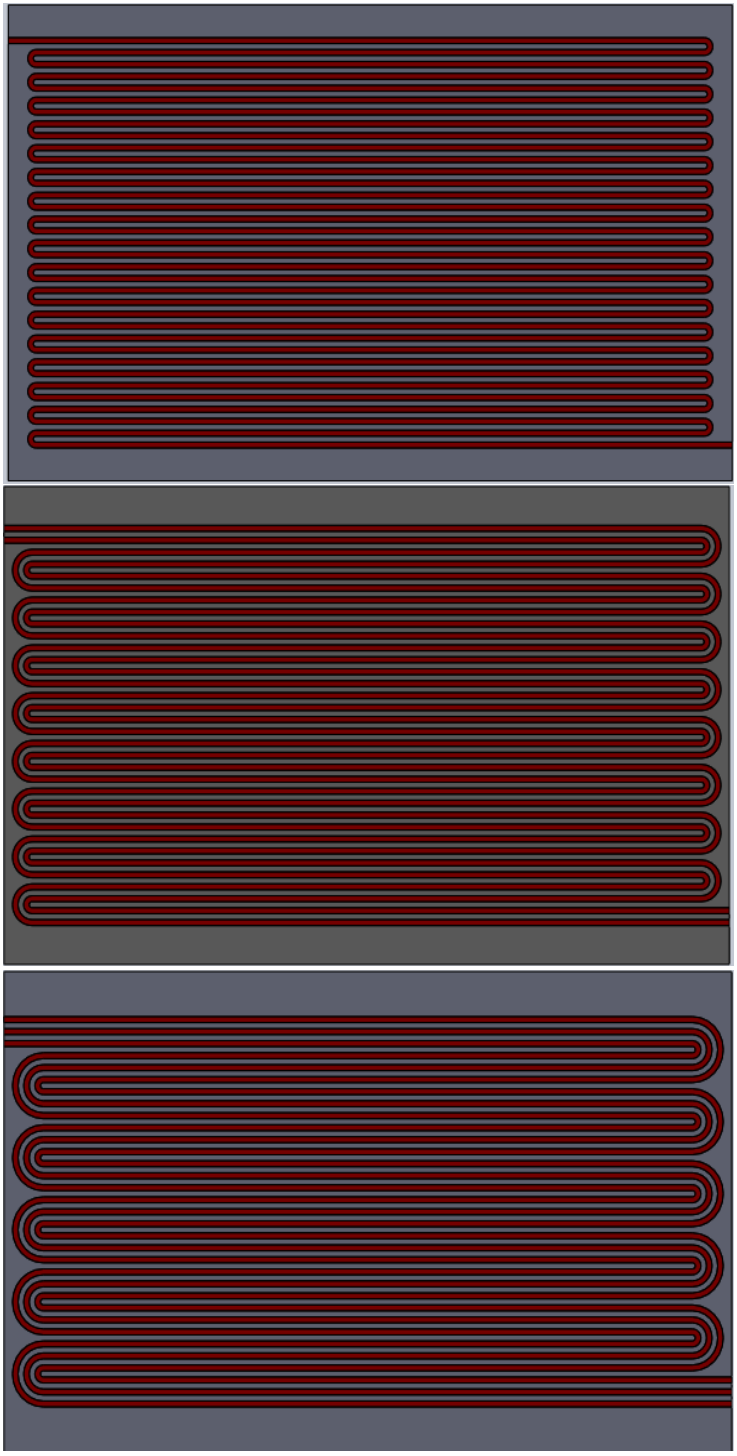

Figure 3.3 7 cm x 12 cm size single (top), double (middle) and triple (bottom) serpentine flow field designs

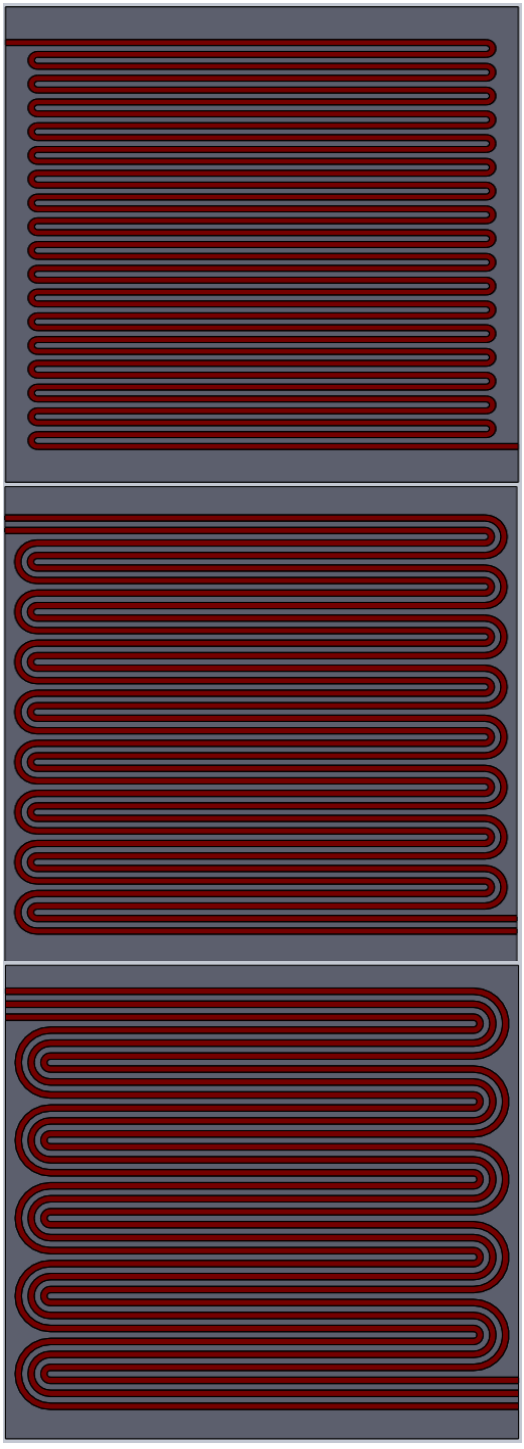

Figure 3.4 7 cm x 7cm size single (top), double (middle) and triple (bottom) serpentine flow field designs

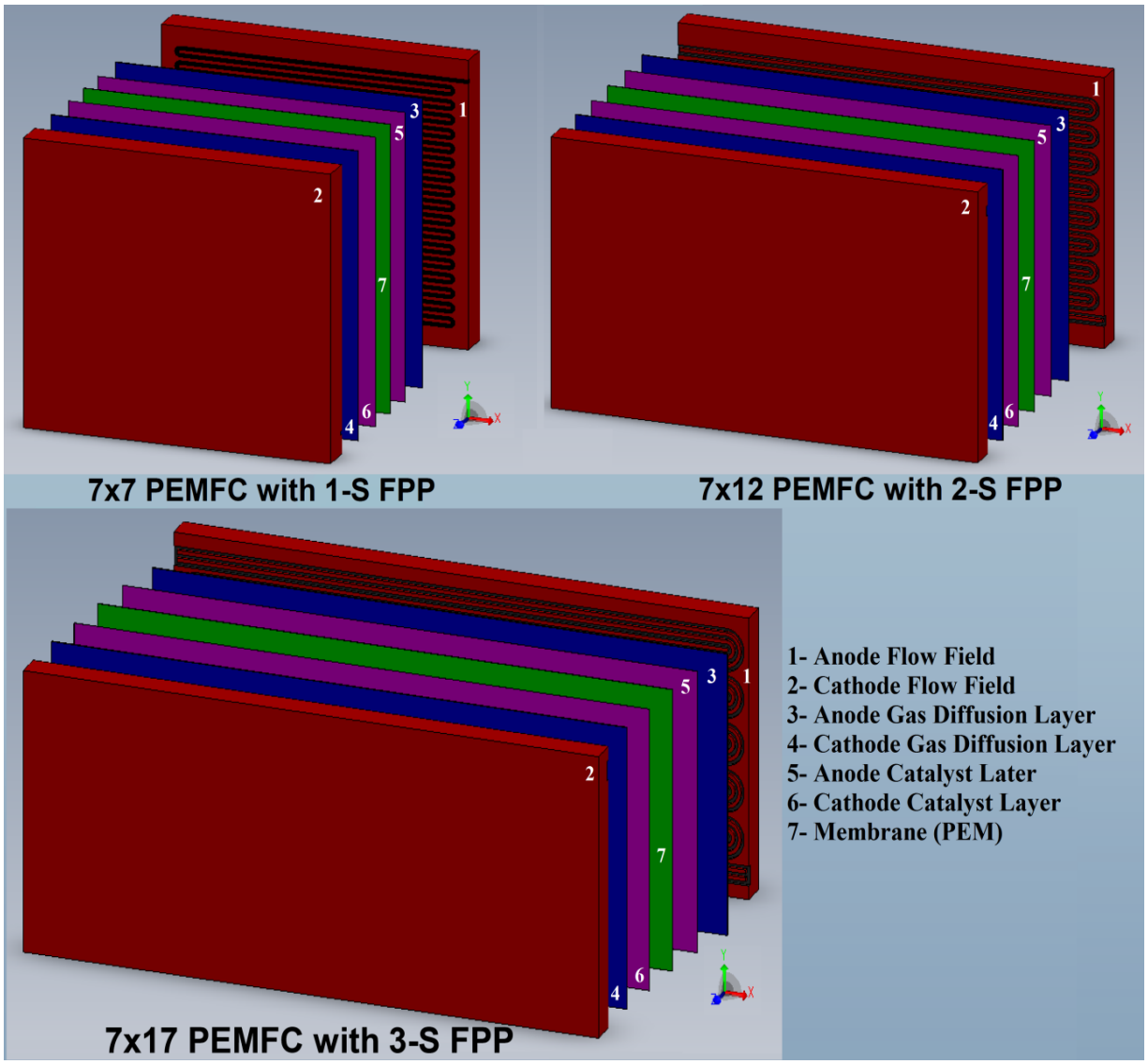

Figure 3.5 Exploded view of three active area PEMFCs with serpentine flow fields

Table 3.1 Geometric dimensions of three PEM fuel cells

Cell	Part	Length (cm)	Width (cm)	Height (cm)
PEMFC 1 (7x7 cm^2)	Gas diffusion layers (GDL)	7	7	**0.025[91]**
	Catalyst Layer (CL)	7	7	**0.005[91]**
	Membrane	7	7	**0.00175[92]**
	Channels	7	0.1	**0.1[93]**
	Rib	7	0.1	**0.1[92]**
PEMFC 2 (7x12 cm^2)	Gas diffusion layers (GDL)	12	7	**0.025[91]**
	Catalyst Layer (CL)	12	7	**0.005[91]**
	Membrane	12	7	**0.00175[92]**
	Channels	12	0.1	**0.1[93]**
	Rib	12	0.1	**0.1[92]**
PEMFC 3 (7x17 cm^2)	Gas diffusion layers (GDL)	17	7	**0.025[91]**
	Catalyst Layer (CL)	17	7	**0.005[91]**
	Membrane	17	7	**0.00175[92]**
	Channels	17	0.1	**0.1[93]**
	Rib	17	0.1	**0.1[92]**

Table 3.2 Naming conventions for boundary surfaces

Surface function		Named surface
Anode flow channel	Inlet	mass_flow_inlet_a
	Outlet	pressure_outlet_a
Cathode flow channel	Inlet	mass_flow_inlet_c
	Outlet	pressure_outlet_c
Anode side electrical contact		terminal_a
Cathode side electrical contact		terminal_c

The second step is generating high quality mesh using ANSYS WORKBENCH MESH. The computational domain is divided into a number of elements as shown in Figure. 3.6. Named selections are required to define the boundary conditions of the mesh and naming conventions used are specified in Table 3.2. Refinement of mesh greatly influences the solution. So, the grid independency test is carried out with three different mesh sizes

namely coarse, medium and fine. The current generated in the MEA is simulated with three different mesh sizes, is shown in Figure 3.7 and noticed very nominal variation of 0.3% in the results. Therefore, mesh with medium size is considered for all the simulations to save computational time and space. Now this mesh can be exported to solver.

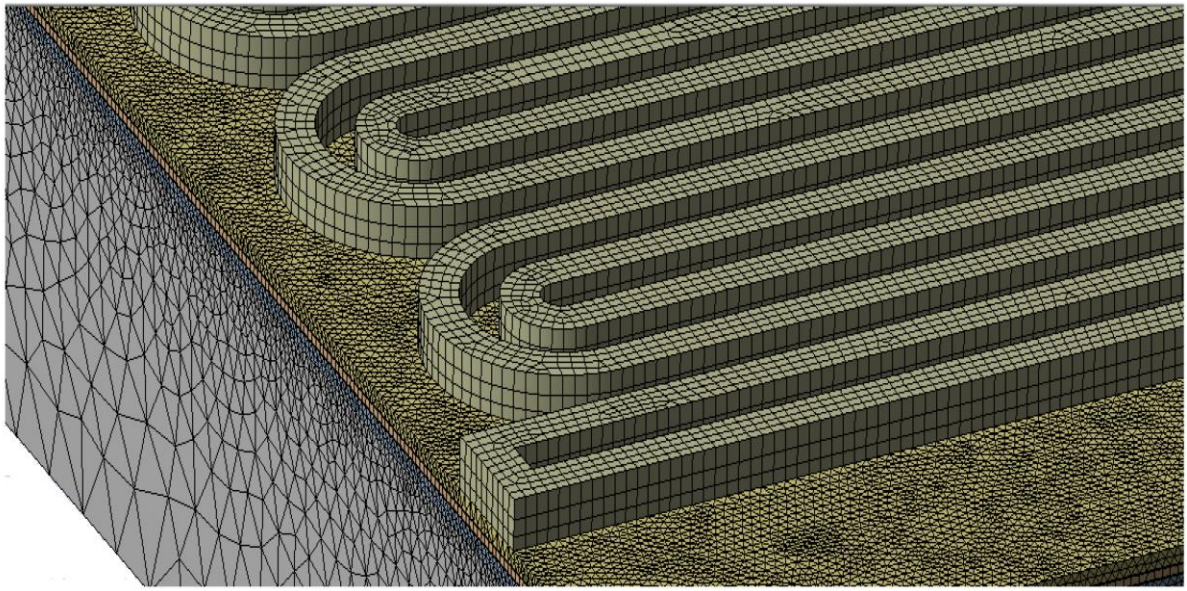

Figure 3.6 Computational mesh of 2-S PEMFC

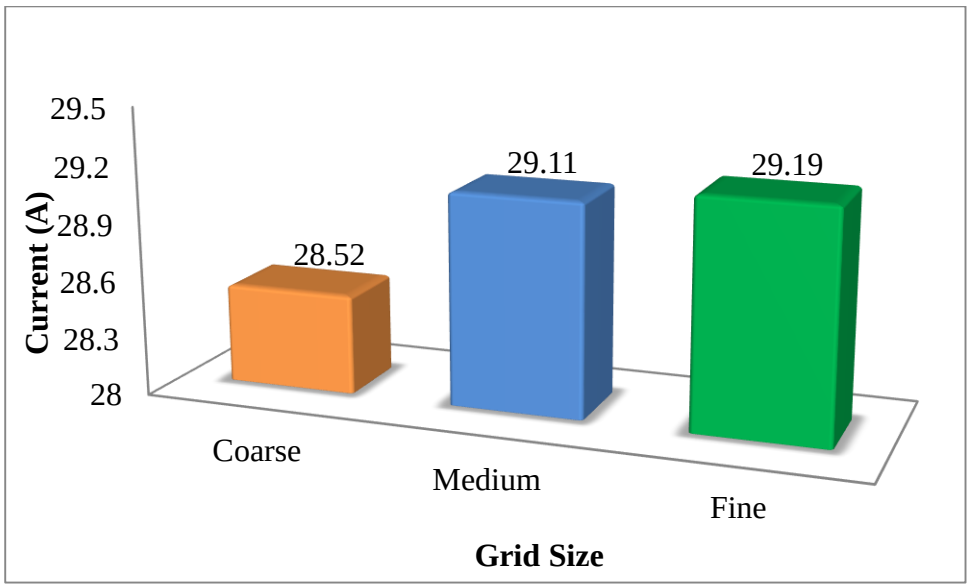

Figure 3.7 Grid test

The third step is to define the boundary conditions with thermo-physical and operating parameters of PEMFC for solving the reaction kinetics. Some of these include gas flow rates, operating pressures and temperatures, heat flux rates, resistances and load. These parameters are not fixed and these will be changed with the requirements of the simulation and the

materials used. The type of models which can be incorporated in the simulation include joule hating, reaction heating, electrochemistry sources, Butler-Volmer rate, membrane water transport, multiphase, multi-component diffusion and anisotropic e-conductivity in porous electrode. A detailed computational procedure is given below.

3.1.4 Computational procedure

The simulation setup is initiated by loading fuel cell module. This is accomplished by typing the following command into the Text User Interface (TUI) and pressing the Enter key.**/define/models/addon-module 3.** Once the module is loaded, it is important to test the mesh with the default settings first. The basic parameters have to be set first. To set operating parameters (Table 3.6) and material properties (Table 3.7), open the Fuel Cells & Electrolysis – PEMFC module as shown in Figure 3.7.

Table 3.3 Operating parameters used in simulation

Specifications		**Value**
Mass fraction ($H_2/O_2/H_2O$) on anode		0.6/0/0.4
Mass fraction ($H_2/O_2/H_2O$) on cathode		0/0.96/0.04
Operating pressure (Pa)		101325
Operating temperature (K)		323
Mass flow rate on anode side (cm^3/min)	PEMFC 1	196
	PEMFC 2	336
	PEMFC 3	476
Mass flow rate on cathode side (cm^3/min)	PEMFC 1	588
	PEMFC 2	1008
	PEMFC 3	1428

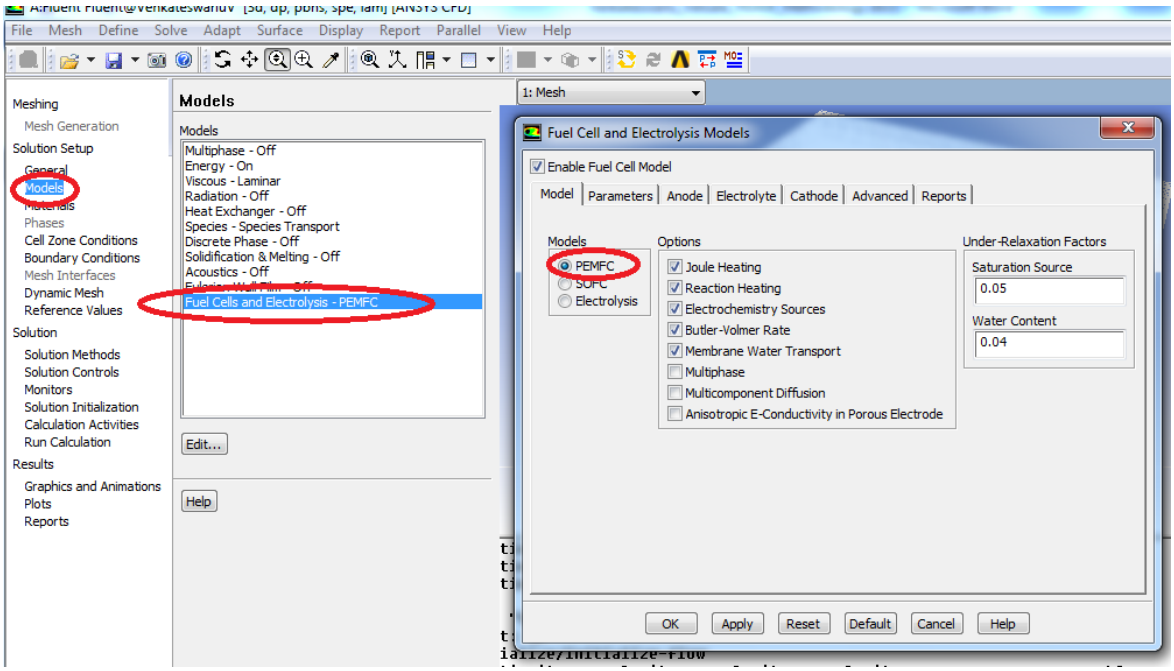

Figure 3.8. Opening the fuel cell module and setting the fuel cell zones

Table 3.4 Key properties used in the simulation

Parameter	Value
Reference concentration at anode	**1 kmol/m^3**
Reference concentration at cathode	**1 kmol/m^3**
Reference current density at anode	**10000 A/m^2**
Reference current density at cathode	**20 A/m^2**
Membrane equivalent weight (g/mol)	**1100**
Porosity of anode GDL	**0.5**
Porosity of cathode GDL	**0.5**
Porosity of anode CL	**0.5**
Porosity of cathode CL	**0.5**

Under the **parameters** tab, key properties given in Table 3.4 are applied. Then, under the **anode** tab, current collector, GDL and CL are assigned for the anode. Similarly, current collector, GDL and CL are for cathode, under **cathode** tab. Under the **electrolyte** tab, electrolyte (membrane) is assigned for the cell. Finally, under the **reports** tab, anode and cathode terminals are assigned. Under the same tab, electrolyte projected area in m^2 (the cell active area) also given. All the steps explained are given in the Figures 3.8 - 3.12.

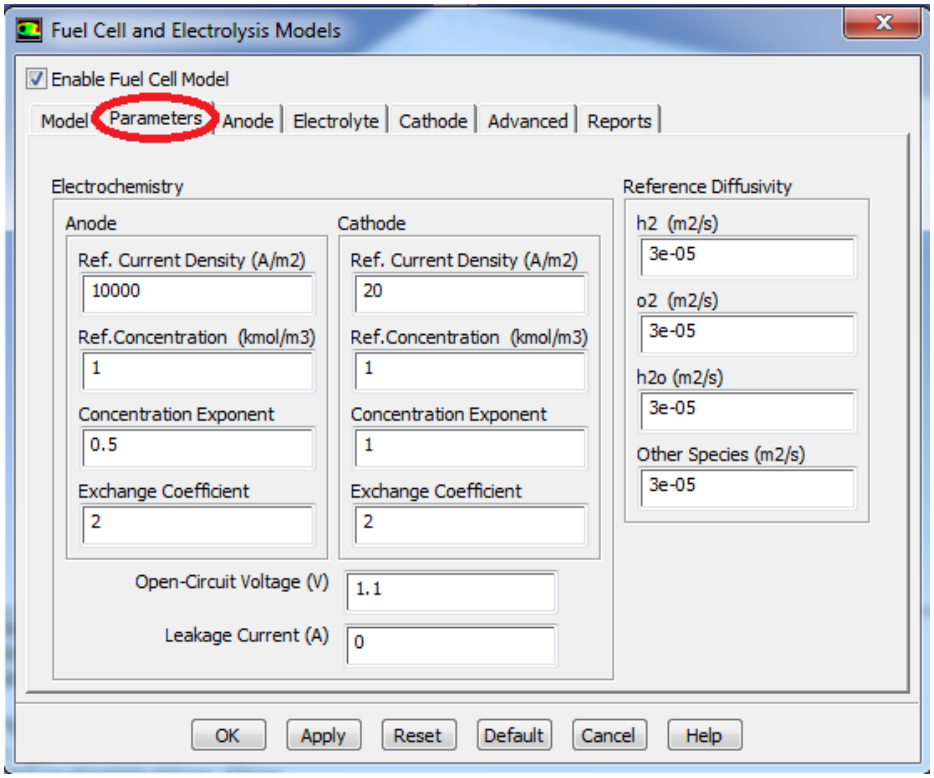

Figure 3.9 setting of model parameters

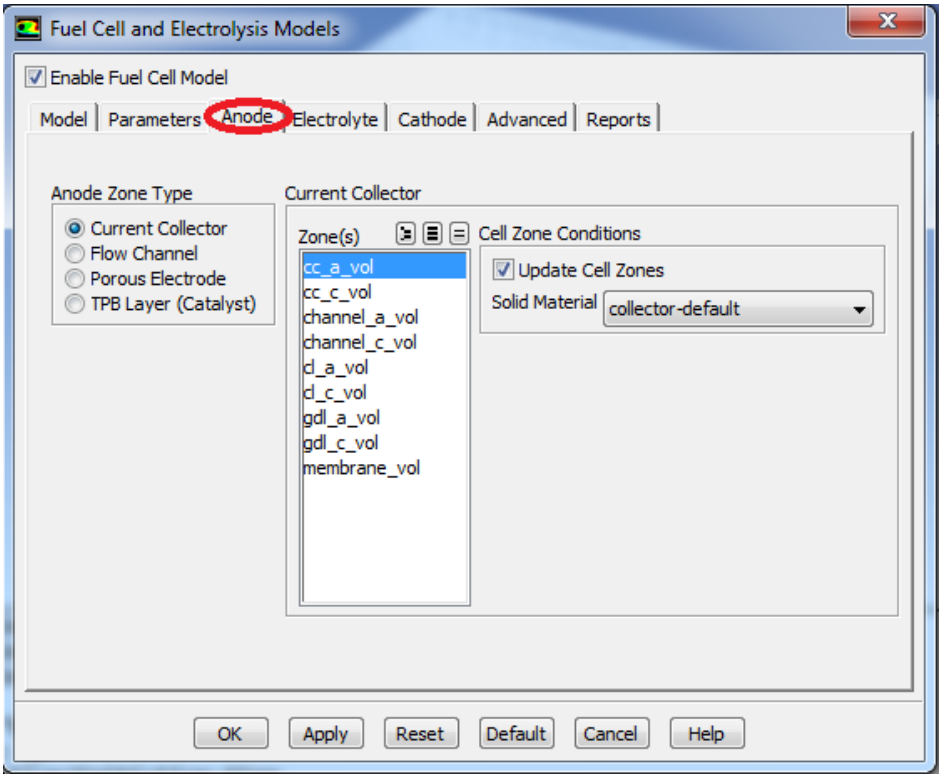

Figure 3.10 setting of anode electrode parameters

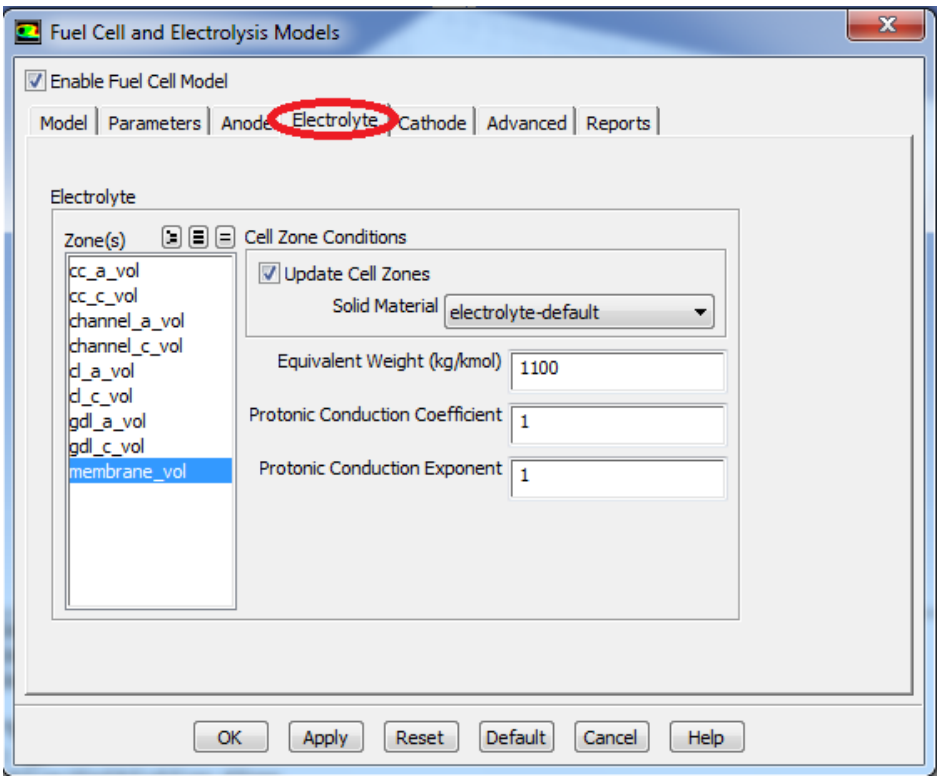

Figure 3.11 setting of membrane parameters

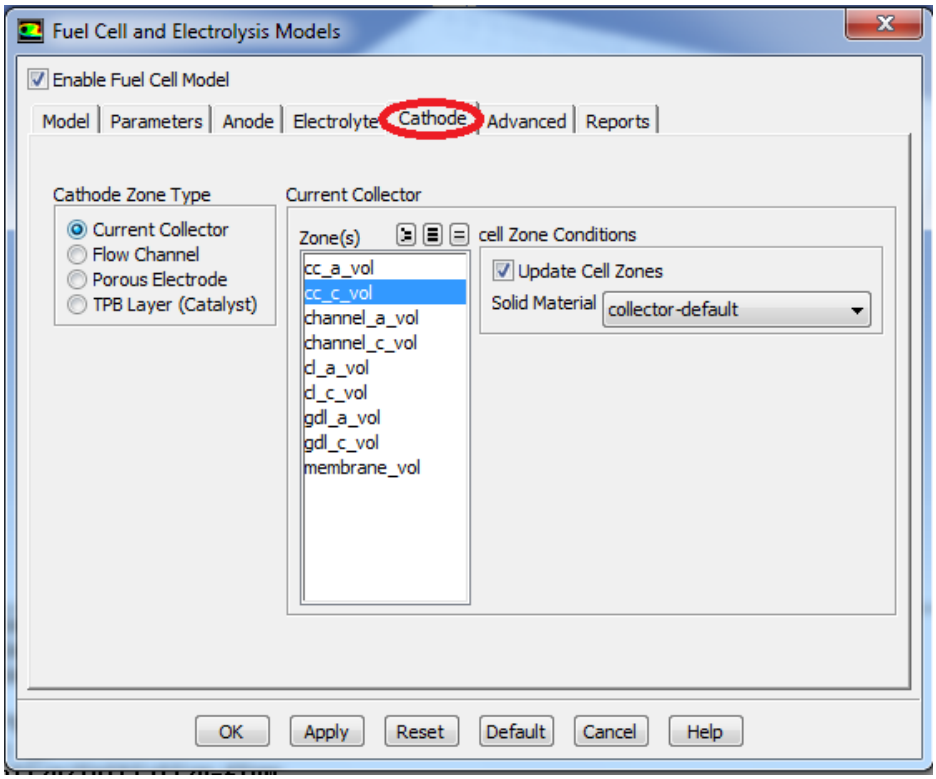

Figure 3.12 setting of cathode electrode parameters

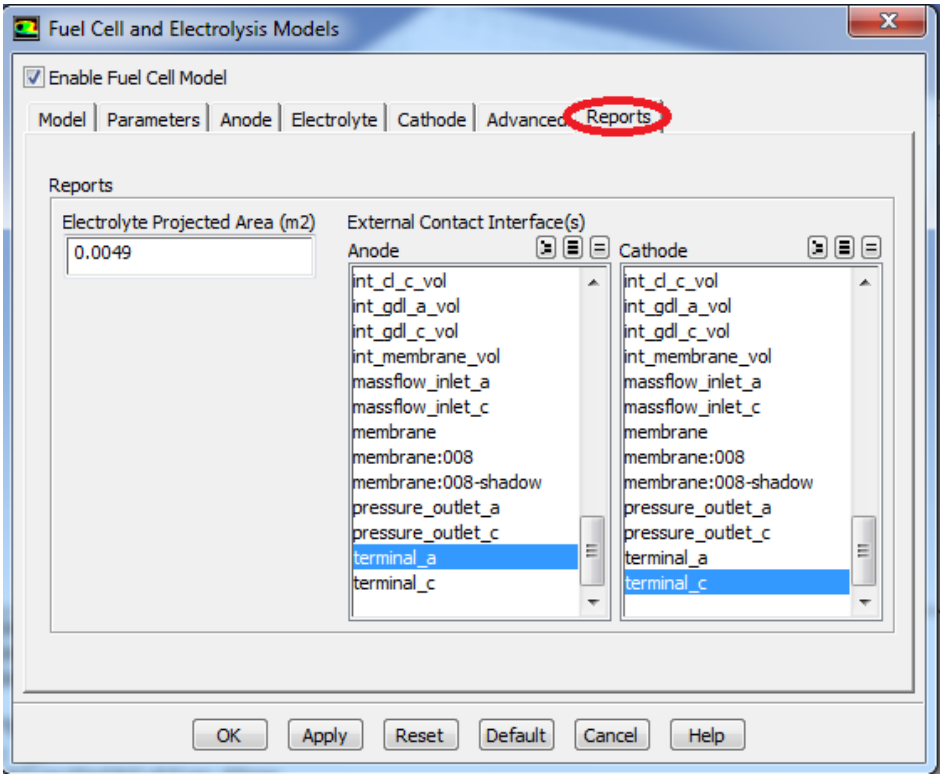

Figure 3.13 assigning of anode and cathode terminals

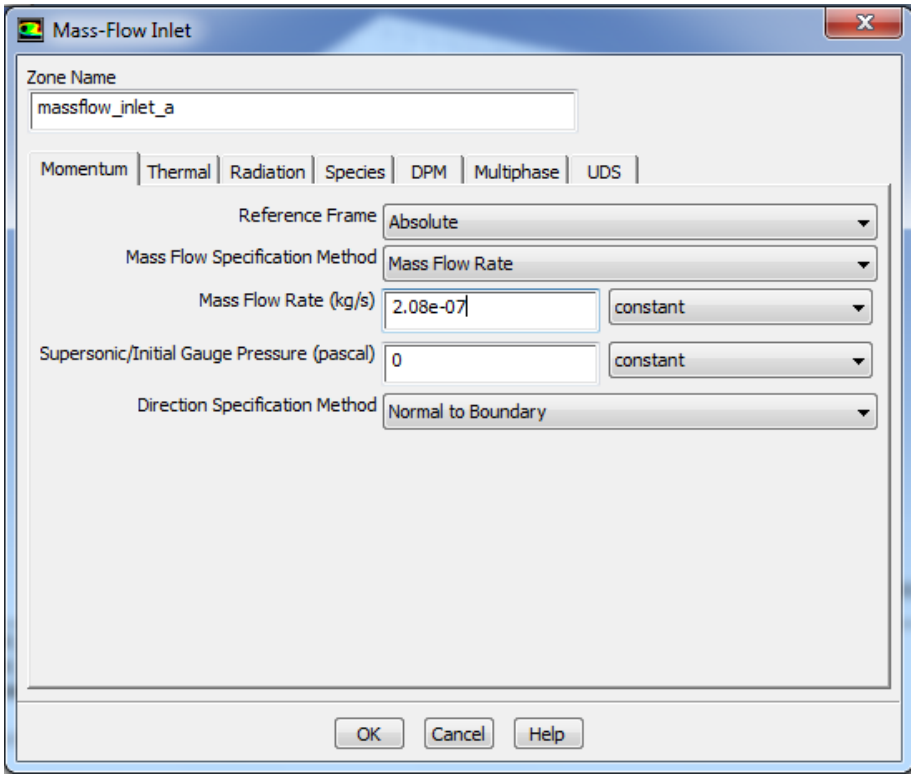

Figure 3.14 setting of anode mass flow inlet

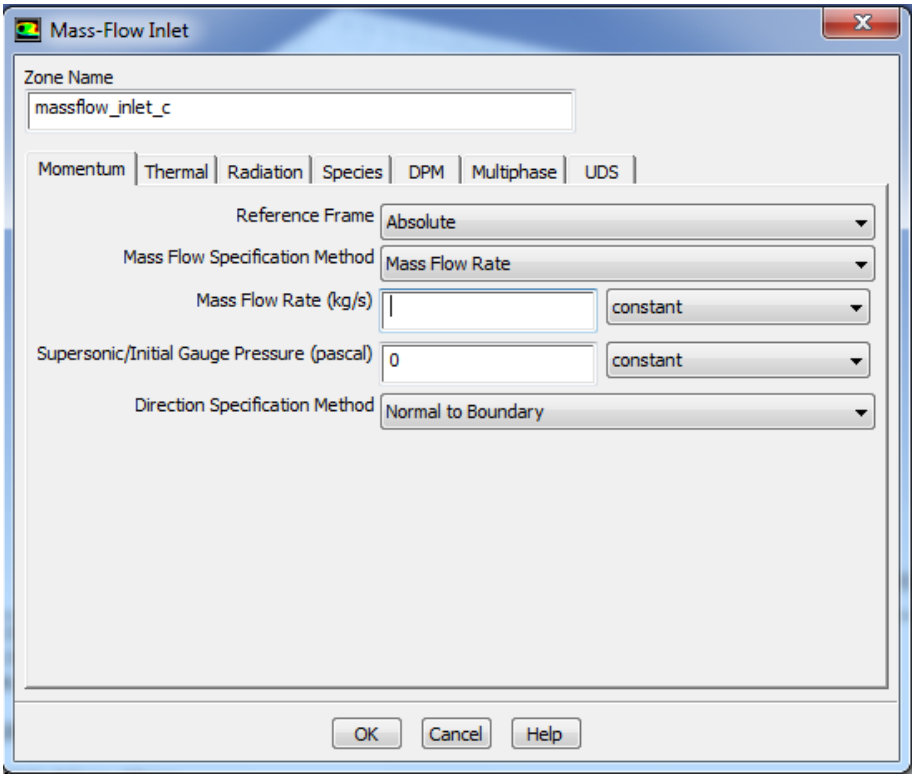

Figure 3.15 setting of cathode mass flow inlet

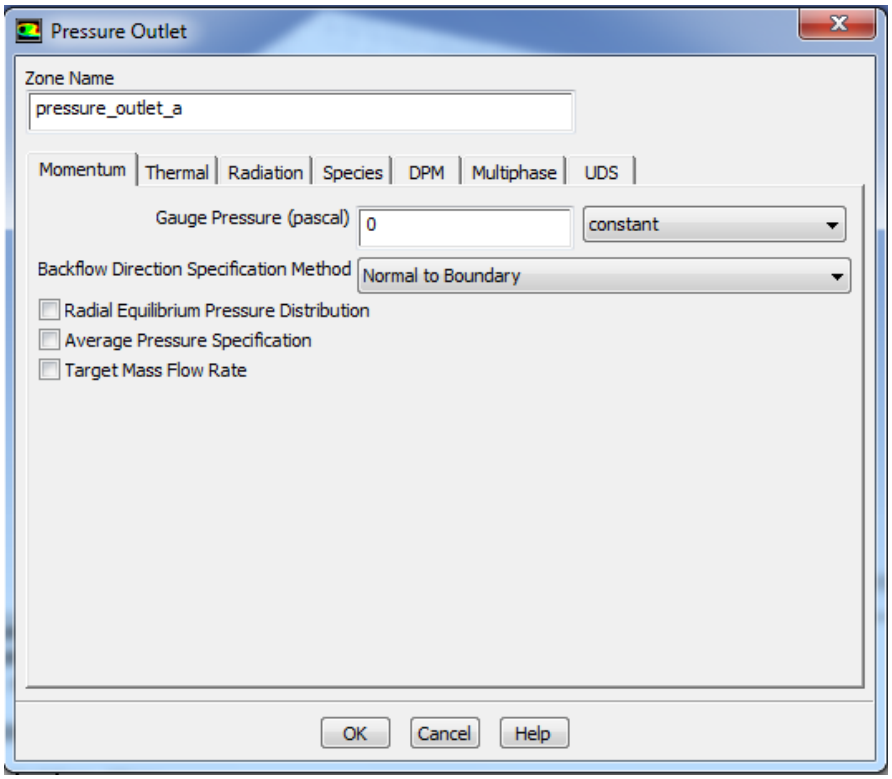

Figure 3.16 setting of anode outlet

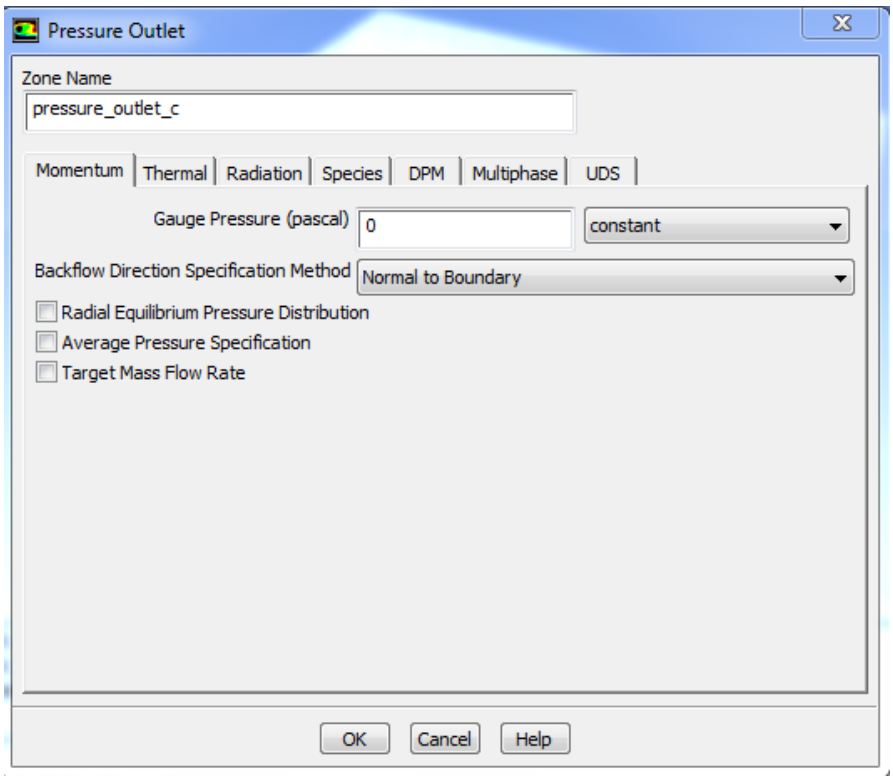

Figure 3.17 setting of cathode outlet

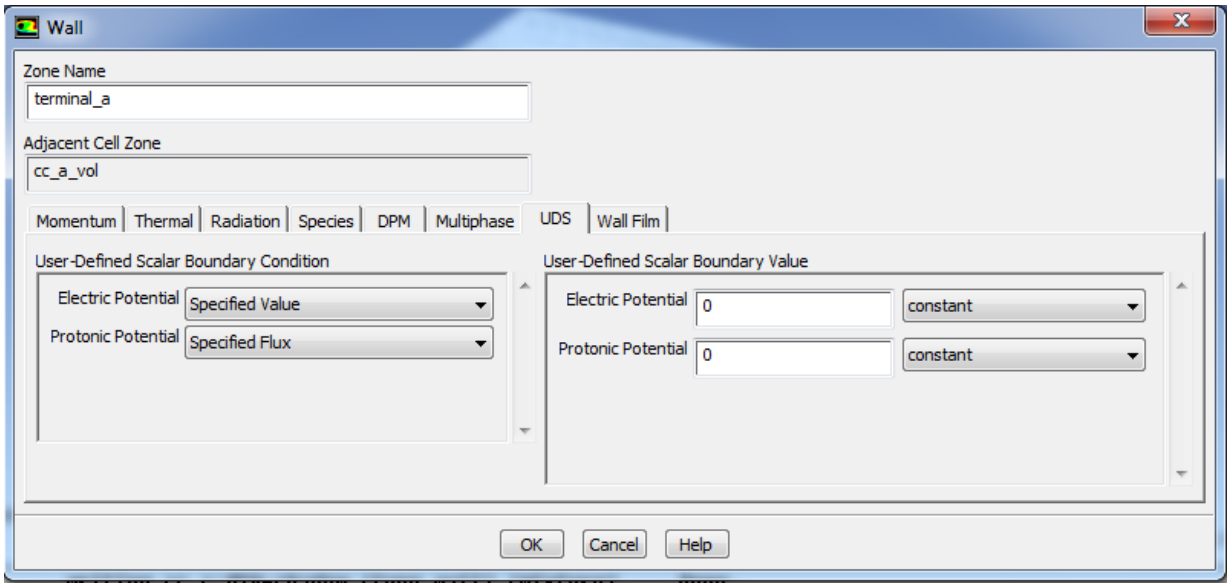

Figure 3.18 setting of anode terminal voltage

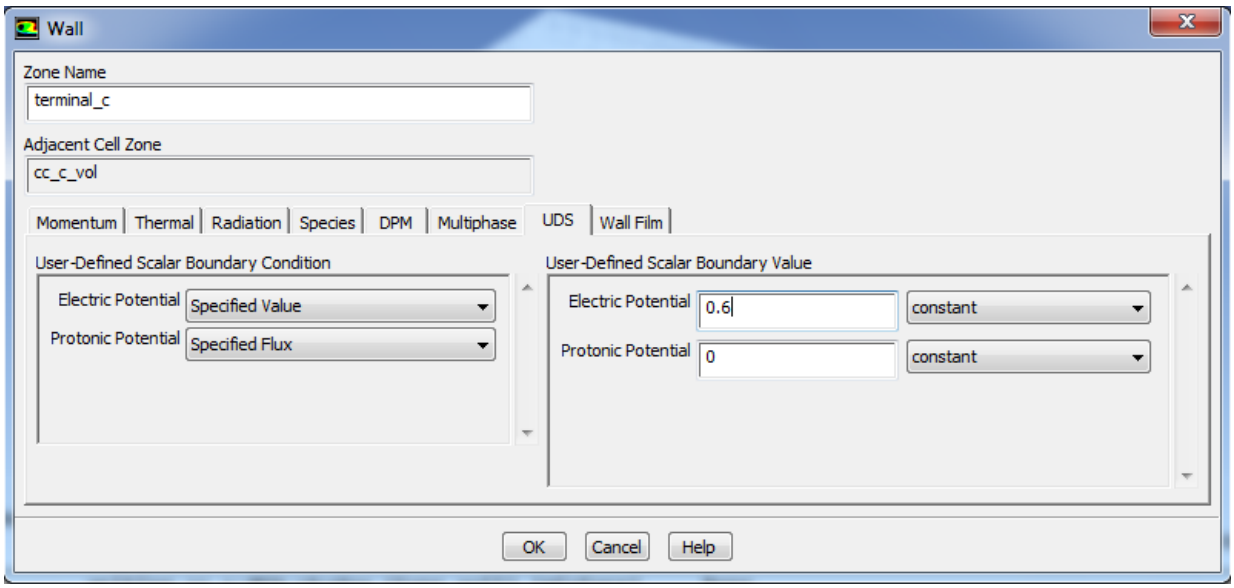

Figure 3.19 setting of cathode terminal voltage

Under-relaxation factors are also used to control the solution and here in this work under-relaxation factor adopted as 0.3 for momentum, 0.7 for pressure and 0.95 for H_2, O_2, H_2O and water saturation. There are 6 boundary conditions that must be set. These are the inlets for the anode and cathode flow channels, outlets for the anode and cathode flow channels, and the anode and cathode terminals. To set inlet mass flow rate on anode and cathode (see Figures 3.13 and 3.14), under the **momentum** tab, fixed the inlet mass flow rate of hydrogen according to the current to be drawn. Similarly, on cathode side also oxygen flow rate is fixed. Under the **thermal** tab, the temperature is set as 323K. This is a typical operating temperature of the fuel cell. Under the **species** tab, the species concentration on the anode side of H_2, O_2, and H_2O are set as 0.8, 0, and 0.2, respectively. While, on the cathode side H_2, O_2, and H_2O are set as 0, 0.2 and 0.1, respectively. These values correspond to a 100% humidified inlet gas. Next, pressure outlet of anode and cathode are set as shown in Figures 3.15 and 3.16. Finally anode electric potential (anode terminal voltage) is set as 0 V (Zero) and cathode electric potential (cathode terminal voltage) is varied from 0.1 to 0.9 V as shown in Figures 3.17 and 3.18. The iteration criterion for convergence has been set at 10^{-6} to ensure the accuracy of simulation results. The simulations have been carried out in an Intel Xeon HP workstation with 32 GB RAM and 2.40 GHz CPU, running on Windows 7 Operating System.

3.2 Parameters to be investigated in the simulation study

3.2.1 Pressure drop

Pressure drop takes place in the flow channel because of friction and bending losses. This is one of the key parameter that must be taken into account while designing the flow channel for fuel cell. This pressure drop helps in deciding the type of blowers or compressors to be used

to maintain sufficient pressure in the channel. This pressure drop also affects the electrochemistry of the FC. The product water produced at the cathode channel should be evacuated from the FC and this needs a high pressure drop. Sometimes too high pressure drops create an extreme parasitic power requirement for the driving of gases into the FC, hence, the effective design of the flow channel is important to ensure a balance in pressure drop requirements at the FC cathode section.

3.2.2 Reactants distribution in flow field plates

Flow field plates (FFPs) distribute the reactants in the FC. If these FFPs fail to distribute the reactant gasses to the reaction active surface via GDL then mass transfer losses takes place in the FC subsequently reduces the FC output. The flow distribution influences the performance of the FC significantly. A uniform distribution of the reactants on the GDL with reasonable pressure drop along the flow channel is important for both effective utilization of reactants and PEMFC performance. Additionally, proper water and thermal management inside the FC are necessary for achieving maximum power output from the FC.

3.2.3 Currents flux density distribution

The uniformity of the current density over the entire active area in operational PEMFC is vital for optimizing the cell performance. Non-uniform current distribution, in conjunction with non-uniform water production in the cathode, has adverse effect on the durability, and reliability of PEMFCs. It is well documented that the overall PEMFC performance is strongly affected by sophisticated interaction of the assembly method, component design, operating conditions as well as the properties and microstructure of fuel cell components. The design and assembly processes include: flow field geometry, reactant flow arrangement, and clamping pressure. The operating conditions include: reactant pressure, cell temperature, relative humidity, and reactant flow rate. However, it has been observed by many studies that the most crucial implication of this complex interaction is an uneven electrochemical reaction rate, which takes place on the surface of the membrane electrode assembly (MEA) active area. As a result, this may lead to low/poor reactions and electro-catalyst utilization, which reduces the overall performance, and accelerates cell aging. For example, reactant reduction along the flow channel causes current variation from the inlet to the exit of the channel, and degrades the FC performance.

3.2.4 Membrane water content

The polymer electrolyte membrane is one of the important components in a PEMFC. An ideal membrane to use in PEMFCs must have a good proton conductivity, low electron

conductivity, low fuel permeability, good chemical and thermal stabilities, and good mechanical properties. A good water balance on the anode and cathode is one of the key issues in FC water management, which is mainly related to the water content in the membrane. If the membrane is not adequately hydrated then ion transport will not take place effectively from anode to cathode, which adversely affects the FC performance. However, if the membrane is hydrated excessively, this will deluge the reaction sites, that will influence the transport of reactant gases. The water content of the membrane should be maintained in certain ranges (λ=14). So in order to avoid dry-out and flooding of the membrane, the water content inside the membrane should be distributed uniformly and which will improve the proton conductivity of the membrane.

3.2.5 Liquid water activity

The low-pressure drop corresponds to generally low gas velocities, which contribute to poor water management properties of this flow field design. Any water build up that occurs in the channels will not be effectively forced to the outlet. Water build up has two immediate negative consequences. First, the liquid water will occupy reaction sites in the catalyst layer which will decrease the reaction rate. Second, the water buildup in the channels can block the flow of the reactant gases which causes large inactive zones to form. When a channel is completely flooded, a limiting current density is reached. This may lead not only to an extremely low efficiency, but also causes the failure of the cell due to high-pressure drops and oxygen starvation. If water removal from the cell could be improved, higher current densities could be reached leading to FCs with higher power using the same materials. This would make FCs cheaper, lighter and smaller. Moreover, operating conditions leading to irreversible degradation of the cell must be avoided thus improves the FC durability. In PEMFCs, the water generates on the cathode side due to oxygen reduction reaction (ORR). Sometimes water molecules may transfer from anode side to cathode side. Some amount of water is necessary to keep the membrane hydrated and excess water must be removed to avoid flooding. Both flooding and dehydration cause drop in cell performance.

3.3 Experimental methodology

Three PEMFCs with an active area of 49 cm^2, 84 cm^2 and 119 cm^2 used in the present study. All PEMFC components with the customized specifications are fabricated with the help of Vinpro Technologies, Hyderabad.

3.3.1 Materials

The main components of PEMFC include flow field plates (single, double and triple serpentine), end plates, copper current collector plates, and gaskets. At the anode and cathode sides of each cell, the flow field and current collector plates are insulated from the end plates by thick rubber sheets. Each flow field plate for the anode/cathode has one inlet and one outlet. The cell assembly is subjected to uniform compression controlled by torque wrench.

Membrane Electrode Assembly (MEAs)

Three types of membrane-electrode assembly (MEAs) are used and mainly contain Nafion membranes namely Nafion™ 112, Nafion™ 117 and Nafion™ 212 with an approximate thickness of 53, 175 and 50 μm respectively. Each membrane is supported by catalysts with a platinum loading of 0.6, 0.8 and 1.0 mg/cm^2 on cathode side and platinum loading is fixed as 0.4 mg/cm^2 on anode side which is illustrated in Figure 3.19. The carbon paper act as gas diffusion layer which has a thickness of 230 μm and is coated with 30% PTFE by weight.

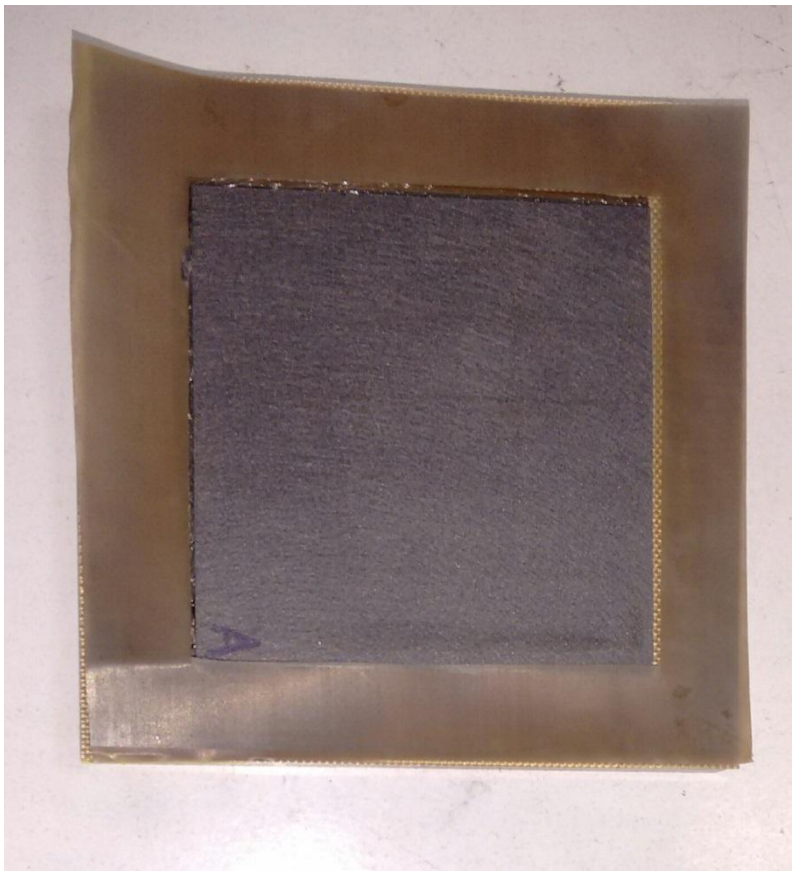

Figure 3.20 Membrane electrode assembly (MEA)

Flow Field Plate

Figure 3.20 shows three types of serpentine (1-S, 2-S and 3-S) flow field plates (FFPs) used in this study and these FFPs are made of graphite. The graphite material is selected due to its desirable properties even though it is brittle. The dimensions of these FFPs are given Table. 3.1

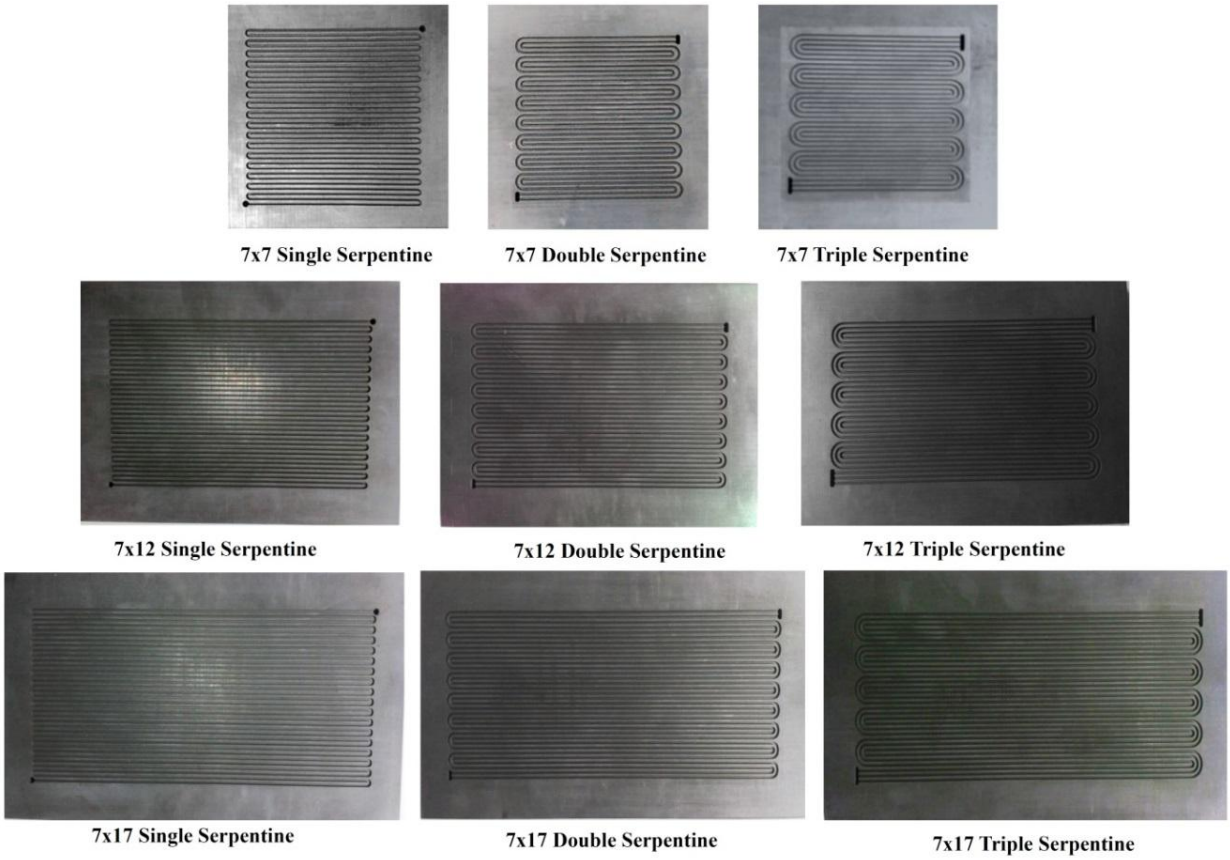

Figure 3.21 Flow fields used in experiments

Endplates

Figure 3.21 shows the end plates made of aluminum are used in this study. Holes are provided to end plates, which are identical to those in flow field plates and current collector plates. The thickness of the plate should be sufficient to accommodate the shear stress at the bolts without deflection because excess deflection of the end plates can result in poor sealing of the PEMFC.

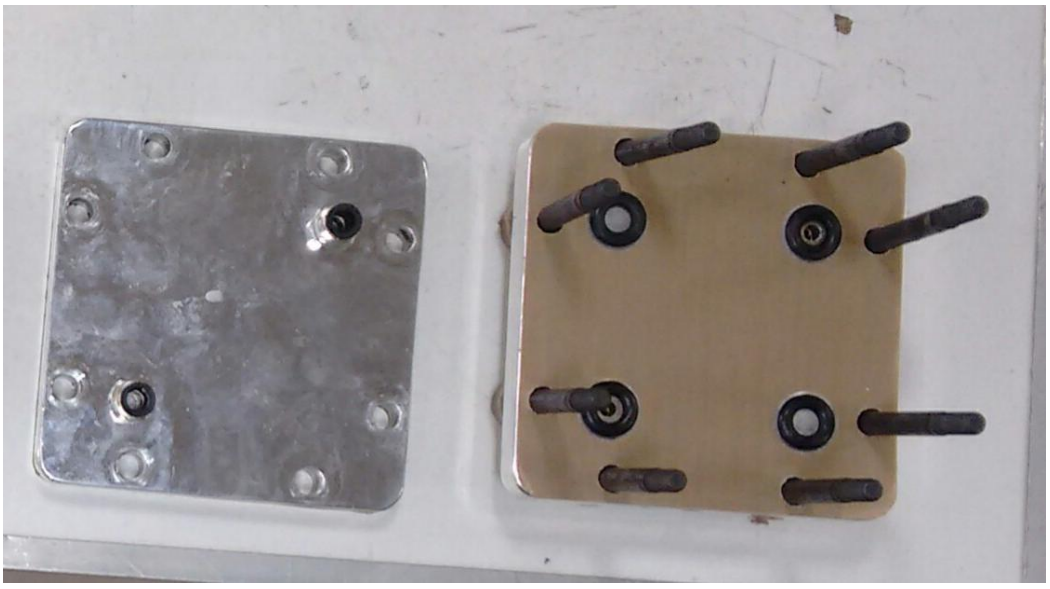

Figure 3.22 End plates of the FC

The desired physical properties of common materials which can be used for the end plate are as follows: low density, excellent electrochemical stability, high electrical insulation, easy to machine, high mechanical strength and stiffness. Therefore, Aluminum alloy 6061 is used to meet the functional requirements of the endplates, high strength (125 MPa tensile strength), high thermal conductivity (180 W/m.K), and it is relatively cheap when compared to other aluminum alloys. The most commonly used materials are aluminum, titanium, and stainless steel alloys.

Current Collector

One of the copper electrical/current collector plates used in this study is shown in Figure 3.22. The plates are designed in house and fabricated in the Engineering Machine Shop. It is made from C15720 copper, which contains 99.6 wt% (weight) copper. The copper provides both excellent electrical and thermal conductivities with 89 S/m and 353 W/m.K at 20 ^{o}C, respectively. The current collector is fastened to the endplate via thick sheet of rubber. The rubber gasket is applied between these two plates to insulate the plates electrically while providing proper sealing for the inlet and outlet flow reactants.

Figure 3.23 current collectors

Rings of silicon were used to seal the reactant flow between the current collector and the flow field plate. Two holes are drilled on opposite corners for the reactant supply, and four small holes were drilled for locating dowel pins.

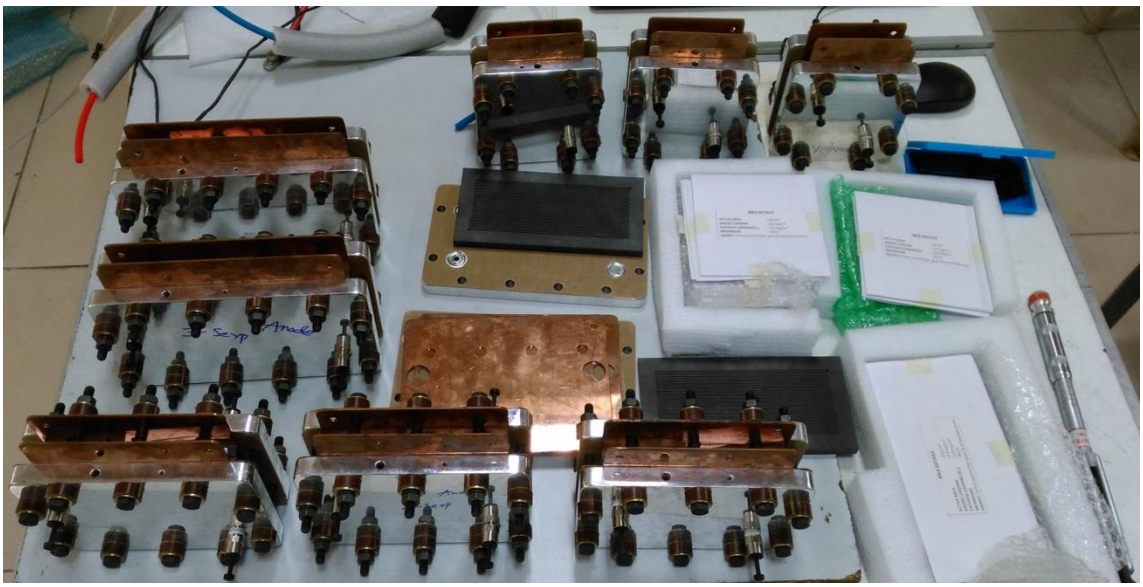

Figure 3.24 PEMFC hardware used in the present work

3.3.2 PEM fuel cell test station

The experimental investigations are carried out on single PEM fuel cell with the help of programmable SMART2 Fuel Cell Test Station (make:WonATech Co Ltd, Korea) which is available in the Centre of Excellence (CoE) at the Department of Mechanical Engineering, NIT Warangal. The fuel cell test station has the provision to vary the reactants mass flow rate, FC temperature, humidification temperature and back pressure on both the anode and cathode sides. Back-pressures are controlled using backpressure regulators. This test station is equipped with data acquisition system and computer-based control. The mass flow rates, cell temperature, humidification temperatures are set at desired value and read through the software called WFTS™. The FC polarization curves are obtained from this system in conjunction with the Electric Load on the cell, which measures the voltage against the current response. The schematic and photograph of the SMART2 Fuel Cell Test Station is shown Figures 3.23 and 3.24.

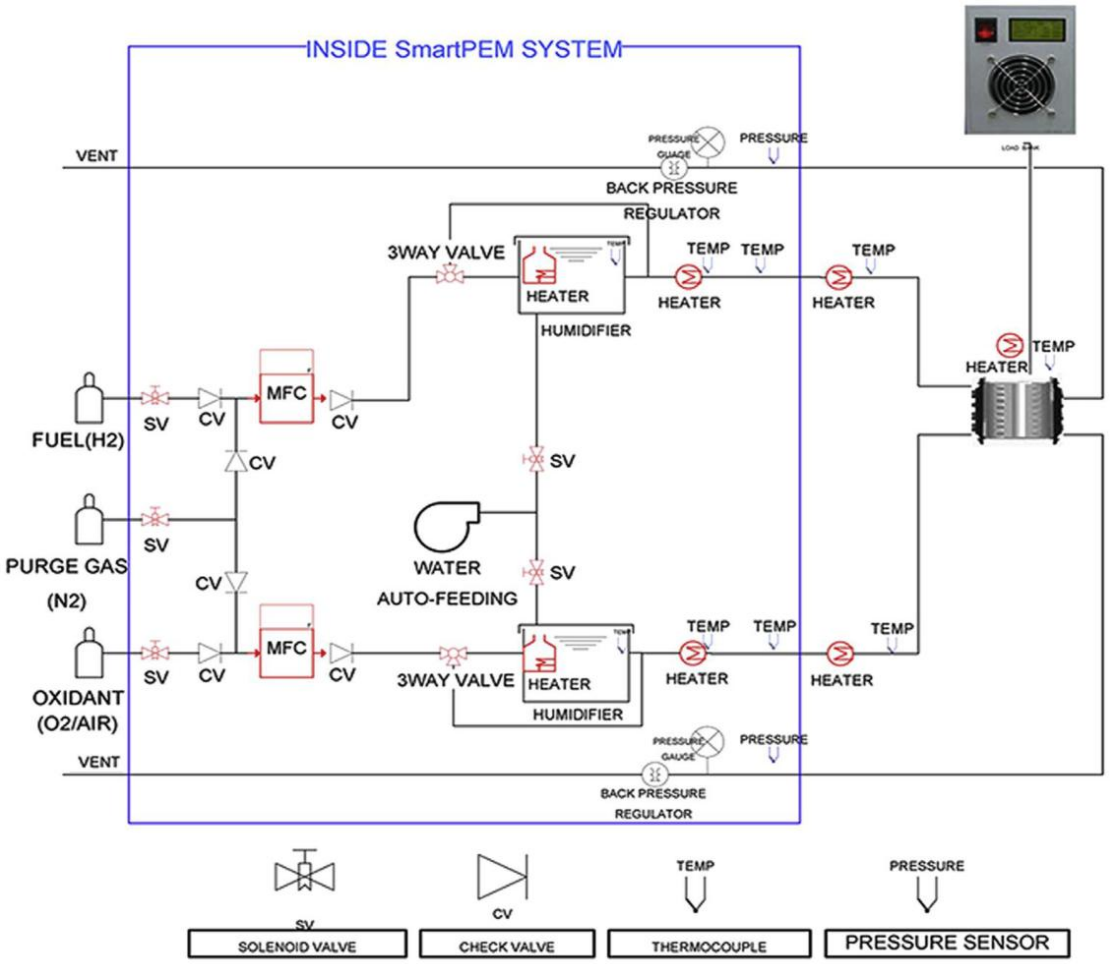

Figure 3.25 schematic of PEMFC test station

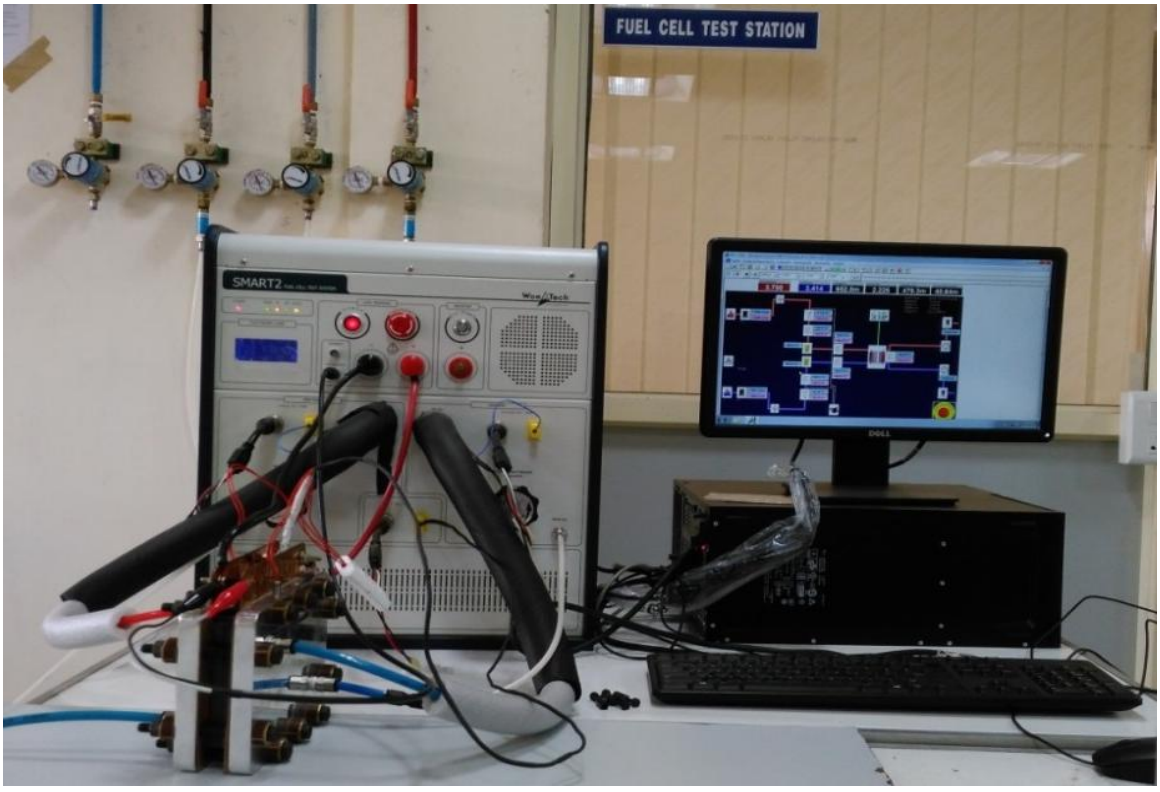

Figure 3.26 SMART2 PEM fuel cell test station

3.3.3 Activation of MEAs

Prior to conduct the experiments on the cell, the MEAs of fuel cell need to be activated. Activation of MEAs is carried out at cell temperature of 70^{o}C. Hydrogen and oxygen humidification temperatures also set at 70°C. During the activation, the fuel cell performance is recorded for every 30 minues. When no further increase in performance is observed, it indicates that, the MEA is activated.

3.3.4 Experimental procedure

The procedure for the experimentation on the fuel cell is given below:

- Connect the reactants inlet and outlets of the PEM fuel cell to the Test Station.
- Connect the electrode terminals of the fuel cell test station to the current collectors of the fuel cell
- Check the availability of distilled water for the humidification processes in the test station.
- Switch-on the Fuel Cell Test Station and WFTS^{TM} software interfaced computer.
- Open the hydrogen, nitrogen and oxygen cylinder valves.
- Prior to start the experimentation, check for any leakage in the connections and then purge the anode side with nitrogen to make sure that no left-over gas is present inside.
- Set the experimental parameters such as mass flow rate, FC temperature, gas humidification temperatures at desired value through the WFTS software interface as shown in Figures 3.25 and 3.26.
- Set the maximum voltage, minimum voltage and voltage increment of the fuel cell.
- Set the delay between every two voltage vs. current data points in the test software interface.
- Start the computer program to automatically control the experiments and collect the data.

The fuel cell is disconnected from the test station and dismantled. Again PEM fuel cell is reassembled by changing flow field design or Membrane. The above experimental procedure is repeated for three active area PEM fuel cells (49, 84 and 119 cm^2) with three flow field designs (1-S, 2-S and 3-S), three MEAs (N112, N117 and N212) having Pt loadings 0.6, 0.8 and 1.0 mg/cm^2.

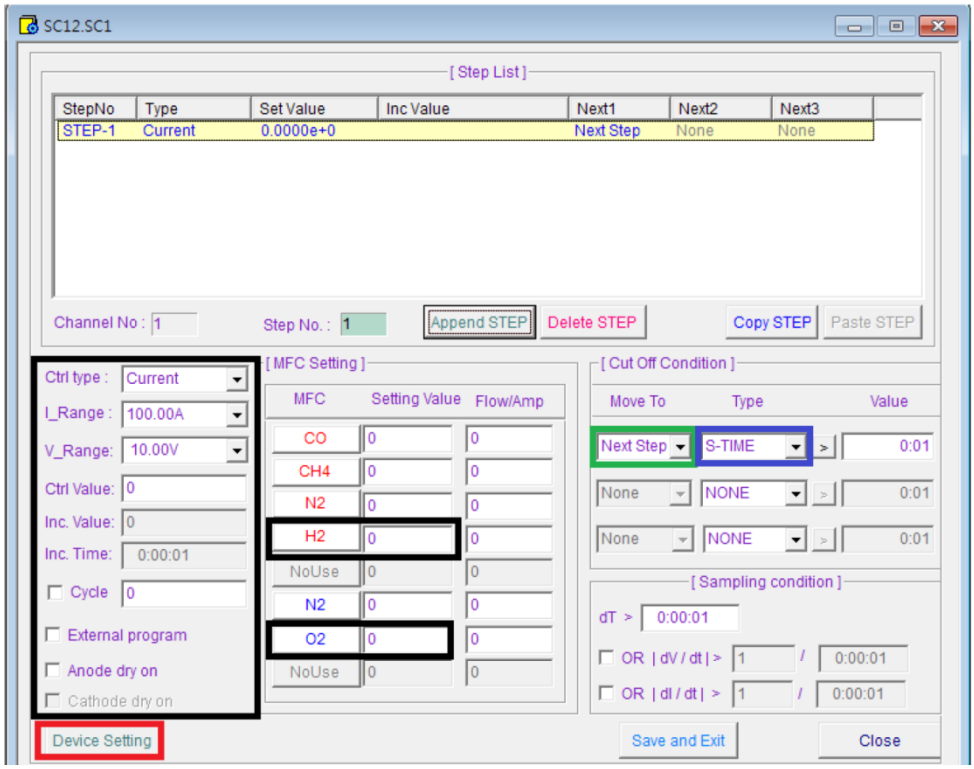

Figure 3.27 setting inlet mass flow rates in through software interface

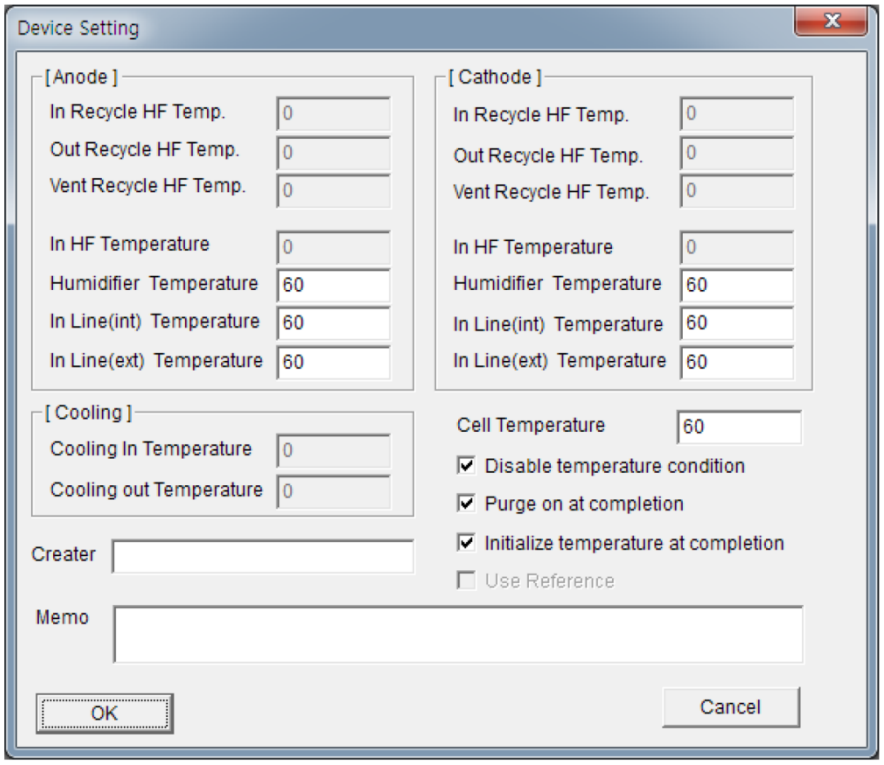

Figure 3.28 setting of cell and humidification temperatures through software interface

CHAPTER 4

4. RESULTS AND DISCUSSION

Computational and experimental investigations on the performance of three active area PEMFCs using single (1-S), double (2-S) and triple (3-S) serpentine flow field configurations has been completed. Numerically predicted pressure drop, mass fraction distribution of hydrogen, oxygen, and liquid water activity along the channel at peak power performance of three PEMFCs with three flow fields presented. To validate the numerical results, experiments were conducted with same flow field configurations used in the simulation for three PEMFCs. After validation of numerical results with experimental results, further experiments are conducted to investigate the influence of platinum loading, membrane thickness, operating conditions such as cell operating temperature, reactants humidification temperature and the reactants flow rate on the performance of three PEMFCs using triple serpentine flow field. It is observed from the simulation results that 3-S flow field is performing better than 1-S and 2-S flow fields.

4.1 Simulation results

4.1.1 Pressure drop

A CFD analysis was carried out on 1-S, 2-S and 3-S flow field models to study the pressure drop from inlet to outlet. Figure 4.1 shows the pressure drop along the 1-S, 2-S and 3-S flow channels of 49 cm^2 active area fuel cell (PEMFC 1). Similarly, Figures 4.2 and 4.3 shows the pressure drop along the 1-S, 2-S and 3-S flow channels of 84 cm^2 active area fuel cell (PEMFC 2) and 119 cm^2 active area fuel cell (PEMFC 3) respectively. From Figures 4.1, 4.2 and 4.3, it is observed that pressure drops are maximum at the inlets and gradually reduced towards the outlets. It is also observed that highest-pressure drops are observed in 1-S flow channels and lowest pressure drops in 3-S flow channels of three PEMFCs. The numerically predicted pressure drops in 1-S, 2-S and 3-S flow fields of three PEMFCs are given in Table 4.1. From this table, it is observed that pressure drops are reduced with increase in the number of flow passages. It is also observed that pressure drops are increased with increase in flow channel length. Therefore, the flow field of multichannel serpentine is prefered to reduce the pressure drop in channels.

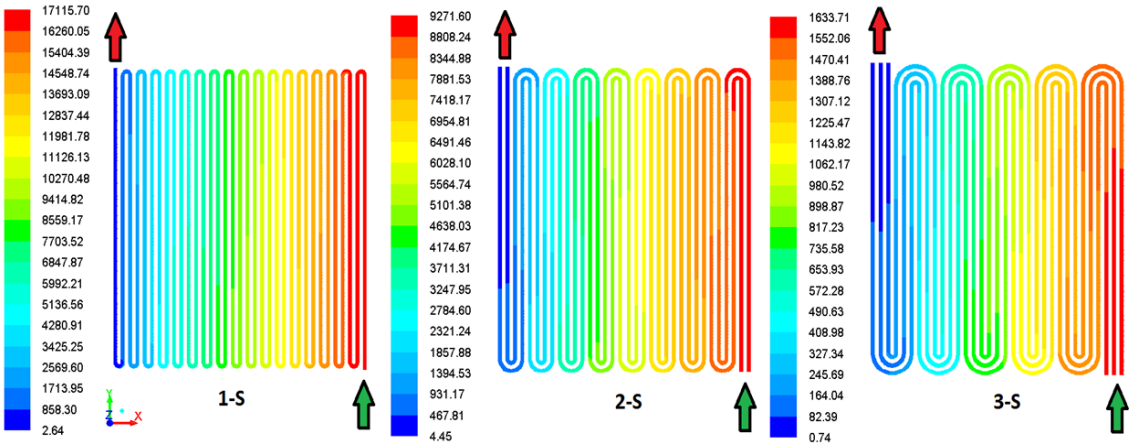

Figure 4.1 Variation of Pressure in cathode channel of PEMFC 1

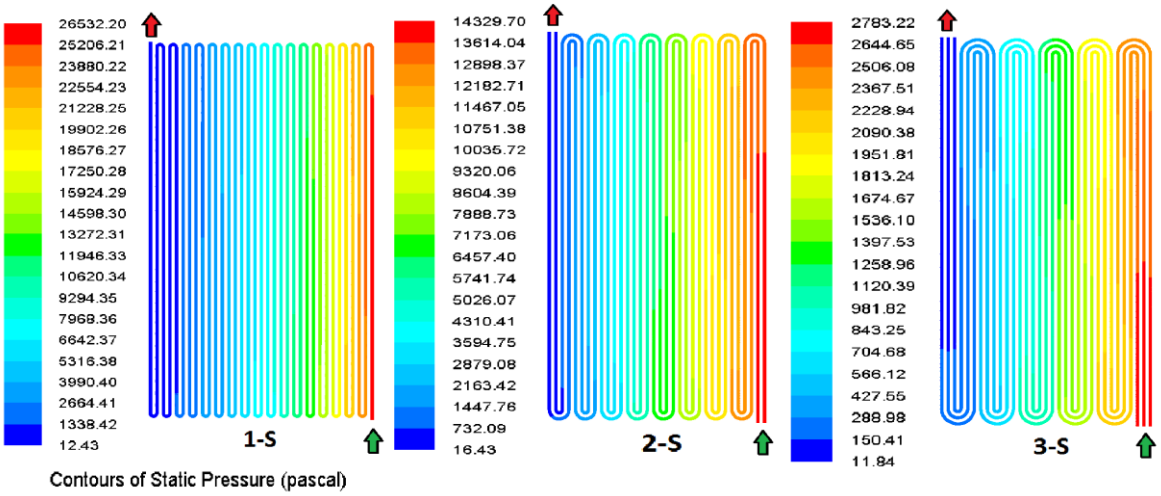

Figure 4.2 Variation of Pressure in cathode channel of PEMFC 2

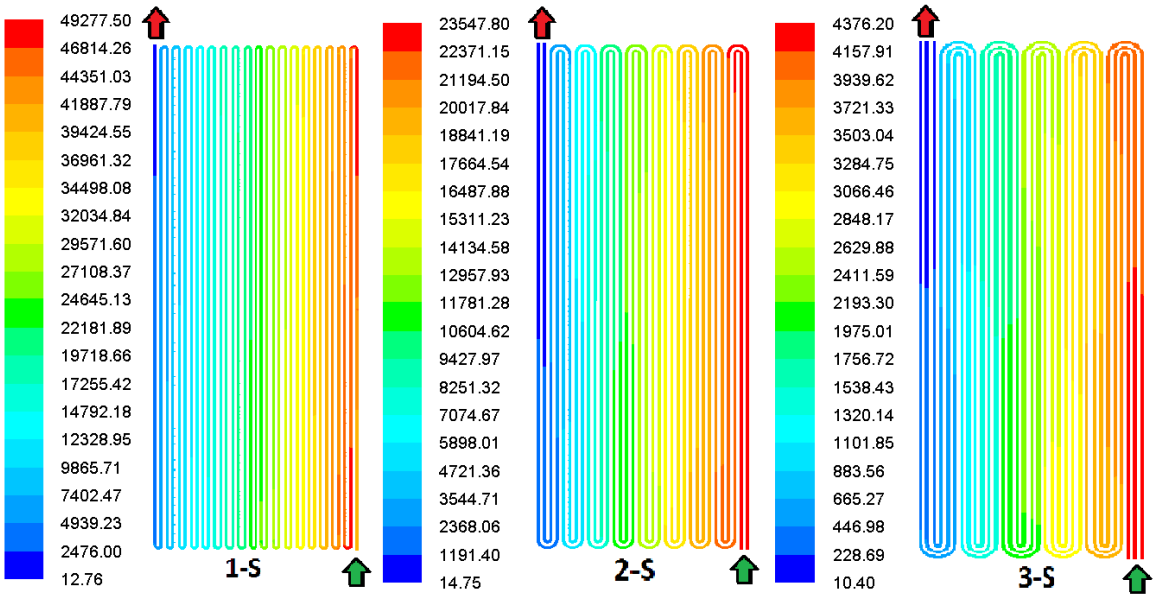

Figure 4.3 Variation of Pressure in cathode channel of PEMFC 3

Table 4.1 Numerically predicted pressure drops in the cathode channels

Cathode Channel	Pressure drop ΔP (Pascal)		
	1-S	2-S	3-S
PEMFC 1 (49 cm^2)	17115	9271	1633
PEMFC 2 (84 cm^2)	26532	14329	2783
PEMFC 3 (119 cm^2)	49277	23457	4376

4.1.2 Hydrogen and oxygen distribution

Figure 4.4 shows the hydrogen mass fraction distribution along the three types of anode flow channels (1-S, 2-S and 3-S) of PEEMFC1 at a cell potential of 0.5 V. Similarly, Figures 4.5 and 4.6 shows the hydrogen mass fraction distribution along the three types of anode flow channels (1-S, 2-S and 3-S) of PEMFC 2 and PEMFC 3 respectively at a cell potential of 0.5 V. From Figures 4.4, 4.5 and 4.6, it is observed that hydrogen mass fractions are high at the channel inlets and gradually decreased along the flow channel and become low at the channel outlets. Figures 4.7, 4.8 and 4.9 shows the oxygen mass fraction distribution along the cathode flow channels (1-S, 2-S and 3-S) of PEMFC 1, PEMFC 2 and PEMFC 3 respectively at cell potential of 0.5 V. From Figures 4.7, 4.8 and 4.9, it is observed that oxygen mass fractions are high at the channel inlets, decreased along the flow channel, and become low at the channel outlets. It is also observed that oxygen mass fraction distribution is more uniform than hydrogen mass fraction distribution. The reduction of species concentration along the channels is due to consumption of reactants in the reaction.

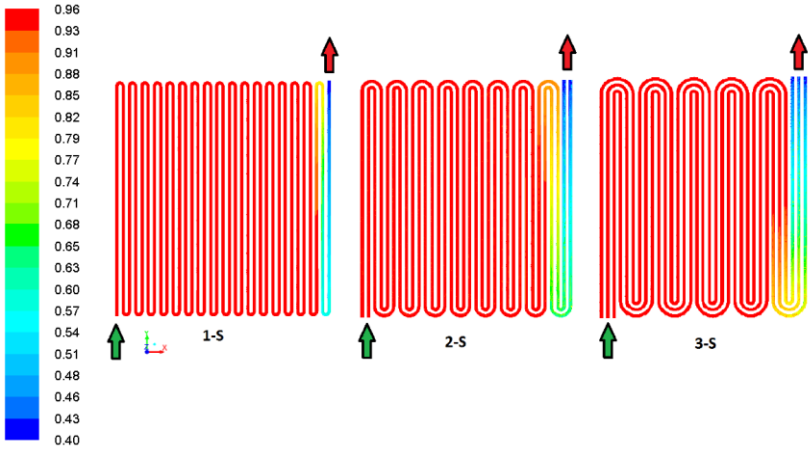

Figure 4.4 H_2 mass fraction distribution in anode channel of PEMFC 1 at 0.5 V

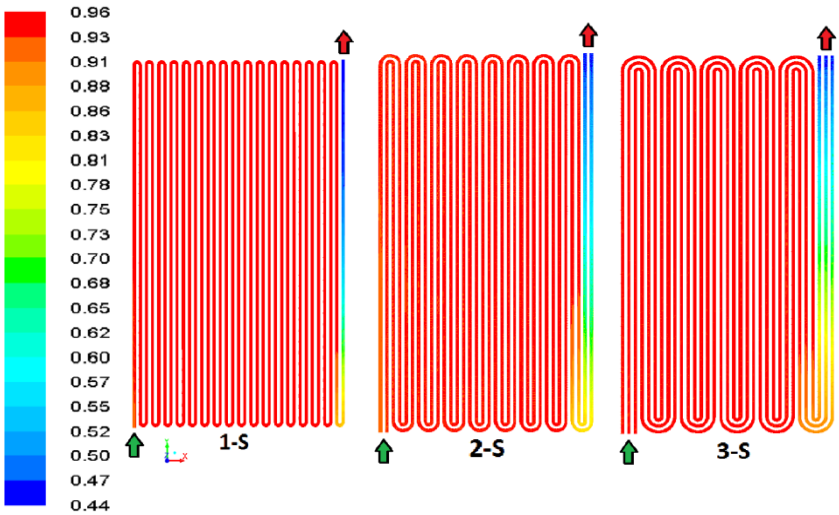

Figure 4.5 H_2 mass fraction distribution in anode channel of PEMFC 2 at 0.5 V

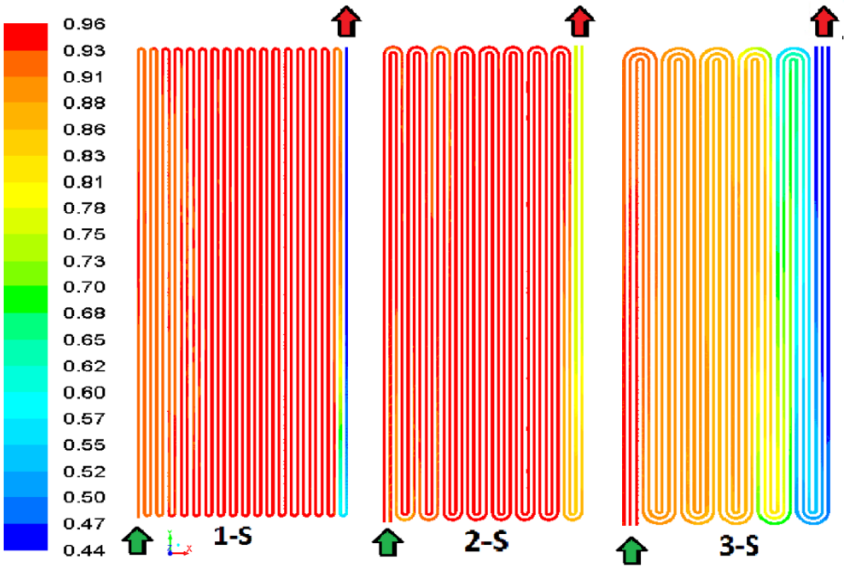

Figure 4.6 H_2 mass fraction distribution in anode channel of PEMFC 3 at 0.5 V

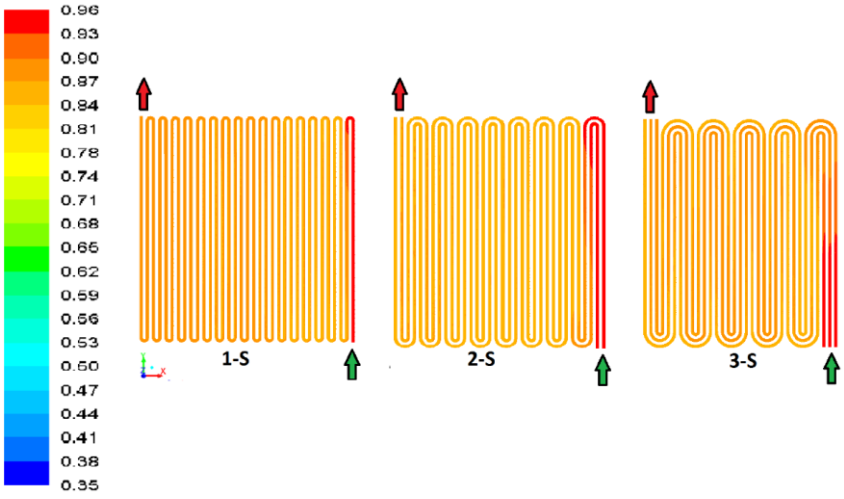

Figure 4.7 O_2 mass fraction distribution in cathode channel of PEMFC 1 at 0.5 V

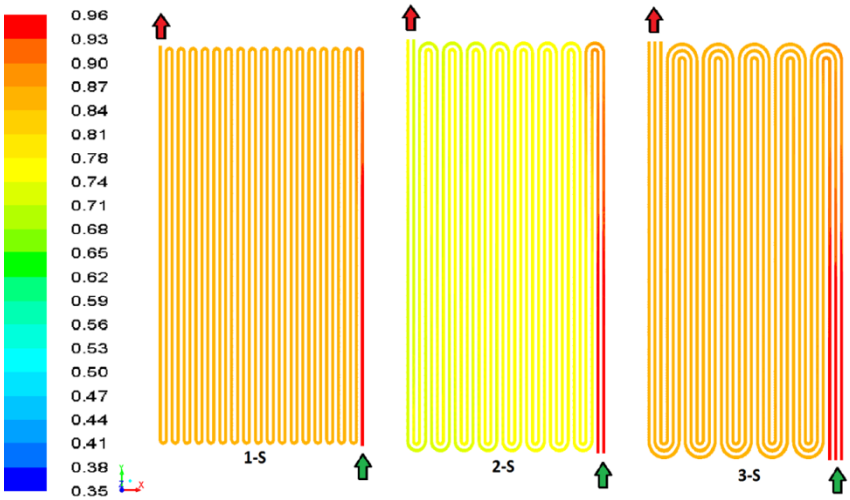

Figure 4.8 O_2 mass fraction distribution in cathode channel of PEMFC 2 at 0.5 V

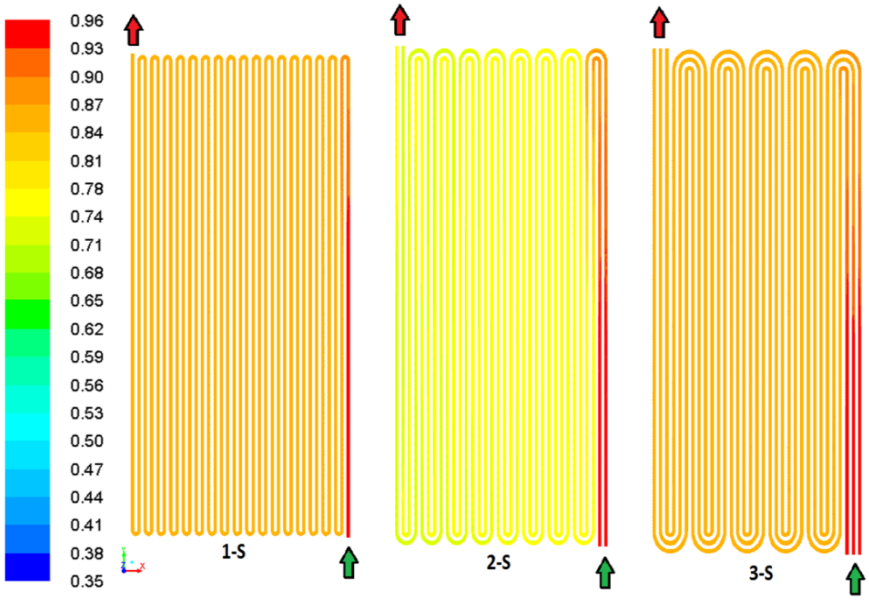

Figure 4.9 O_2 mass fraction distribution in cathode channel of PEMFC 3 at 0.5 V

4.1.3 Current flux density distribution

Figure 4.10 shows the current flux density distribution over the cathode catalyst layer of three flow field configurations (1-S, 2-S and 3-S) of PEMFC 1 at a cell potential of 0.5 V. Similarly, Figures 4.11 and 4.12 shows the current flux density distribution over the cathode catalyst layer of three flow field configurations (1-S, 2-S and 3-S) PEMFC 2 and PEMFC 3 respectively at a cell potential of 0.5 V. The simulation results showed that the current densities are the maximum in the region close the anode inlet and decreased along the direction of the flow. The drop in the local current densities is because of the reactant depletion. It is also observed that the current flux density distribution over the CL of 3-S flow fields PEMFCs is better than 1-S and 2-S flow field PEMFCs.

4.1.4 Liquid water activity

Figure 4.13 shows the liquid water activity in the three types of cathode flow field (1-S, 2-S and 3-S) of PEMFC 1 at a cell potential of 0.5 V. Similarly, Figures 4.14 and 4.15 shows the liquid water activity in the three types cathode channels (1-S, 2-S and 3-S) PEMFC 2 and PEMFC 3 respectively at 0.5 V cell potential. From Figures 4.13, 4.14 and 4.16, it is observed that liquid water activity is less at the inlet and gradually increased and become more at the outlet. This is due to movement of the liquid water molecules along the flow direction of the oxygen. It is also observed that liquid water concentrations are less in 3-S type flow field channels than 1-S and 2-S type flow field channels. From these contours, it is concluded that triple serpentine flow field has ability to remove liquid water from the cell.

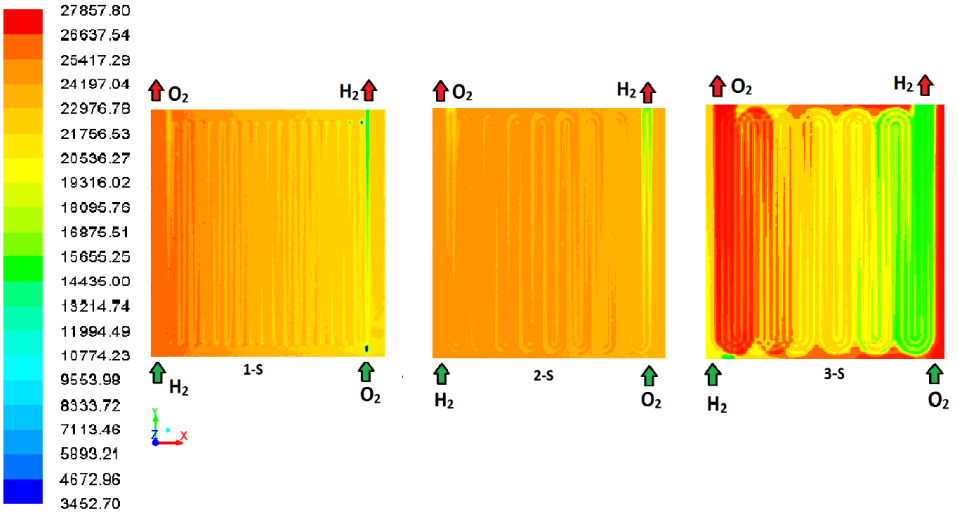

Figure 4.10 Current flux density distribution on cathode CL of PEMFC 1 at 0.5 V

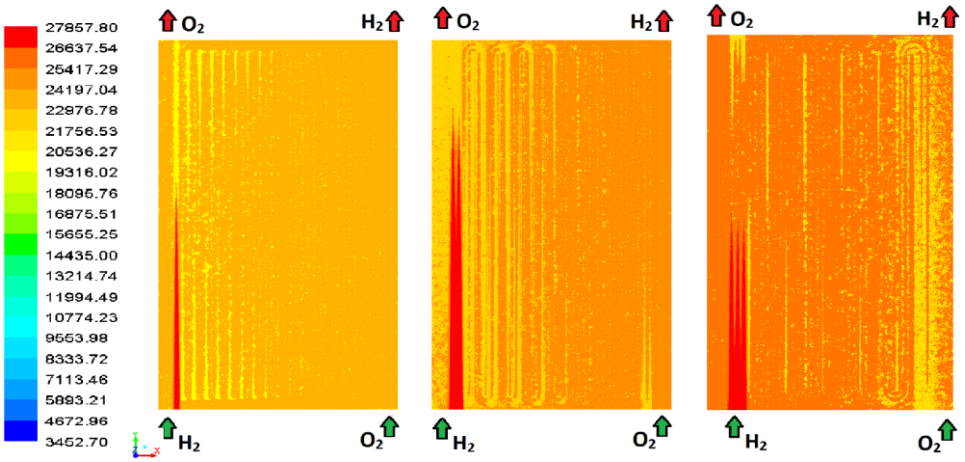

Figure 4.11 Current flux density distribution on cathode CL of PEMFC 2 at 0.5 V

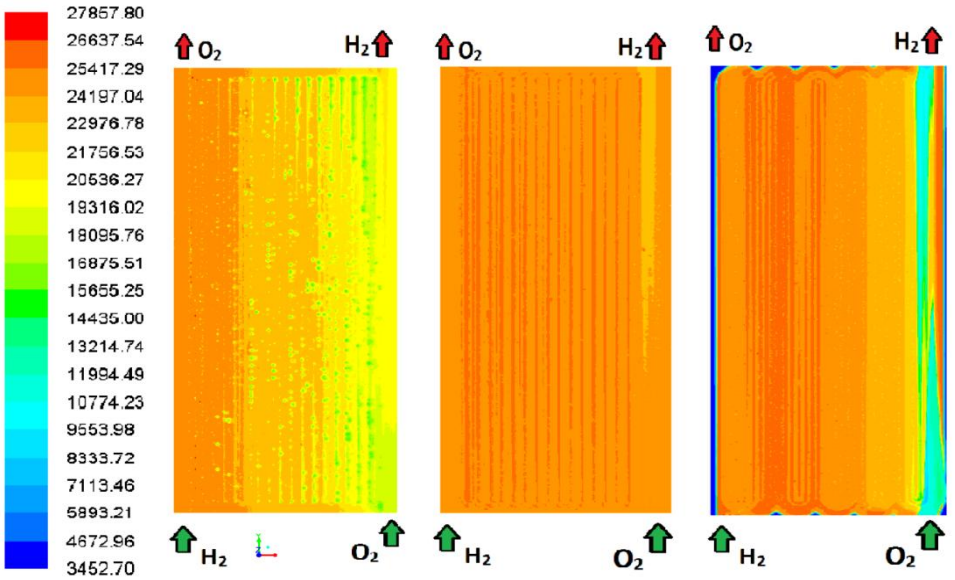

Figure 4.12 Current flux density distribution on cathode CL of PEMFC 3 at 0.5 V

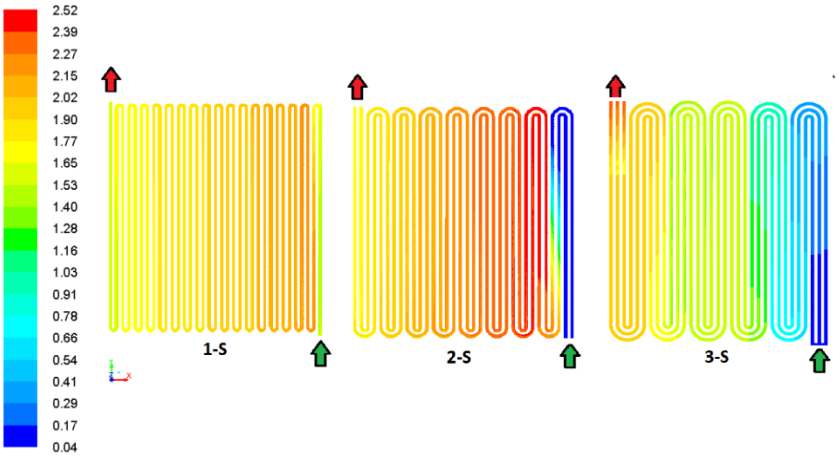

Figure 4.13 Liquid water activity in cathode channel of PEMFC 1 at 0.5 V

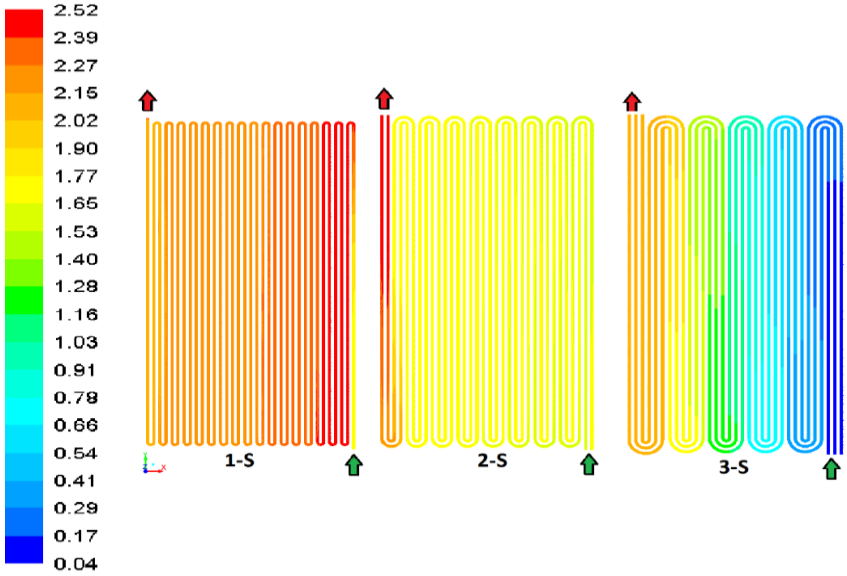

Figure 4.14 Liquid water activity in cathode channel of PEMFC 2 at 0.5 V

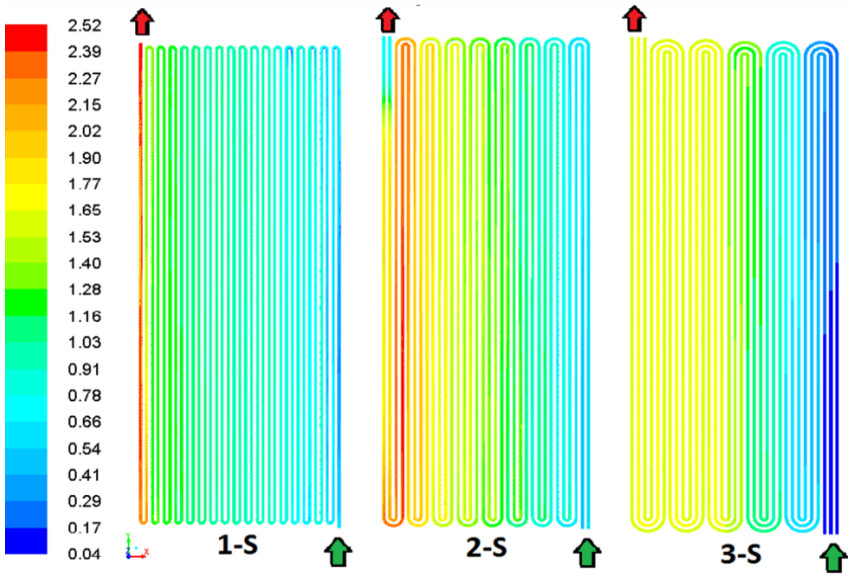

Figure 4.15 Liquid water activity in cathode channel of PEMFC 3 at 0.5 V

4.1.5 Membrane water content

Figure 4.16 shows the water distribution in the membrane of three flow field configurations (1-S, 2-S and 3-S) of PEMFC 1 at a cell potential of 0.5 V. Similarly, Figures 4.17 and 4.18 shows the water content in the membrane water distribution in the membrane of three flow field configurations of PEMFC 2 and PEMFC 3 at a cell potential of 0.5 V. From Figures 4.16, 4.17 and 4.18, it is observed that the water content distribution is somehow good in PEMFCs of 3-S flow fields and the values of this water content are good enough to keep the membrane hydrated, which resulted in enhanced proton conductivity. This water content distribution in the membrane is identical to the current density distribution in Figures 4.10, 4.11 and 4.12 because water production is dependent on generated.

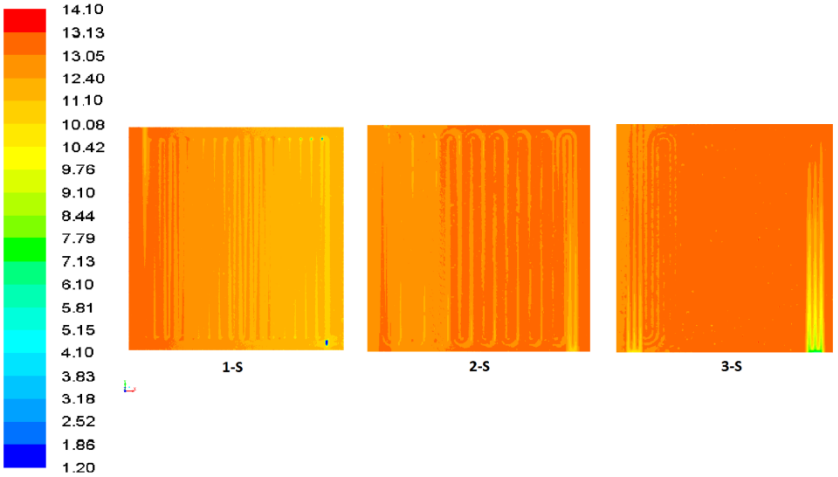

Figure 4.16 Membrane water content in PEMFC 1 at 0.5 V

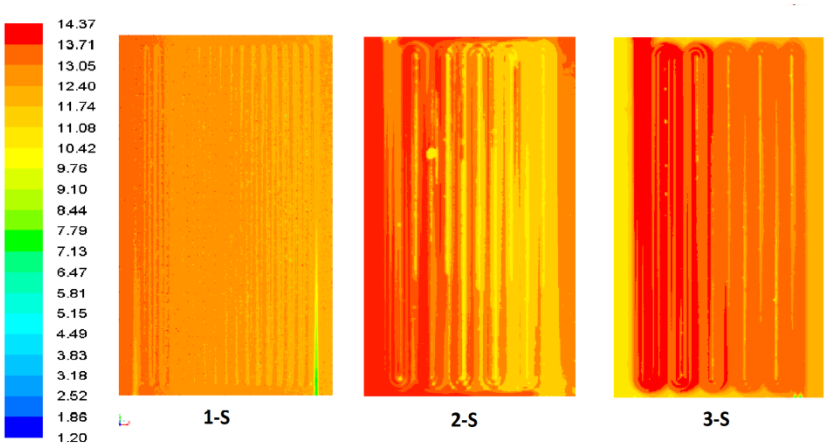

Figure 4.17 Membrane water content in PEMFC 2 at 0.5 V

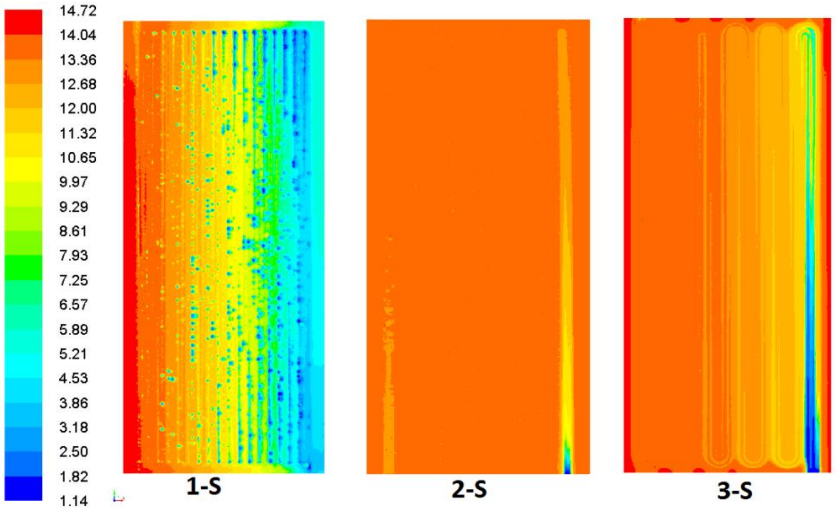

Figure 4.18 Membrane water content in PEMFC 3 at 0.5 V

4.2 Validation

Numerical results may be reckoned as reliable and accurate when the numerical model is well resolved and has been systematically validated with experimental results. An experimental study is carried out to correlate the present numerical results with the experimental results. From numerically and experimentally obtained data, polarization as well as power curves have been drawn and compared as shown in Figure 4.19. It is observed that numerical data are in good agreement with experimental data. It is also observed that the 3-S PEMFCs performance is better than 1-S and 2-S PEMFCs. Further experiments have been carried out with 3-S flow field to study the influence of membrane thickness, platinum loading, operating parameters such as cell temperature, reactant gas humidification temperature, reactant gas flow rate on PEMFCs performance.

Table 4.2 Difference between numerical and experimental results

	Flow Field	Simulation	Experiment	% deviation
PEMFC 1	1-S	14.2	13.71	3.57
	2-S	15.13	14.63	3.41
	3-S	16.59	16.01	3.62
PEMFC 2	1-S	21.86	20.86	4.79
	2-S	23.56	22.56	4.43
	3-S	26.16	25.16	3.97
PEMFC 3	1-S	29.97	29.11	2.95
	2-S	33.54	32.61	2.85
	3-S	36.15	35.25	2.79

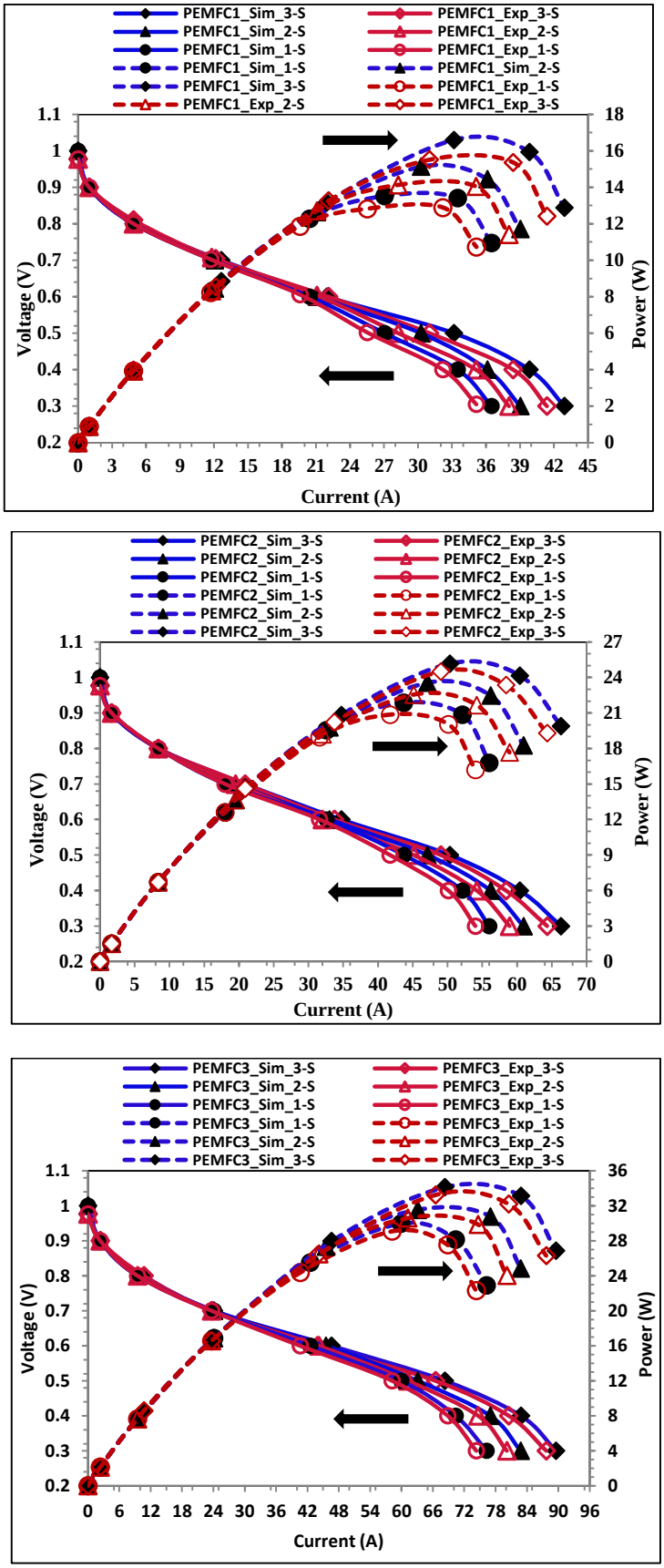

Figure 4.19 Polarization and performance curve of three PEMFCs having three types of flow fields

4.2.1 Calculation of power output with respect to pressure drop

The pressure drop is one of the crucial issue that should be considered while designing the flow channel. In this study, pressure drop loss associated to the power density is calculated for the three flow fields of PEMFC 1, PEMFC 2 and PEMFC 3 as follows.

$$W_{net} = W_{cell} - W_p \qquad (\mathbf{4.1})$$

$$W_{cell} = i * V_{cell} \qquad (\mathbf{4.2})$$

$$W_p = \frac{\Delta P * A_{cha} * V}{A_{total}} \qquad (\mathbf{4.3})$$

Where W_{net} is the net power density, W_{cell} is the cell power density, W_p is the pressure drop loss in cathode, ΔP is the total cathode pressure drop, $A_{cha}$is the cathode flow channel inlet cross-sectional area, V is the velocity of the oxidant at the cathode inlet, and A_{total} is the cell active area. The calculated pressure drop loss and power output for the three proposed flow field configurations at 0.5 V are given in Table 4.3. The results show that as the number of flow passes increase the pressure drop losses decrease. It is observed that the pressure drop loss is minimum in 3-S flow fields and high in 1-S flow fields. It is also observed that the pressure drop losses (W_P) are far less than the cell output power (W_{Net}). Therefore, the pressure drop losses can be neglected.

Table 4.3 Calculated pressure drops in the cathode channels at the operating voltage of 0.5 V

	Flow Field	**ΔP (Pa)**	**W_{Cell} (W)**	**W_P (W)**	**W_{Net} (W)**
PEMFC 1	1-S	17115	14.2	0.87	13.33
	2-S	9271	15.13	0.28	14.85
	3-S	1633	16.59	0.10	16.49
PEMFC 2	1-S	26532	21.86	1.12	20.74
	2-S	14329	23.56	0.52	23.04
	3-S	2783	26.16	0.12	26.04
PEMFC 3	1-S	49277	29.97	1.26	28.71
	2-S	23457	33.54	0.61	32.93
	3-S	4376	36.15	0.22	35.93

4.3 Experimental results

It is well known that the performance of the FC is influenced by numerous parameters, such as the cell operating temperature, cell operating pressure, reactant gas humidification temperature, and reactant flow rate, in addition to design parameters such as membrane, catalyst particle size, quantity, and nature of gas diffusion layers. Every single parameter, depending on the conditions, may influence the reactions. In order to explore the influence of these parameters on the FC performance, experimental analyses has been conducted.

4.3.1 Effect of membrane thickness

Effect of membrane thickness on cell performance is analysed with three membranes having different thickness namely N212 (50 μm), N112 (51 μm) and N117 (178 μm). Figure 4.20 shows the effect of the membrane thickness on the performance of three active area PEM fuel cells. Experimental tests were conducted at 70^{o}C cell temperature and 1 bar pressure. The highest power output of 16 W, 23 W, and 34 W have been obtained when N212 membrane was used in PEMFC 1, PEMFC 2 and PEMFC 3 respectively. The peak power delivered by the PEMFC loaded with N112 and N117 membrane are less than PEMFC loaded with N212 membrane because the ohmic resistance of N112 and N117 is higher than N212. From these results, it is concluded that a thin membrane (N212) offers less ohmic resistance and gives high performance.

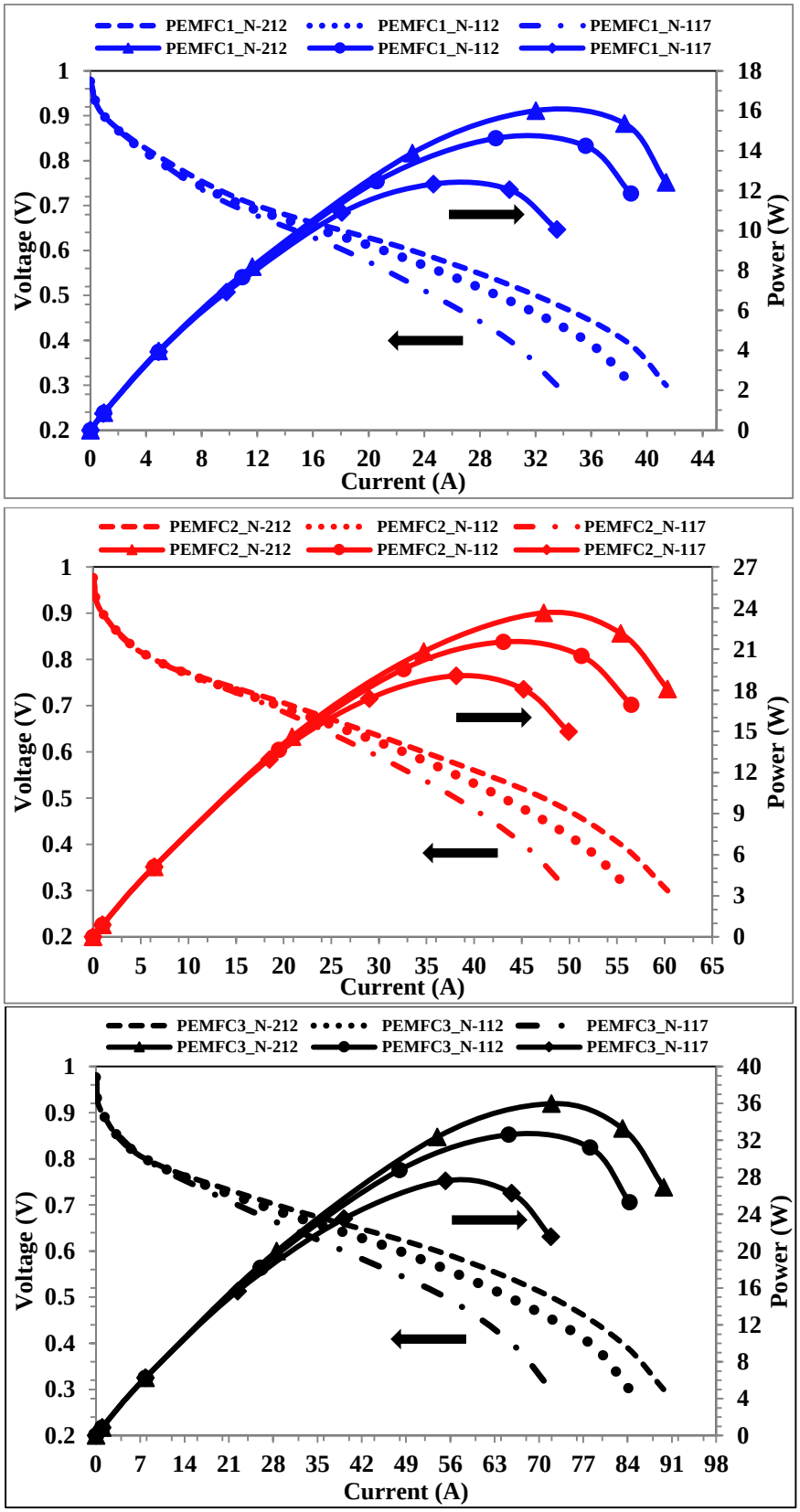

Figure 4.20 Effect of membrane thickness on performance of PEMFC 1(top), PEMFC 1 (middle) and PEMFC 3(bottom)

4.3.2 Effect of catalyst (Pt) loading

The effect of catalyst (Pt) loading on the performance of PEMFCs with an active area of 49, 84 and 119 cm^2 were analysed experimentally by incorporating N212 membrane. The platinum loading on the cathode side is taken as 0.6, 0.8 and 1.0 mg/cm^2 and on anode side is 0.4 mg/cm^2. The catalyst loading is more critical on the cathode side due to the significant activation polarization/kinetic loss for the oxygen reduction reaction (ORR). Figure 4.21 shows the effect of catalyst (Pt) loading on the i-V characteristics of three PEMFCs. It is observed that the cell performance has increased with increase in platinum loading. A larger catalyst loading facilitates higher surface area for electrochemical reactions, as a result, more reactant species involve in the reactions, generate more current and decrease the activation loss. It is also observed that the rate of increase in performance is more when the platinum loading increased from 0.6 to 0.8 mg/cm^2 than 0.8 to 1.0 mg/cm^2. Too high platinum loadings (more than 1 mg/cm^2) negatively influence the FC performance due to mass transport resistance caused by the thick electrode layer. In this study, all the cells delivered maximum performance with 1.0 mg/cm^2 platinum loading.

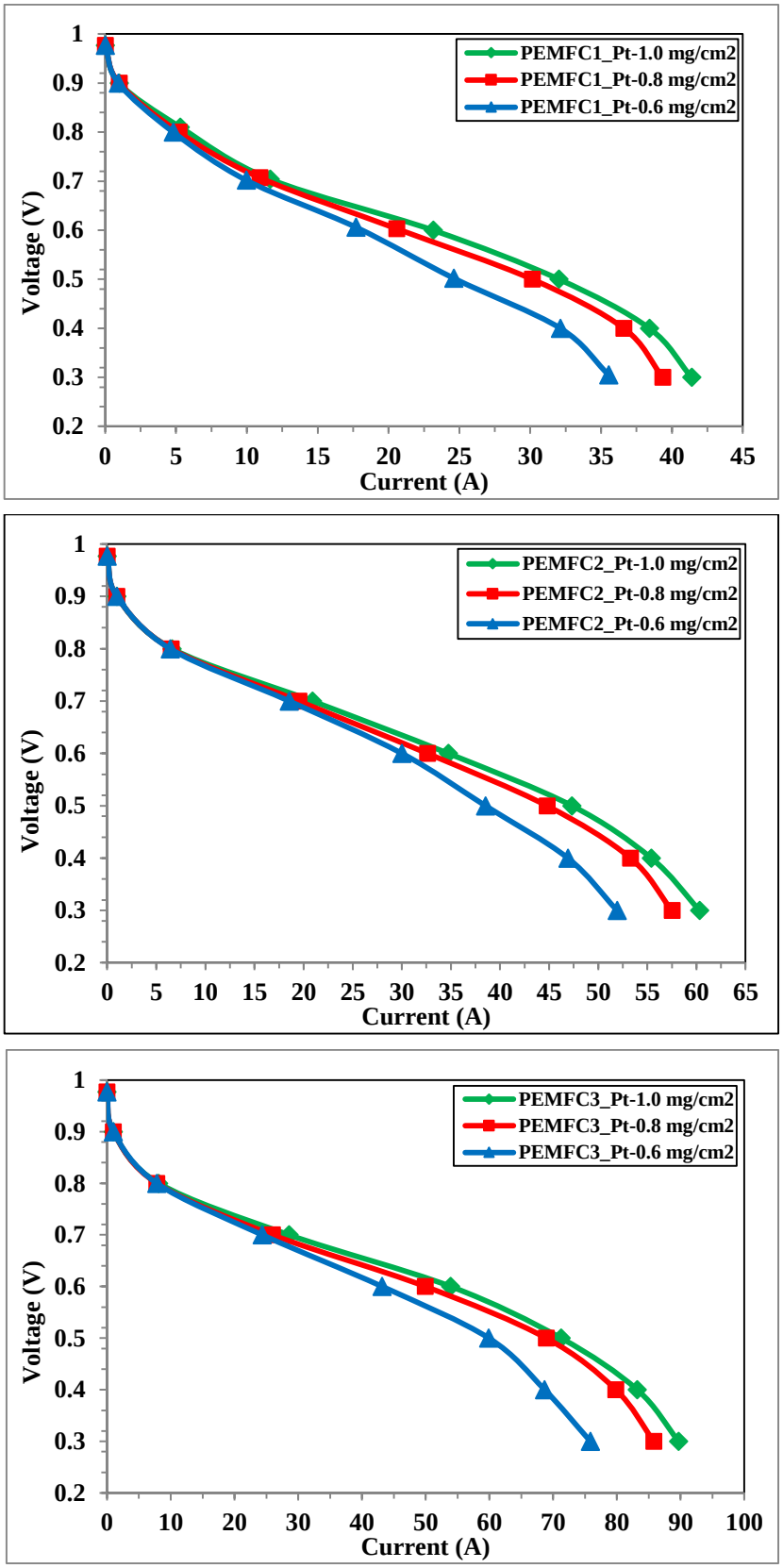

Figure 4.21 Effect of catalyst loading on performance of PEMFC 1 (top), PEMFC 2 (middle) and PEMFC 3 (bottom)

4.3.3 Effect of cell temperature

The effect of cell operating temperature on the performance of three PEMFCs has been studied. All the PEMFCs were assembled with 1.0 mg/cm^2 Pt loaded N212 MEA and the experiments have been carried out at different cell temperatures ranging from 40 ^{o}C to 80^{o}C, with an increment of 10^{o}C while the anode and cathode humidification temperatures were kept at 70◦C. The experimental results are shown in Figure 4.22. It is observed that when the temperatures increased from 40^{o}C to 70^{o}C, the performance of PEMFCs is increased due to improvement in the catalytic activity, and as a result, the chemical reaction rate increases. Also increasing the cell temperature facilitates the reactant transfer in the electrodes. When the cell temperatures increase further from 70^{o}C to 80^{o}C (T_{cell}>T_{humid}) then the performance of FCs is decreased due to membrane dehydration (extreme evaporation of liquid water in the cell), which significantly increase ohmic resistance of membrane (the active catalyst surface area may also reduced.). This is mostly because of increase in exchange current density with temperature. The effect of the cell temperature is more significant in the high current region. At low current region, the cell performance does not change much with the increase in the cell temperature.

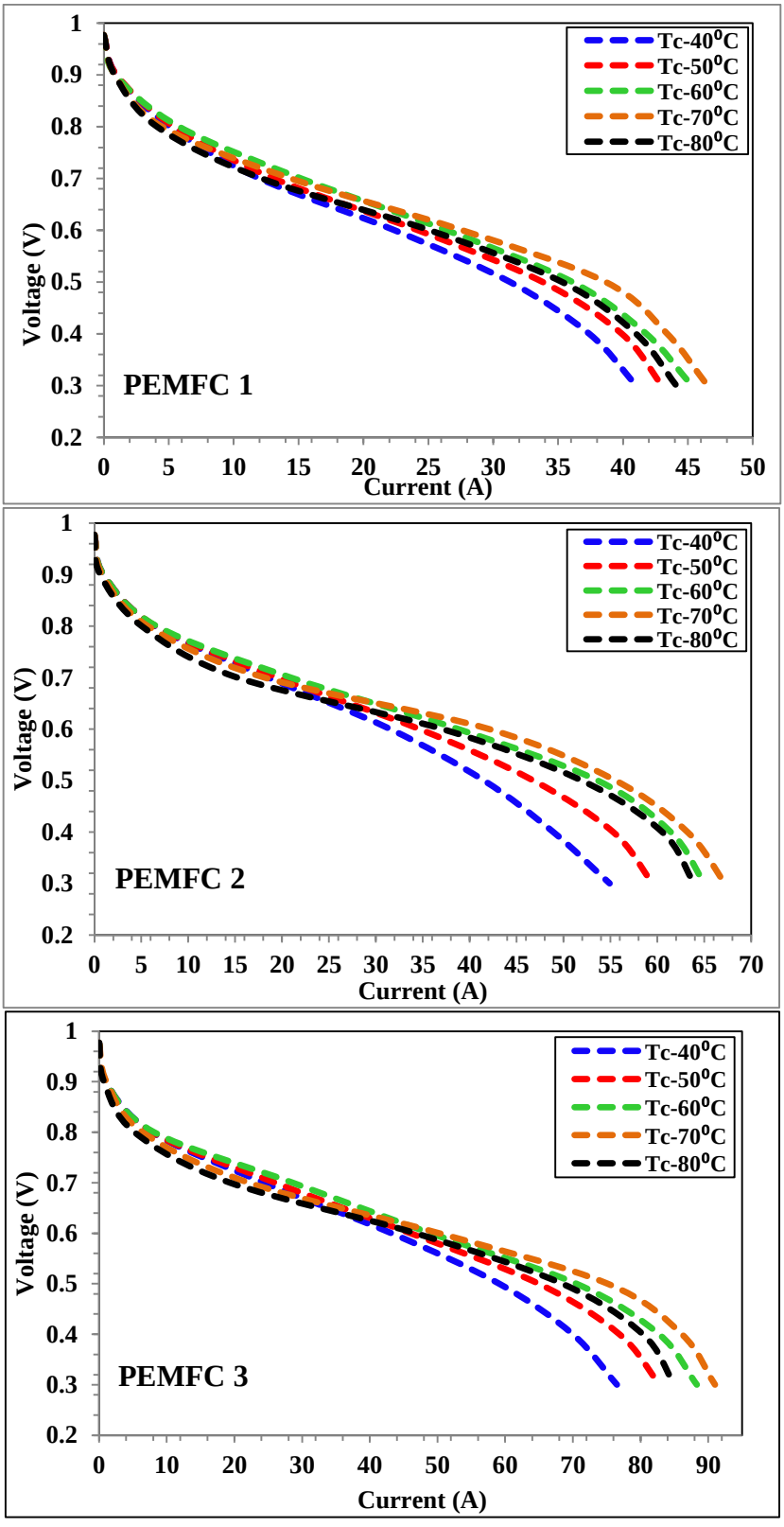

Figure 4.22 Effect of temperature on cell performance of PEMFC 1 (top), PEMFC 2 (middle) and PEMFC 3 (bottom)

4.3.4 Effect of anode and cathode gas humidification temperature

The effect of anode and cathode gas humidification temperature on the performance of three PEMFCs was studied with two sets of experiments. In first set of the experiments, anode gas humidification temperatures ($T_{h,a}$) are varied from 40^{o}C to 80^{o}C with an increment of 10^{o}C and the cathode humidification temperature is fixed at 70^{o}C. In the other set of experiments, cathode humidification temperatures ($T_{h,c}$) are varied from 40^{o}C to 80^{o}C with an increment of 10^{o}C and anode humidification temperature fixed at 70^{o}C. For both cases, the cell temperature (T_c) is kept at 70^{o}C. From Figure 4.23, it is observed that increase in the anode humidification temperatures indicated a positive influence on FCs performance till it reaches the cell temperature i.e. from 40^{o}C to 70^{o}C. This increase in anode humidification temperature keeps the membrane hydrated thus the ionic resistance of the membrane decreases. With further increase in the anode humidification temperature from 70^{o}C to 80^{o}C (i.e $T_{h,a} > T_c$), the cells performance decreases significantly due to back diffusion.

The effect of cathode humidification temperature on performance three PEMFCs is shown in Figure 4.24. It is observed that increase in the cathode humidification temperatures (from 40^{o}C to 60^{o}C) exhibited a positive influence on the FCs performance. This increase in humidification temperature keeps the membrane hydrated thus the ionic resistance of the membrane decreases. With further increase in cathode humidification temperature (from 60^{o}C to 80^{o}C), the membrane become over hydrated due to both electro-osmosis and water production at the cathode, leads to significant reduction in the FCs performance. The influence of the gas humidification temperature is more significant at low cell potential. At high cell potential, the performance of FCs does not change much with the increase in the gas humidification temperatures. In this study, the peak powers were obtained from the FCs at 70^{o}C and 60^{o}C anode humidification temperature and cathode humidification temperatures.

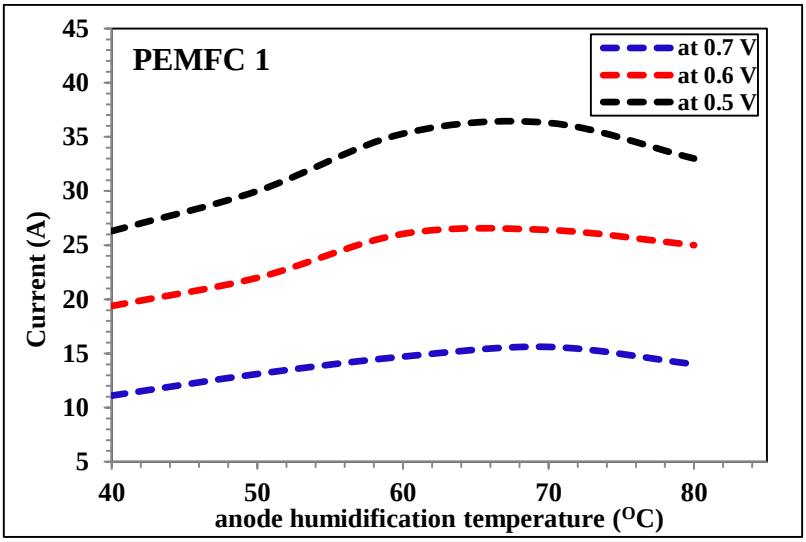

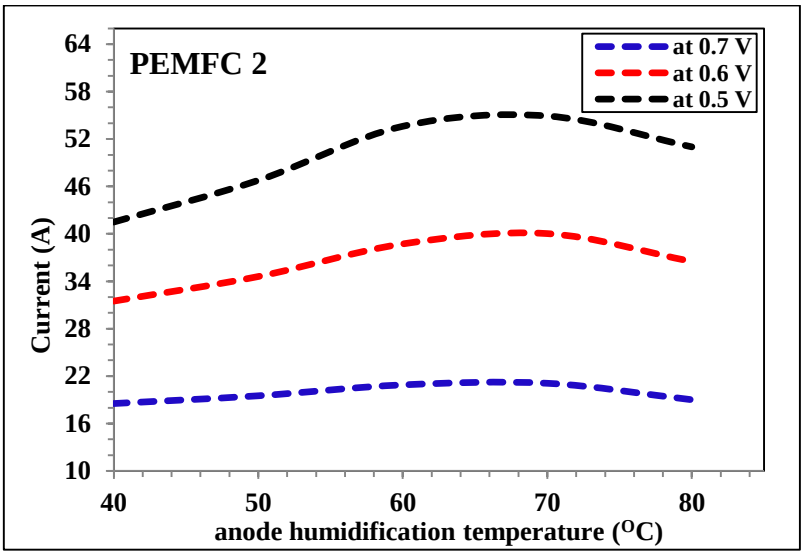

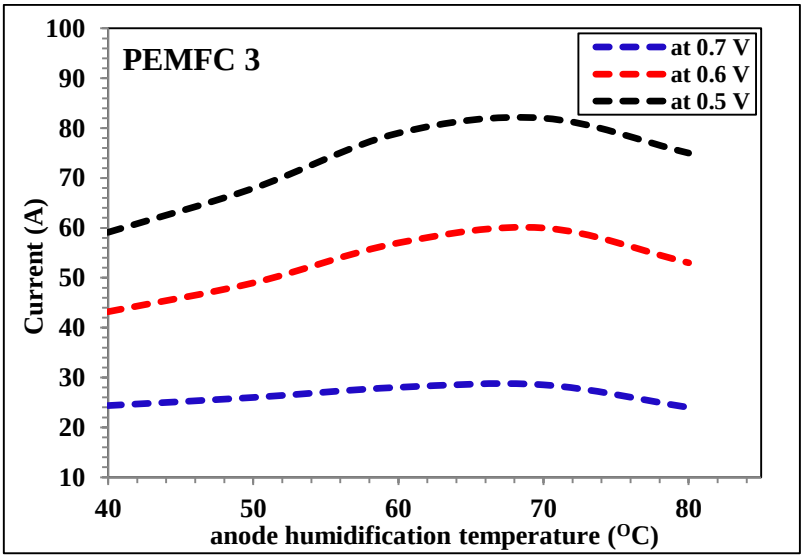

Figure 4.23 Effect of anode gas humidification on performance of PEMFC 1, PEMFC 2 and PEMFC 3

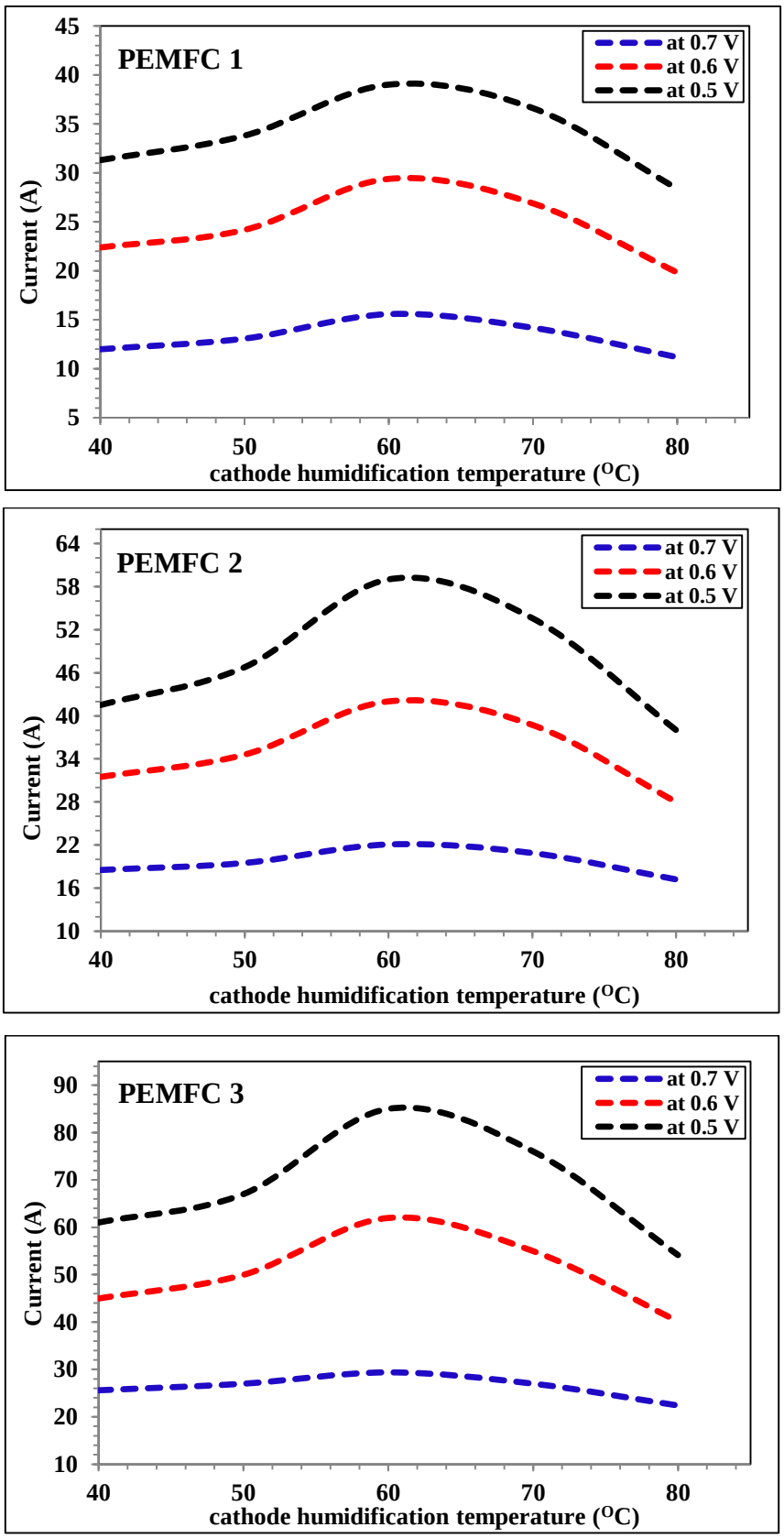

Figure 4.24 Effect of cathode gas humidification on performance of PEMFC 1, PEMFC 2 and PEMFC 3

4.3.5 Effect of hydrogen and oxygen flow rate

Two series of experiments are carried out to study the effect of reactants flow rate on the performance of three active area PEMFCs. In one set of the experiments hydrogen flow rates are varied and oxygen flow rate is fixed. In the other set of experiments oxygen flow rates are varied and hydrogen flow rate is fixed. In both sets of experiments, the cell and gas humidification temperatures are kept at 70^{o}C.

Figure 4.25 shows the influence of hydrogen flow rate on FCs performance and Figure 4.26 shows the influence of hydrogen flow rate on the current generated in the FCs at different cell potential. From Figures 4.25 and 4.26, it is observed that the FCs performance is increased when the hydrogen flow rate increases from 200 to 400 ccm for PEMFC 1, 400 to 600 ccm for PEMFC 2, from 600 to 800 ccm for PEMFC 3. Similarly, Figure 4.27 shows the influence of oxygen flow rate on FCs performance and Figure 4.28 shows the influence of oxygen flow rate on the current generated in the FCs at different cell potential. From Figures 4.27 and 4.28, it is observed that when the oxygen flow rate increased from 400 to 800 ccm for PEMFC 1, 800 to 1400 ccm for PEMFC 2, from 1200 to 1800 ccm for PEMFC 3. Increase in the reactants flow rate allows more fuel and oxidizer transport from GDL to the reaction sites (CL) and enhances the electrochemical reaction as well as FCs performance. But,with further increase in the flow rate of hydrogen and oxygen, the performance of FCs found to be decreased because transportation of fuel to the GDL decreases and they come out from the channel without involving in electrochemical reaction. From this study, it is also found that at high cell potentials the reactants flow rate is not significant and more significant at low cell potentials.

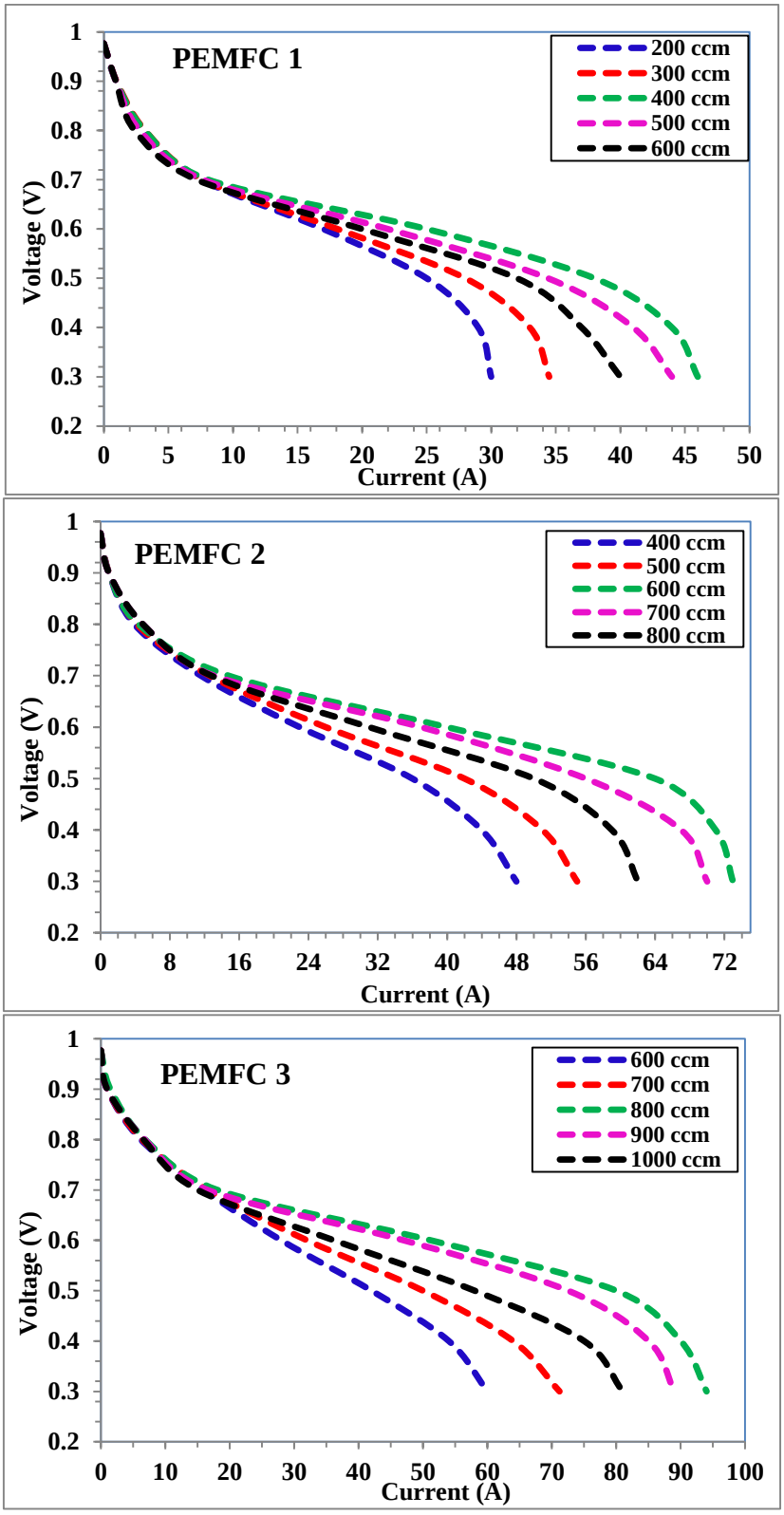

Figure 4.25 Influence of hydrogen flow rate on performance of PEMFC 1 (top), PEMFC 2 (middle) and PEMFC 3 (bottom)

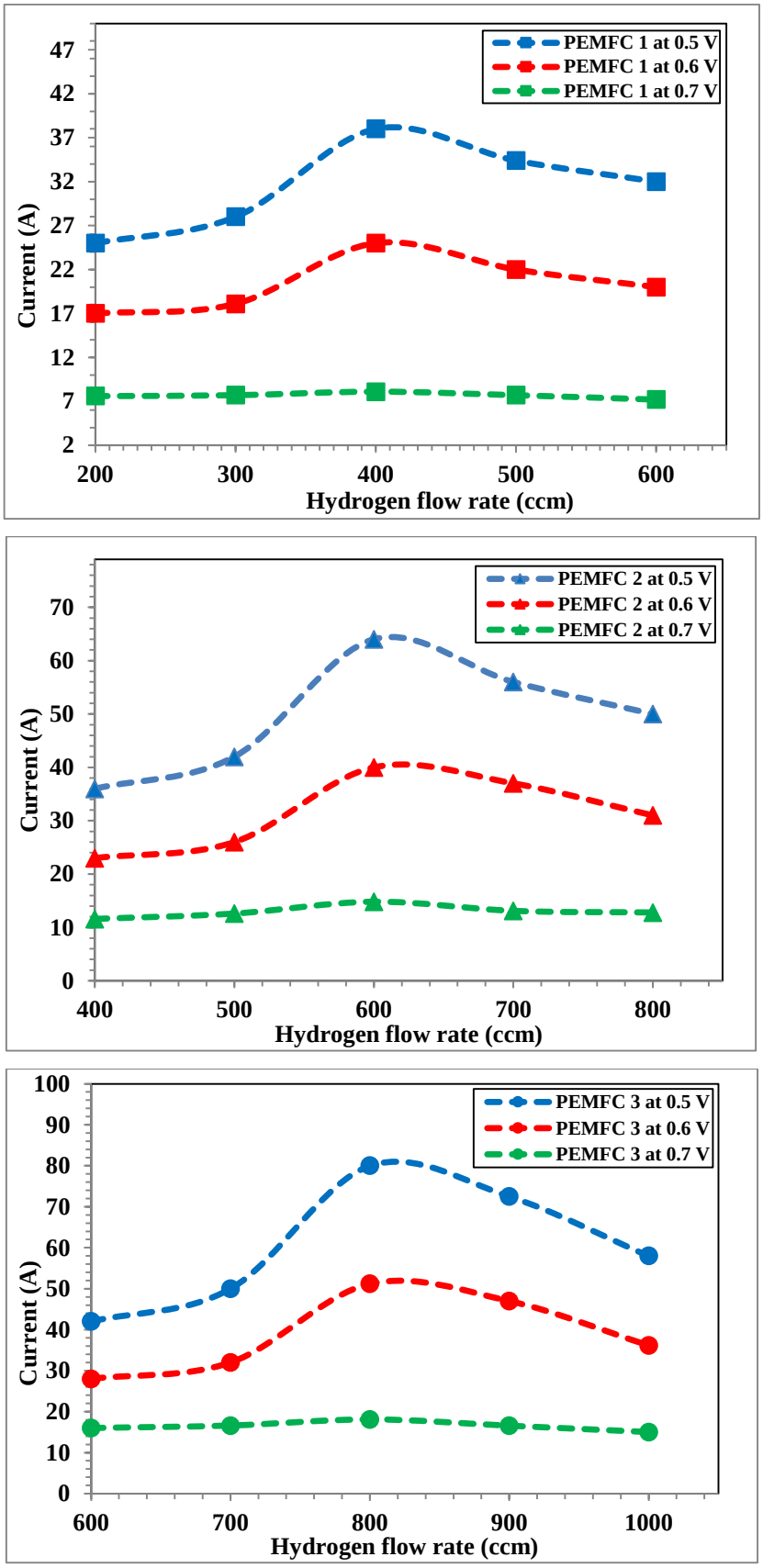

Figure 4.26 Effect of hydrogen flow rate on the current generated in PEMFC 1 (top), PEMFC 2 (middle) and PEMFC 3 (bottom)

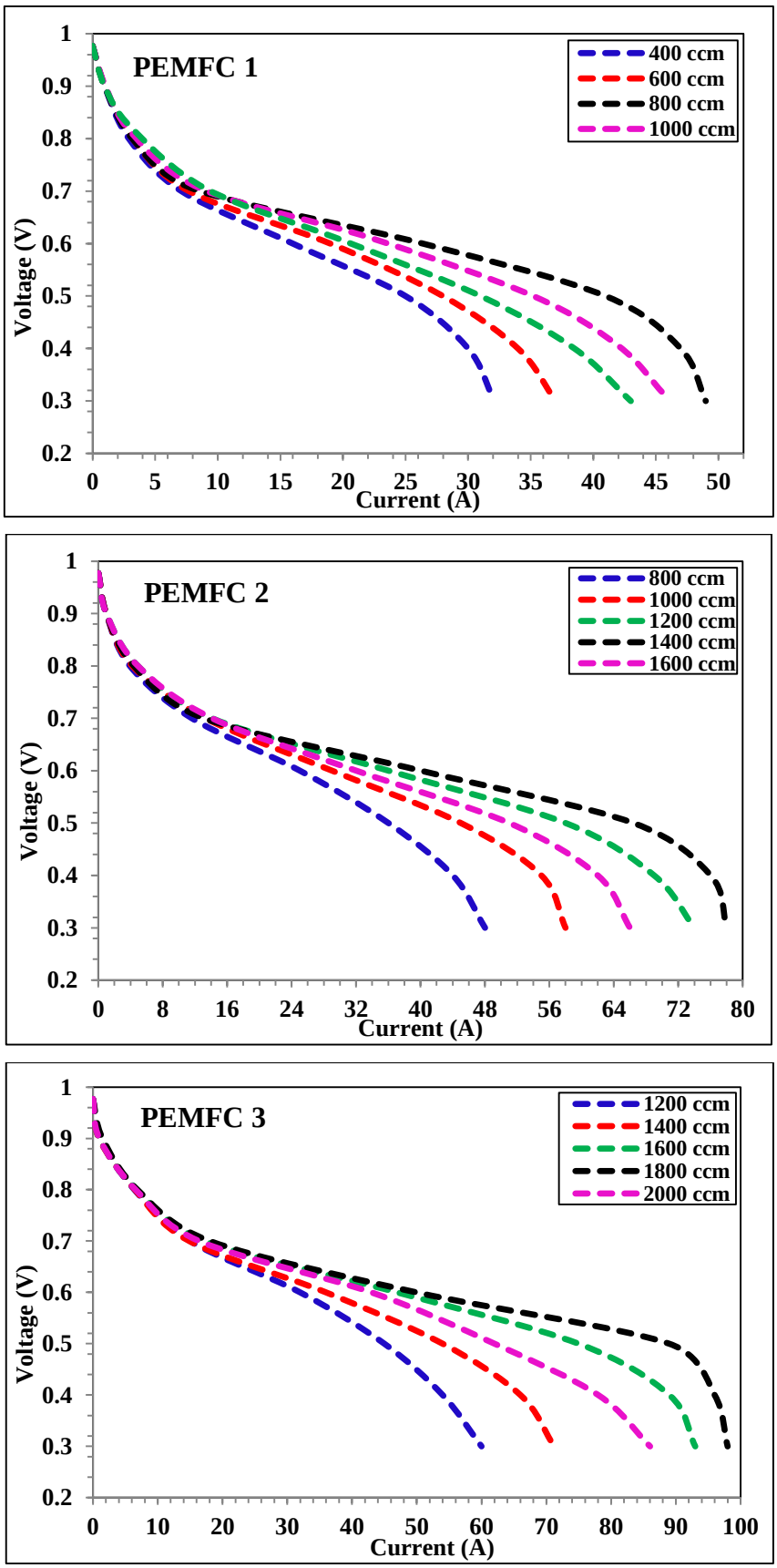

Figure 4.27 Effect of oxygen flow rate on cell performance of PEMFC 1(top), PEMFC 2 (middle) and PEMFC 3 (bottom)

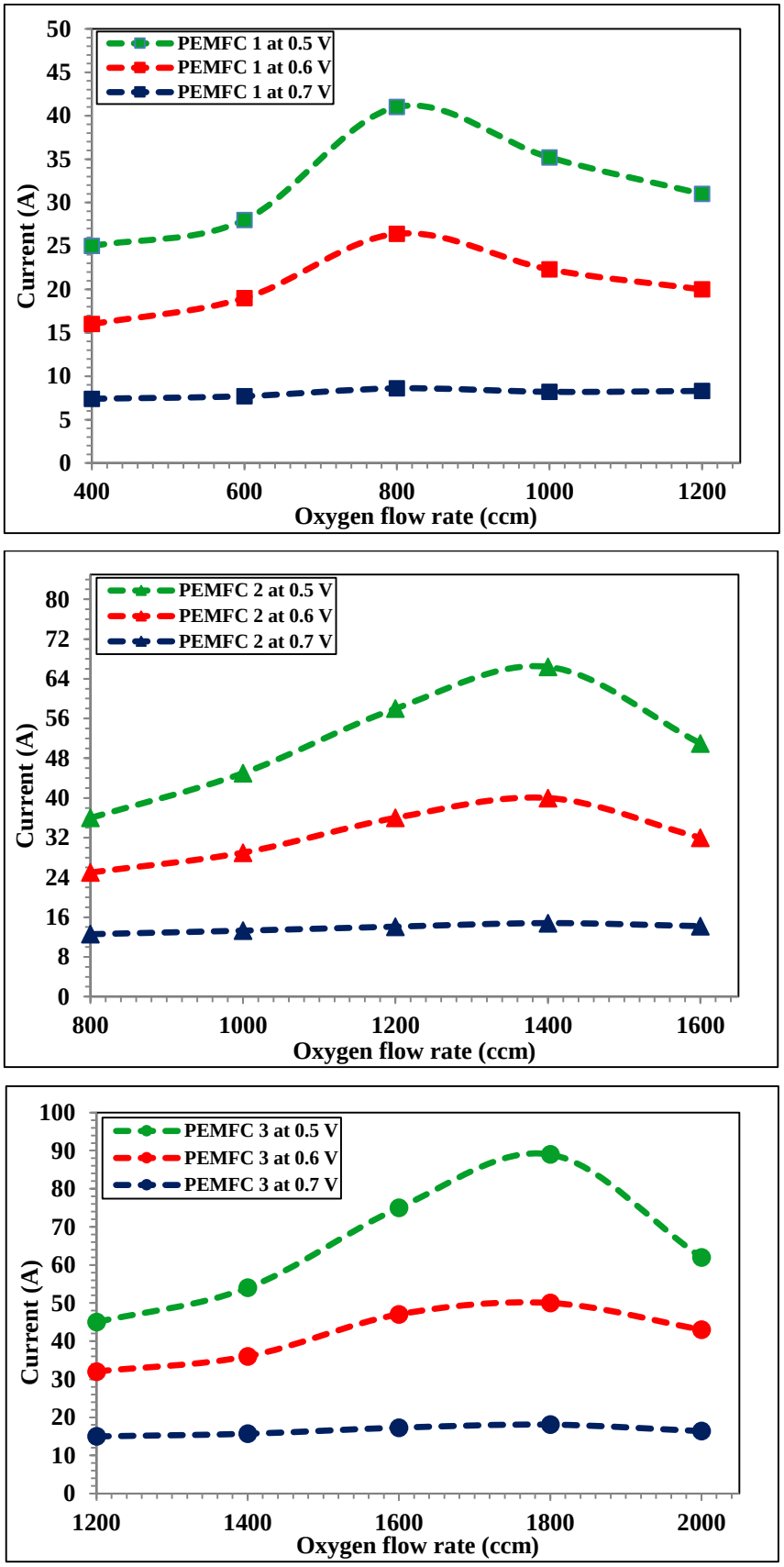

Figure 4.28 Effect of oxygen flow rate on the current generated in PEMFC 1 (top), PEMFC 2 (middle) and PEMFC 3 (bottom)

Finally, the optimized parameters of the PEMFC 1, PEMFC 2 and PEMFC 3 are presented in Table 4.4. Polarization curves (solid lines) and power density curves (dotted lines) of three

PEMFCs are obtained with the optimized parameters and presented in Figure 4.29. The fuel cell of active area 49 cm^2 with 50 µm membrane thickness and 1.0 mg/cm^2 platinum loading produced a peak power density of 418 mW/ cm^2 at 0.5 V when the cell was operated at 70°C cell temperature, 70°C anode humidification temperature, 60°C cathode humidification temperature, 400 ccm H_2 flow rate and 800 ccm O_2 flow rate. In the same way the cell of active areas 84 cm^2 and 119 cm^2 produced a peak powers of 395 mW/cm^2 and 374 mW/cm^2 respectively at 0.5 V. From this analysis, it is observed that the power density of smaller active area (49 cm^2) cell is higher than the larger active area (84 and 119 cm^2) fuel cells. From this investigation, it is concluded that instead of going for larger active area cell one can choose smaller active area cell with more number (i.e stack) of cells.

Table 4.4 optimized parameters for PEMFC 1, PEMFC 2 and PEMFC 3

Parameter	PEMFC 1	PEMFC 2	PEMFC 3
Flow field type (1-S, 2-S and 3-S)	3-S	3-S	3-S
Membrane thickness (µm)	50	50	50
Platinum loading (mg/cm^2)	1.0	1.0	1.0
Cell temperature (°C)	70	70	70
Anode gas humidification temperature (°C)	70	70	70
Cathode gas humidification temperature (°C)	60	60	60
Anode gas flow rate (ccm)	400	600	800
Cathode gas flow rate (ccm)	800	1400	1800

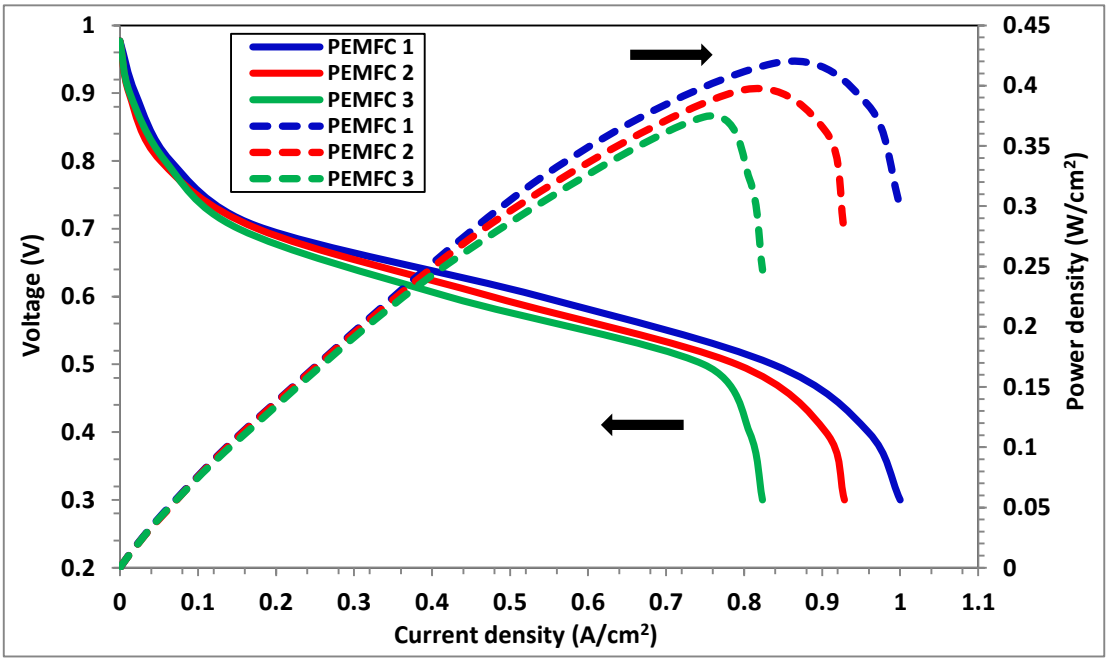

Figure 4.29 Performance comparison of PEMFC 1, PEMFC2 and PEMFC 3

CHAPTER 5

5. CONCLUSIONS

First, a computational fluid dynamics study on three active area PEMFCs with three types of serpentine flow fields (1-S, 2-S and 3-S) has been carried out and key parameters such as pressure drop, reactants mass fraction, liquid water activity, the membrane water content, polarization and performance of the PEMFC were presented. Then, experiments were conducted to validate the simulation results as well as to find out the best flow field design. Finally, experimental study has been carried out to examine the influence of operating parameters namely cell operating temperature, gas flow rates and gas humidification temperatures and design parameters such as membrane thickness and platinum loading on FC performance with best flow field design for three active area PEMFCs. The following conclusions were drawn from this study.

- Highest pressure drops were observed in single (1-S) and lowest pressure drops were observed in triple (3-S) serpentine flow fields. Therefore the 3-S flow field is considered for further investigations.
- Oxygen mass fraction distributions were more uniform than hydrogen mass fraction distributions.
- Liquid water activity in the cathode channels is less at inlet and increases gradually towards outlet and 3-S flow field has the better water removal capability.
- From experimental investigations the following observations were made
    - PEMFCs with triple serpentine flow field performs better than PEMFCs with single and double serpentine flow fields.
    - A thin membrane (N212) offers less ohmic resistance than thick membrane (N112 and N117) and results in improvement in the cell performance.
    - Fuel cell performance was increased with increase in platinum loading from 0.6 to 1.0 mg/cm^2. Rate of increase in performance is more when the platinum loading increased from 0.6 to 0.8 mg/cm^2 than 0.8 to 1.0 mg/cm^2.
    - The increase in the cell temperature show positive influence on the fuel cells performance up to 70 ^{o}C and negative influence after 70 ^{o}C.
    - The increase in the anode gas humidification temperature indicated positive influence on the fuel cells performance up to 70 ^{o}C and negative influence after 70 ^{o}C.

- The increase in the cathode gas humidification temperature has positive influence on the fuel cells performance up to 60 ^{o}C and negative influence after 60 ^{o}C.
- PEMFC1 (49 cm^2) produced a peak power of 20.5 W at 0.5 V when the cell was operated at 70^{o}C cell temperature, 70^{o}C anode humidification temperature, 60^{o}C cathode humidification temperature, 400 ccm H_2 flow rate and 800 ccm O_2 flow rate.
- Similarly, PEMFC2 (84 cm^2) developed peak power of 33.2 W at 0.5 V when the cell was operated at 70^{o}C cell temperature, 70^{o}C anode humidification temperature, 60^{o}C cathode humidification temperature, 600 ccm H_2 flow rate and 1400 ccm O_2 flow rate.
- PEMFC3 (119 cm^2) generated a peak power of 44.5 W at 0.5 V when the cell was operated at 70^{o}C cell temperature, 70^{o}C anode humidification temperature, 60^{o}C cathode humidification temperature, 800 ccm H_2 flow rate and 1800 ccm O_2 flow rate.

From this study it is observed that the power density (418 mW/ cm^2 at 0.5 V) of smaller active area (49 cm^2) cell is higher than the larger active area viz. 84 and 119 cm^2 (395 mW/cm^2 and 374 mW/cm^2) fuel cells. From this investigation, it is concluded that instead of going for larger active area fuel cell, one can choose smaller active area cell with more number (i.e stack) of cells.

5.1 Scope for future work

In the present study the fuel cell with different active area, design and operating parameters were investigated. However, there is scope to investigate the parameters for the end use application of fuel cell.

- The effect porosity and thickness of gas diffusion layer can be analysed.
- The MEA of fuel cell other than Nafion membrane can be explored to reduce cost of fuel cell.
- The power electronic circuit can be designed for the PEM fuel cell to run the portable power devices.

REFERENCES

[1] A. Beicha and R. Zaamouche, "Electrochemical model for proton exchange membrane fuel cells systems," *J. Power Technol.*, vol. 93, no. 1, pp. 27–36, 2013.

[2] J. Larminie and A. Dicks, Fuel Cell Systems Explained, 2nd ed., *John Wiley & Sons Ltd, London,* 2003.

[3] D. D. Boettner, G. Paganelli, Y. G. Guezennec, G. Rizzoni, and M. J. Moran, "Proton Exchange Membrane Fuel Cell System Model for Automotive Vehicle Simulation and Control," *J. Energy Resour. Technol. Trans. ASME*, vol. 124, no. 1, pp. 20–27, 2002.

[4] H. Zhao and A. F. Burke, "Optimization of fuel cell system operating conditions for fuel cell vehicles," *J. Power Sources*, vol. 186, no. 2, pp. 408–416, 2009.

[5] M. Shichun, W. Xiaoen, T. Haolin, L. Peigang, L. Ming, P. Mu, and Y. RunZhang, "A Self-Humidifying Composite Membrane with Self-Assembled Pt Nanoparticles for Polymer Electrolyte Membrane Fuel Cells," *J. Electrochem. Soc.*, vol. 153, no. 10, pp. A1868–A1872, 2006.

[6] P. K. Das, X. Li, and Z. S. Liu, "A three-dimensional agglomerate model for the cathode catalyst layer of PEM fuel cells," *J. Power Sources*, vol. 179, no. 1, pp. 186–199, 2008.

[7] C. Lim and C. Y. Wang, "Effects of hydrophobic polymer content in GDL on power performance of a PEM fuel cell," *Electrochim. Acta*, vol. 49, no. 24, pp. 4149–4156, 2004.

[8] P. Choopanya and A, "Computational Fluid Dynamics Modelling of a Polymer Electrolyte Membrane Fuel Cell under Transient Automotive Operations," *PhD Thesis Univ. Sussex*, 2015.

[9] F. B. P. Ryan O'hare, Suk-Won Cha, Whitney G. Colella, *Fuel Cell Fundamentals*. .

[10] J. T. Pukrushpan, H. Peng, and A. G. Stefanopoulou, "Control-Oriented Modeling and Analysis for Automotive Fuel Cell Systems," *Trans. ASME*, vol. 126, no. March 2004, pp. 14–25, 2004.

[11] F. Barbir, "PEM Fuel Cells: Theory and Practice," *Elsevier Inc*, 2013.

[12] V. Gurau, F. Barbir, and H. Liu, "An Analytical Solution of a Half-Cell Model for

PEM Fuel Cells," *J. Electrochem. Soc.*, vol. 147, no. 7, p. 2468, 2000.

[13] D. M. Bernardi and M. W. Verbrugge, "A Mathematical Model of the Solid-Polymer-Electrolyte Fuel Cell," *J. Electrochem. Soc.*, vol. 139, no. 9, pp. 2477–2491, 1992.

[14] A. Parthasarathy, S. Srinivasan, a. J. Appleby, and C. R. Martin, "Temperature dependence of the electrode kinetics of oxygen reduction at the platinum/Nafion interface - A microelectrode investigation," *J. Electrochem. Soc.*, vol. 139, no. 9, pp. 2530–2537, 1992.

[15] J. C. Amphlett, R. F. Mann, B. A. Peppley, P. R. Roberge, and A Rodrigues, "A practical PEM fuel cell Model for Simulating Vehicle Power Sources," *Proceedings of the Tenth Annual Battery Conference on Applications and Advances, USA*, 1995.

[16] S. S. and C. E. C. Junbom Kim, Seong-Min Lee, "Modeling of Proton Exchange Membrane Fuel Cell Performance with an Empirical Equation," *J. Electrochem. Soc.*, vol. 142, no. 8, pp. 2670–2674, 1995.

[17] A. Kazim, H. T. Liu, and P. Forges, "Modelling of performance of PEM fuel cells with conventional and interdigitated flow fields," *J. Appl. Electrochem.*, vol. 29, no. 12, pp. 1409–1416, 1999.

[18] R. F. Mann, J. C. Amphlett, M. a. I. Hooper, H. M. Jensen, B. a. Peppley, and P. R. Roberge, "Development and application of a generalised steady-state electrochemical model for a PEM fuel cell," *J. Power Sources*, vol. 86, no. 1–2, pp. 173–180, 2000.

[19] M. W. Fowler, R. F. Mann, J. C. Amphlett, B. A. Peppley, and P. R. Roberge, "Incorporation of voltage degradation into a generalised steady state electrochemical model for a PEM fuel cell," *J. Power Sources*, vol. 106, no. 1–2, pp. 274–283, 2002.

[20] Q. Wang, D. Song, T. Navessin, S. Holdcroft, and Z. Liu, "A mathematical model and optimization of the cathode catalyst layer structure in PEM fuel cells," *Electrochim. Acta*, vol. 50, no. 2–3 SPEC. ISS., pp. 725–730, 2004.

[21] S Dutta, S Shimpalee, Van Zee "Three Dimensional numerical simulation of straight channel PEM Fuel Cells," *J. Appl. Electrochem.*, vol. 30, no. 2, pp. 135–146, 2000.

[22] T. Berning, D. M. Lu, and N. Djilali, "Three-dimensional computational analysis of transport phenomena in a PEM fuel cell," *J. Power Sources*, vol. 106, no. 1, pp. 284–294, 2002.

[23] A. Kumar and R. G. Reddy, "Effect of channel dimensions and shape in the flow-field distributor on the performance of polymer electrolyte membrane fuel cells," *J. Power Sources*, vol. 113, no. 1, pp. 11–18, 2003.

[24] T. Berning and N. Djilali, "Three-dimensional computational analysis of transport phenomena in a PEM fuel cell - A parametric study," *J. Power Sources*, vol. 124, no. 2, pp. 440–452, 2003.

[25] P. T. Nguyen, T. Berning, and N. Djilali, "Computational model of a PEM fuel cell with serpentine gas flow channels," *J. Power Sources*, vol. 130, no. 1–2, pp. 149–157, 2004.

[26] K. W. Lum and J. J. McGuirk, "Three-dimensional model of a complete polymer electrolyte membrane fuel cell – model formulation, validation and parametric studies," *J. Power Sources*, vol. 143, no. 1–2, pp. 103–124, 2005.

[27] Y. Lin and S. B. Beale, "Numerical predictions of transport phenomena in a proton exchange membrane fuel cell," *J. Fuel Cell Sci. Technol.*, vol. 2, no. 4, pp. 213–218, 2005.

[28] W.M. Yan, H.C. Liu, C.Y. Soong, F.Chen, and C.H. Cheng, "Numerical study on cell performance and local transport phenomena of PEM fuel cells with novel flow field designs," *J. Power Sources*, vol. 161, no. 2, pp. 907–919, 2006.

[29] Wei Mon Yan, Hung Yi Li, Wei Che Tsai"Three-Dimensional Analysis of PEMFCs with Different Flow Channel Designs," *J. Electrochem. Soc.*, vol. 153, no. 10, p. A1984, 2006.

[30] X. Liu, W. Tao, Z. Li, and Y. He, "Three-dimensional transport model of PEM fuel cell with straight flow channels," *J. Power Sources*, vol. 158, no. 1, pp. 25–35, 2006.

[31] J.-H. Jang, W.-M. Yan, H.-Y. Li, and W.-C. Tsai, "Three-dimensional numerical study on cell performance and transport phenomena of PEM fuel cells with conventional flow fields," *Int. J. Hydrogen Energy*, vol. 33, no. 1, pp. 156–164, 2008.

[32] Sadiq Al-Baghdadi, "Three-dimensional computational fluid dynamics model of a tubular-shaped PEM fuel cell," *Renew. Energy*, vol. 33, no. 6, pp. 1334–1345, 2008.

[33] X.D. Wang, Y.Y. Duan, W.M. Yan, and F.B Weng, "Effects of flow channel geometry on cell performance for PEM fuel cells with parallel and interdigitated flow fields,"

Electrochim. Acta J., vol. 53, pp. 5334–5343, Jan. 2008.

[34] W.C. Weng, W.M. Yan, H.Y. Li, and X.-D. Wang, "Numerical Simulation of Cell Performance in Proton Exchange Membrane Fuel Cells with Contracted Flow Field Design," *J. Electrochem. Soc.*, vol. 155, no. 9, pp. B877–B886, 2008.

[35] B. Rismanchi and M. H. Akbari, "Performance prediction of proton exchange membrane fuel cells using a three-dimensional model," *Int. J. Hydrogen Energy*, vol. 33, no. 1, pp. 439–448, 2008.

[36] X.D. Wang, X. Zhang, T. Liu, Y.Y. Duan, W.M. Yan, and D.J. Lee, "Channel geometry effect for proton exchange membrane fuel cell with serpentine flow field using a three-dimensional two-phase model.," *J. Fuel Cell Sci. Technol.*, vol. 7, no. 5, p. 051019/1-051019/9, 2010.

[37] A. P. Manso, F. F. Marzo, M. G. Mujika, J. Barranco, and A. Lorenzo, "Numerical analysis of the influence of the channel cross-section aspect ratio on the performance of a PEM fuel cell with serpentine flow field design," *Int. J. Hydrogen Energy*, vol. 36, no. 11, pp. 6795–6808, 2011.

[38] D. Juarez-Robles, A. Hernandez-Guerrero, B. Ramos-Alvarado, F. Elizalde-Blancas, and C. E. Damian-Ascencio, "Multiple concentric spirals for the flow field of a proton exchange membrane fuel cell," *J. Power Sources*, vol. 196, no. 19, pp. 8019–8030, 2011.

[39] K.S. Choi, H.M. Kim, and S.M. Moon, "Numerical studies on the geometrical characterization of serpentine flow-field for efficient PEMFC," *Int. J. Hydrogen Energy*, vol. 36, no. 2, pp. 1613–1627, 2011.

[40] I. Khazaee and M. Ghazikhani, "Three-Dimensional Modeling and Development of the New Geometry PEM Fuel Cell," *Arab. J. Sci. Eng.*, vol. 38, no. 6, pp. 1551–1564, 2013.

[41] J. M. Sierra, S. J. Figueroa-Ramirez, S. E. Diaz, J. Vargas, P. J. Sebastian, "Numerical evaluation of a PEM fuel cell with conventional flow fields adapted to tubular plates," *Int. J. Hydrogen Energy*, vol. 39, pp. 1–12, 2014.

[42] S. H. Han, N. H. Choi, and Y. D. Choi, "Performance and flow characteristics of large-sized PEM fuel cell having branch channel," *Int. J. Hydrogen Energy*, vol. 40, no. 14, pp. 4819–4829, 2015.

[43] N. Limjeerajarus and P. Charoen-Amornkitt, “Effect of different flow field designs and number of channels on performance of a small PEFC,” *Int. J. Hydrogen Energy*, vol. 40, no. 22, pp. 7144–7158, 2015.

[44] L. Rostami, P. Mohamad, G. Nejad, and A. Vatani, “A numerical investigation of serpentine fl ow channel with different bend sizes in polymer electrolyte membrane fuel cells,” *Energy*, vol. 97, pp. 400–410, 2016.

[45] A. L. R. Paulino, E. F. Cunha, E. Robalinho, M. Linardi, I. Korkischko, and E. I. Santiago, “CFD Analysis of PEMFC Flow Channel Cross Sections,” *Fuel Cells*, no. 0, pp. 1–10, 2017.

[46] T. V Nguyen, “A gas distributor design for proton-exchange-membrane fuel cells,” *J. Electrochem. Soc.*, vol. 143, no. 5, pp. L103–L105, 1996.

[47] A. Kazim, P. Forges, and H. T. Liu, “Effects of cathode operating conditions on performance of a PEM fuel cell with interdigitated flow fields,” *Int. J. Energy Res.*, vol. 27, no. 4, pp. 401–414, 2003.

[48] A. Kumar and R. G. Reddy, “Effect of gas flow-field design in the bipolar/end plates on the steady and transient state performance of polymer electrolyte membrane fuel cells,” *J. Power Sources*, vol. 155, no. 2, pp. 264–271, 2006.

[49] L. Sun, P. H. Oosthuizen, and K. B. McAuley, “A numerical study of channel-to-channel flow cross-over through the gas diffusion layer in a PEM-fuel-cell flow system using a serpentine channel with a trapezoidal cross-sectional shape” *Int. J. Therm. Sci.*, vol. 45, no. 10, pp. 1021–1026, 2006.

[50] S. Shimpalee, S. Greenway, and J. W. Van Zee, “The impact of channel path length on PEMFC flow-field design,” *J. Power Sources*, vol. 160, no. 1, pp. 398–406, 2006.

[51] A. Su, F.-B. Weng, P.-H. Chi, S.-M. Lu, G.-B. Jung, C. H. Tu, and Y.-M. Ferng, “Effect of channel step-depth on the performance of proton exchange membrane fuel cells,” *Proc. Inst. Mech. Eng. Part A J. Power Energy*, vol. 221, pp. 617–625, 2007.

[52] K. Hongthong, K. Pruksathorn, P. Piumsomboon, and P. Sripakagorn, “Effect of the geometry and pattern of the flow channel on the performance of polymer electrolyte membrane fuel cell,” *Korean J. Chem. Eng*, vol. 24, no. 4, pp. 612–617, 2007.

[53] M. A. R. S. Al-baghdadi and H. A. K. S. Al-janabi, “Numerical analysis of a proton

exchange membrane fuel cell . Part 2 : parametric study," *J. Power Energy*, vol. 221, pp. 931–940, 2007.

[54] Y. M. Ferng and A. Su, "A three-dimensional full-cell CFD model used to investigate the effects of different flow channel designs on PEMFC performance," *Int. J. Hydrogen Energy*, vol. 32, no. 17, pp. 4466–4476, 2007.

[55] W. M. Yan, H. Y. Li, P. C. Chiu, and X. D. Wang, "Effects of serpentine flow field with outlet channel contraction on cell performance of proton exchange membrane fuel cells," *J. Power Sources*, vol. 178, no. 1, pp. 174–180, 2008.

[56] Jeon, S. Greenway, S. Shimpalee, "The effect of serpentine flow-field designs on PEM fuel cell performance," *Int. J. Hydrogen Energy*, vol. 33, pp. 1052–1066, 2008.

[57] C.-H. Min, "Performance of a proton exchange membrane fuel cell with a stepped flow field design," *J. Power Sources*, vol. 186, no. 2, pp. 370–376, 2009.

[58] A. Iranzo, M. Munoz, E. Lopez, J. Pino, and F. Rosa, "Experimental fuel cell performance analysis under different operating conditions and bipolar plate designs," *Int. J. Hydrogen Energy*, vol. 35, no. 20, pp. 11437–11447, 2010.

[59] J. G. Carton and A. G. Olabi, "Design of experiment study of the parameters that affect performance of three flow plate configurations of a proton exchange membrane fuel cell," *Energy*, vol. 35, no. 7, pp. 2796–2806, 2010.

[60] S. Bansode, T. Sundararajan, and S. K. Das, "Computational and Experimental Studies on the Effect of Flow-Distributors on the Performance of PEMFC," *J. Fuel Cell Sci. Technol.*, vol. 7, no. 5, p. 051014, 2010.

[61] Xiao-Dong Wang, Wei-Mon Yan, Yuan-Yuan Duan, Fang-Bor Weng, Guo-Bin Jung, "Numerical study on channel size effect for proton exchange membrane fuel cell with serpentine flow field," *Energy Convers. Manag.*, vol. 51, no. 5, pp. 959–968, 2010.

[62] É. Fontana, E. Mancusi, A. Da Silva, V. C. Mariani, A. A. Ulson De Souza, "Study of the effects of flow channel with non-uniform cross-sectional area on PEMFC species and heat transfer," *Int. J. Heat Mass Transf.*, vol. 54, pp. 4462–4472, 2011.

[63] W.M. Yan, X.D. Wang, D.J. Lee, X.X. Zhang, Y.F. Guo, and A. Su, "Experimental study of commercial size proton exchange membrane fuel cell performance," *Appl. Energy*, vol. 88, pp. 392–396, 2011.

[64] P. V. Suresh, S. Jayanti, A. P. Deshpande, and P. Haridoss, “An improved serpentine flow field with enhanced cross-flow for fuel cell applications,” *Int. J. Hydrogen Energy*, vol. 36, no. 10, pp. 6067–6072, 2011.

[65] H.C. Chiu, J.H. Jang, W.M. Yan, H.Y. Li, and C.C. Liao, “A three-dimensional modeling of transport phenomena of proton exchange membrane fuel cells with various flow fields,” *Appl. Energy*, vol. 96, pp. 359–370, 2012.

[66] J.-Y. Jang, C.-H. Cheng, W.-T. Liao, Y.-X. Huang, and Y.-C. Tsai, “Experimental and numerical study of proton exchange membrane fuel cell with spiral flow channels,” *Appl. Energy*, vol. 99, pp. 67–79, 2012.

[67] N. B, Sreenivasulu, G, Vasu, V, Dharma Rao, SV, “Effect of Back Pressure and Flow Geometry on PEM Fuel Cell Performance-An Experimental Study,” *Int. J. Appl. Sci. Eng.*, vol. 11, no. 1, pp. 1–11, 2013.

[68] H. Liu, P. Li, D. Juarez-Robles, K. Wang, and A. Hernandez-Guerrero, “Experimental Study and Comparison of Various Designs of Gas Flow Fields to PEM Fuel Cells and Cell Stack Performance,” *Front. Energy Res.*, vol. 2, no. 2, pp. 1–8, 2014.

[69] I. Khazaee, “Experimental investigation and numerical comparison of the performance of a proton exchange membrane fuel cell at different channel geometry,” *Heat Mass Transf.*, vol. 51, no. 8, pp. 1177–1187, 2015.

[70] A. Torkavannejad, H. Sadeghifar, N. Pourmahmoud, and F. Ramin, “Novel architectures of polymer electrolyte membrane fuel cells: Efficiency enhancement and cost reduction,” *Int. J. Hydrogen Energy*, vol. 40, no. 36, pp. 12466–12477, 2015.

[71] A. Iranzo, J. Biesdorf, M. Cochet, A. Salva, P. Boillat, and F. Rosa, “Effect of Serpentine Multi-pass Flow Field Channel Orientation in the Liquid Water Distributions and Cell Performance,” *Fuel Cells*, vol. 16, no. 6, pp. 777–783, 2016.

[72] W. Li, Q. Zhang, C. Wang, X. Yan, S. Shen, G. Xia, F. Zhu, and J. Zhang, “Experimental and numerical analysis of a three-dimensional flow field for PEMFCs,” *Appl. Energy*, vol. 195, pp. 278–288, 2017.

[73] L. Wang, A. Husar, T. Zhou, and H. Liu, “A parametric study of PEM fuel cell performances,” *Int. J. Hydrogen Energy*, vol. 28, no. 11, pp. 1263–1272, 2003.

[74] L. Wang and H. Liu, “Performance studies of PEM fuel cells with interdigitated flow

fields," *J. Power Sources*, vol. 134, no. 2, pp. 185–196, 2004.

[75] S. Hsieh, S. Yang, J. Kuo, C. Huang, and H. Tsai, "Study of operational parameters on the performance of micro PEMFCs with different flow fields," *Energy Convers. Manag.*, vol. 47, pp. 1868–1878, 2006.

[76] W.M. Yan, C.H. Yang, C.Y. Soong, F. Chen, and S.C. Mei, "Experimental studies on optimal operating conditions for different flow field designs of PEM fuel cells," *J. Power Sources*, vol. 160, no. 1, pp. 284–292, 2006.

[77] M. Amirinejad, S. Rowshanzamir, and M. H. Eikani, "Effects of operating parameters on performance of a proton exchange membrane fuel cell," *J. Power Sources*, vol. 161, no. 2, pp. 872–875, 2006.

[78] W. Yu, S. Wu, and S. Shiah, "Parametric analysis of the proton exchange membrane fuel cell performance using design of experiments," *Int. J. Hydrogen Energy*, vol. 33, no. 9, pp. 2311–2322, 2008.

[79] W. M. Yan, X. D. Wang, S. S. Mei, X. F. Peng, Y. F. Guo, and A. Su, "Effects of operating temperatures on performance and pressure drops for a 256 cm2 proton exchange membrane fuel cell: An experimental study," *J. Power Sources*, vol. 185, no. 2, pp. 1040–1048, 2008.

[80] M. Tohidi, S. H. Mansouri, and H. Amiri, "Effect of primary parameters on the performance of PEM fuel cell," *Int. J. Hydrogen Energy*, vol. 35, no. 17, pp. 9338–9348, 2010.

[81] F. Ting, C. Hsieh, W. Weng, and J. Lin, "Effect of operational parameters on the performance of PEMFC assembled with Au-coated Ni-foam," *Int. J. Hydrogen Energy*, vol. 37, no. 18, pp. 13696–13703, 2012.

[82] N. M. Zahari and A. A. Aziz, "Effect of platinum catalyst loading on membrane electrode assembly (MEA) in proton exchange membrane fuel cell (PEMFC)," in *10th IEEE International Conference on Semiconductor Electronics, ICSE 2012 - Proceedings*, 2012, pp. 669–673.

[83] A. C. Okafor and H.-M. Mogbo, "Effects of gas flow rate and catalyst loading on polymer electrolyte membrane (PEM) fuel cell performance and degradation," *Proc. ASME 2010 Eighth Int. Fuel Cell Sci. Eng. Technol. Conf. June 14-16, 2010, Brooklyn, New York, USA*, pp. 1–11.

[84] Y.Q. Meng, C. Wang, Q.L. Zhang, S.Y. Shen, Z. Feng-Juan, Y. Hong, and J.L. Zhang, "The Effects of Cathode Platinum Loading and Operating Backpressure on PEMFC Performance," *Acta Phys. -Chim. Sin.*, vol. 32, no. 6, pp. 1460–1466, 2016.

[85] P. Gazdzicki, J. Mitzel, A. M. Dreizler, M. Schulze, and K. A. Friedrich, "Impact of Platinum Loading on Performance and Degradation of Polymer Electrolyte Fuel Cell Electrodes Studied in a Rainbow Stack," *Fuel Cells*, no. 0, pp. 1–9, 2017.

[86] C.H. Chen, C.H. Chen, and T.Y. Chen, "The numerical study of geometric influence of flow channel patterns on performance of proton exchange membrane fuel cells.," *J. Fuel Cell Sci. Technol.*, vol. 9, no. 2, p. 021015/1-021015/17, 2012.

[87] P. K. Takalloo, E. S. Nia, and M. Ghazikhani, "Numerical and experimental investigation on effects of inlet humidity and fuel flow rate and oxidant on the performance on polymer fuel cell," *Energy Convers. Manag.*, vol. 114, pp. 290–302, 2016.

[88] D. N. Ozen, B. Timurkutluk, and K. Altinisik, "Effects of operation temperature and reactant gas humidity levels on performance of PEM fuel cells," *Renew. Sustain. Energy Rev.*, vol. 59, pp. 1298–1306, 2016.

[89] N. Pourmahmoud, S. Rezazadeh, I. Mirzaee, and V. Heidarpoor, "Three-dimensional numerical analysis of proton exchange membrane fuel cell," *J. Mech. Sci. Technol.*, vol. 25, no. 10, pp. 2665–2673, 2011.

[90] J. A. Salva, A. Iranzo, F. Rosa, and E. Tapia, "Validation of cell voltage and water content in a PEM (polymer electrolyte membrane) fuel cell model using neutron imaging for different operating conditions," *Energy*, vol. 101, pp. 100–112, 2016.

[91] S. Shimpalee and J. W. Van Zee, "Numerical studies on rib & channel dimension of flow-field on PEMFC performance," *Int. J. Hydrogen Energy*, vol. 32, no. 7, pp. 842–856, 2007.

[92] A. Iranzo, M. Muñoz, F. Rosa, and J. Pino, "Numerical model for the performance prediction of a PEM fuel cell. Model results and experimental validation," *Int. J. Hydrogen Energy*, vol. 35, no. 20, pp. 11533–11550, 2010.

[93] A. Iranzo, F. Rosa, and J. Pino, "A simulation tool for geometrical analysis and optimization of fuel cell bipolar plates: Development, validation and results," *Energies*, vol. 2, no. 3, pp. 582–594, 2009.

Appendix

List of publications

World Journal of Engineering 12(6) (2015) 591-606

World Journal of Engineering

Review on challenges of direct liquid fuel cells for portable application

Venkateswarlu Velisala*, G. Naga Srinivasulu, B. Srinivasa Reddy and K. Venkata Koteswara Rao

Department of Mechanical Engineering, National Institute of Technology, Warangal, 506004, India

**E-mail: 2venkee@gmail.com*

(Received 29 June 2015; Accepted 29 September 2015)

Abstract

Fuel cells technologies are the most promising green energy technologies for diverse applications. One of the fastest growing areas is the portable electronic applications where the power range is the order of 1–100 W. For most of the portable electronic devices, rechargeable battery is the major energy source. Due to limitations like limited capacity, requirement of external power for recharge have led many researchers to look for alternative power sources to power portable electronic devices. The high energy density of fuel cells makes them very attractive alternative to batteries for portable power applications. There are a variety of fuel cell technologies being considered to replace batteries in portable electronic equipment. Direct Liquid Fuel Cells (DLFCs) have attracted much attention due to their potential applications as a power source for portable electronic devices. The advantages of DLFCs over hydrogen fed PEM fuel cells include a higher theoretical energy density and efficiency, a more convenient handling of the streams, and enhanced safety. Unlike batteries, fuel cells need not be recharged, merely refueled. This paper provides an overview on challenges of DLFCs (Direct Liquid Fuel Cells), like fuel crossover, cost, durability, water management, weight and size along with approaches being investigated to solve these challenges. Portable Fuel Cell Commercialization Targets for future and producers of portable fuel cells across the globe are also discussed in this paper.

Key words: *Green energy, Portable electronic devices, Battery, Direct Liquid fuel cell, Challenges*

1. Introduction

Energy needs for portable electronic devices such as laptop, smartphone, and other broadband mobile computing are rising rapidly in the past few years due to the increasing their functionalities. The major energy source for most of portable electronic devices is the rechargeable battery. The disadvantage of using a rechargeable battery as a power source is the battery needs an external electrical power source to recharge, and this is a limitation to the mobility of the device because it can only be used with an electrical power source and has limited battery capacity. In remote areas, where no availability of electric power, charging for battery is a problem. These disadvantages of rechargeable batteries have led many researchers to look for alternative power sources to replace the battery technology. As an alternative to battery, fuel cell

ISSN:1708-5284

may be considered as best suited power source for powering portable electronic devices due to practical advantages such as high-energy density, light weight, compactness, simplicity as well as easy and fast recharging via a replacement or a refilled fuel cartridge. The ability of the fuel cell is to provide more energy from the same volume over battery power systems. Small fuel cells normally produce power between 0.5 and 100 W, which is sufficient for portable electronic devices. Fuel cells working with liquid fuels, like methanol, ethanol or formic acid, are closer to practical application in the range of 1–100W. Table 1 gives the Properties of some state of the art portable systems, including size, power requirement, power supply characteristics and autonomy.

For portable applications, Direct Liquid fed Fuel Cell (DLFC) is the most promising fuel cell technology (Klaus *et al*., 2003). Liquid fuels such as Methanol, Ethanol, Formic Acid and Borohydride solutions can be used as fuels for DLFCs without reforming process. DMFCs have 5–10 times higher energy densities than batteries, can operate for a longer time. But the problems with DMFCs are fuel crossover, slower anode electrochemical oxidation of methanol and cost of the components of fuel cell (Kamarudin *et al*., 2009).

Ethanol is also an attractive and promising fuel in DLFCs for portable fuel cell applications due to its: (i) non-toxicity, (ii) natural availability, (iii) renewability and (iv) higher power density. The current direct ethanol fuel cell (DEFC) technologies are able to meet the two important features: efficiency and total operation cost in order to realize the DEFC into commercialization. The well-known sluggish anode electro catalyst activities are at relatively low temperature (20°C – 120°C) due to problem in C-C bond breaking which lead to the low performance remains as the major technological problem. Another major issues facing by DEFC is ethanol permeated through membrane caused mixed potential effects at cathode which lead to reduce cathode performance and fuel utilizations. Another critical obstacle that limits the wide application of acid DEFCs is the cost:

Table 1.
Properties of some state-of-the-art portable systems, including size, power consumption, power supply characteristics and autonomy (Fernandez *et al*., 2013)

Class	Device	Device dimensions (cm^3)	Power requirements	Battery characteristics	Battery dimensions (cm^3)	Power density (Whl^{-1})	Autonomy
Medical implantable	Pace maker	5 × 5 × 0.6	25 μJ/pulse	Lithium iodine 2 Ah @ 2.2 V 0.15 Wh	0.5	300	5–7 years
	Defibrillator	6 × 5 × 1.5	15–40J/ pulse	Lithium silver vanadium oxide 1 Ah @ 2.8 V	0.5	600	3–5 years
	Cochlear implant	5	8 mA DC + 24 mA (pulse 100 ms)	Zn air 0.49 Ah @ 1.05 V	0.56	920	45 h
Medical	Hearing aid	2	5 mA cc + 15 mA (100 ms)	Zn air 0.6 Ah @ 1.05 V	0.5	1260	300 h
	Insulin pump	70	10 mW	Zn/MnO^2 (alkal ine) 2.5 Ah@1.5 V	8	470	400 h
Portable electronics	Smart phone	10 × 7 × 0.7	2 W	Li-ion 1.2 Ah @ 3.7 V	5 × 5 × 0.3	600	6 h
	Video camera	10 × 4 × 5	7 W	Li-ion 1.8 Ah @ 3.6 V	2 × 3 × 4	270	1 h
	Laptop	20 × 20 × 2	40 W	Li-ion 1.4 Ah @ 3.7 V	20 × 5 × 2	235	6 h
Toys	Car	20 × 20 × 5	5–15 W	Ni mh (× 6) 1.2 Ah @ 1.2 V	5 × 14 × 2	30	0.5 h
	Airplane	20 × 20 × 5 (1 kg)	110 W/kg	Ni mh, Ni Cd 1.7 Ah @ 1.2 V	5 × 14 × 2	15	0.3 h

acid electrolyte membranes (typically Nafion® material) are expensive; and a considerable amount of precious Pt is needed to achieve decent performance in acid DEFCs (Li *et al*., 2009).

Direct Formic Acid fuel cells (DFAFCs) are also promising alternatives to hydrogen fed PEMFCs. Very high-power densities have been achieved in direct formic acid fuel cell (DFAFC) systems. DFAFCs also faces several challenges, the most important of these challenges are poor anodic reaction kinetics compared to hydrogen, and fuel crossover. The primary challenge is the tendency for formic acid oxidation to proceed through a –CO-type intermediate, a species that poisons Pt-based catalyst matervials. The second challenge is crossover of fuel, formic acid diffuses from the anode, through the membrane to the cathode. At the cathode, the fuel can react directly with oxygen, creating unwanted heat without producing electricity, thus reducing the overall fuel efficiency of the system.

Sodium borohydride aqueous solution also an interesting alternative as a liquid fuel for fuel cells. Direct borohydride fuel cell (DBFC) uses a sodium borohydride ($NaBH_4$) solution as fuel, and electricity is produced. A direct borohydride fuel cell (DBFC) is a device that converts chemical energy stored in borohydride ion (BH_4^-) and an oxidant directly into electricity by redox processes. DBFC is similar to PEMFC and DMFC according to the usage of membrane electrolyte, similar to AFC because of its alkaline media, and similar to DMFC according to the usage of liquid fuel. Compared with other fuel cells, a DBFC has many advantageous features such as high open circuit potential, ease of electro-oxidation of BH_4^- on non-precious metals such as nickel, low operational temperature, high power density, low fuel crossover, and safety because it eliminates hydrogen storage problem (Celik *et al*., 2008). Hydrogen evolution due to the hydrolysis reaction during operation not only decreases the fuel utilization but also causes some problems in the system designing. In addition to this, BH_4^- crossover, NaOH accumulation at the cathode and $NaBO_2$ accumulation at the anode are other problems that need to be solved (Park *et al*., 2006).

2. Challenges

2.1. Fuel crossover

A common challenge for any direct liquid fuel cell is fuel crossover. In order to encourage the development of DLFC system this challenge need to be solved. For any type of PEM-based fuel cell, the fuel fed to the anode, can permeate to the cathode through membrane. To examine and quantify the fuel crossover behavior in DLFCs a number of studies were conducted (Rhee *et al*., 2003; Wang *et al*., 2004; Song *et al*., 2005;Liu *et al*.,2006; Jeong *et al*., 2007). High concentration of liquid fuel provides higher achievable energy density, but it also causes severe fuel crossover to the electrolyte membrane, it is a very serious problem that severely reduces cell voltage, current density, fuel utilization, and hence cell performance. The rate of crossover decreases with increasing current density, due to higher rate of fuel consumption at the anode (Yu *et al*., 2008). Several approaches have been proposed to reduce fuel crossover in DLFCs during the last decade. One common approach to reduce fuel crossover is the development of new proton conducting membranes with low fuel permeability and high proton conductivity, e.g. the acid-doped polybenzimidazole (PBI), sulfonated-poly (arylene ether ketone)s (SPAEKs), sulfonated-poly(ether sulfone)s (SPES), polyamides, sulfonated-polyimide (SPI), etc (Kerres., 2001; Wan and Lin., 2013). Another approach is the modification of Nafion membranes to make them suitable for DLFC utilization. Another approach is forming hybrid membranes by blending different types of polymers, such as the one being done with zirconium and phosphate, it is shown that the inorganic compound reduces the methanol permeability while the phosphate layer allows for more water to permeate rather than methanol (Bauer and Porada, 2004). Chien *et al*. (2013) developed a low methanol-crossover sulfonated graphene oxide (SGO)/Nafion composite membrane by simply blending well-exfoliated $SGO_{(aq)}$ and Nafion. In the DMFCs test, the SGO/ Nafion composite membrane exhibited performance superior to the commercial membrane Nafion 115 in 1 M and 5 M methanol solutions. SGO is a promising material for reducing methanol crossover and shows great potential for commercial applications. SPEEK is considered one of the most promising candidates for replacing Nafion because it offers lower cost, easier preparation, controllable conductivity, excellent chemical-thermal stability and low methanol crossover (Zhong *et al*., 2008; Tirupathi and Shahi, 2009; Gosalawit *et al*., 2009; Ismail *et al*., 2009; Lin *et al*., 2009). The assembly of Palladium nano-particles onto the Nafion membrane surface yields a good result in reducing methanol crossover up to 8 orders of magnitude compared to

the unmodified membrane, and with no reduction in its ionic conductivity. The results demonstrate the promises of the application of such Pd-PDDA nano-particle self-assembled Nafion™ membrane in DMFC (Tang *et al*., 2005). Thiam *et al* (2013) adopted Palladium–silica nanofibres (Pd–SiO_2 fibre) as an additive to Nafion recast membranes in order to reduce methanol crossover and improve the cell performance. PVA has a good resistance to methanol permeability, but has low conductivity (Bhat *et al*., 2009; Yang *et al*., 2009; Huang *et al*., 2009). The performance of cells with double-layer membranes suggests they have promising applications in DMFCs when compared to SPEEK and PVA in single membrane cells (Yang *et al*., 2008; Maab *et al*., 2009). Abdelkareem and Nakagawa (2006) employed a hydrophobic porous carbon plate and a 2 mm gap between the fuel reservoir and the MEA as a methanol barrier layer and significantly reduced methanol crossover. Zhang and Hsing (2007) adopted a flexible graphite plate between the flow channel and the MEA in an active liquid feed DMFC to decrease the methanol crossover. Yuan *et al*. (2014) developed a novel methanol-blocking membrane prepared by layer-by-layer assembly of poly (diallyldimethylammonium chloride) (PDDA) and graphene oxide (GO) nanosheets onto the surface of Nafion® membrane. This PDDA-GO multilayer onto the Nafion film not only reduces the methanol crossover but also enhances the membrane strength. Yuan *et al*. (2013) fabricated a porous metal fiber sintered felt (PMFSF) as the anodic methanol barrier to control methanol crossover (MCO) in order to feed the fuel cell with a higher concentration of methanol fuel for a passive air-breathing direct methanol fuel cell (PAB-DMFC). This PMFSF helps greatly reduce the effects of methanol crossover. Wan and Lin (2013) proposed a new approach to mitigate methanol crossover, they prepared a composite membrane with a 5 bi-layers of poly (allylamine hydrochloride) (PAH)/polystyrene sulfonic acid sodium salt (PSS) containing Pt_{35}–Ru_{65} catalyst are self-assembled on the Nafion membrane surface through the layer-by-layer technique. A layer of Pt_{35}–Ru_{65} with a thickness of 87.5 nm deposited on Nafion acts as a methanol barrier. MEA with self-assembled Pt_{35}–Ru_{65} layers suppresses methanol crossover by 22% and improves power density by 48% (at 0.30 V) at 80°C.

Ethanol crossover remains the main issue that impedes the widespread use and application of DEFCs. Ethanol is well known for having a lower crossover rate and affecting cathode performance less severely than methanol because of its lower permeability through the Nafion membrane and its slower electrochemical oxidation kinetics on the Pt/C cathode (Song *et al*., 2005). The negative effects of ethanol crossover include decreasing the cathode potential and cathode depolarization (Kamarudin *et al*., 2013). The overall efficiency of direct ethanol fuel cells will decrease due to ethanol crossover. It also results in wasting fuel while in operation (Xu *et al*., 2011; Thiam *et al*., 2011). At the same time, the permeated ethanol and its oxidation intermediate products have the potential to poison the cathode catalyst (Song *et al*., 2007). Ethanol crossover rate is affected by temperature, current densities and feed concentration. The ethanol crossover rate increases with temperature, current densities and feed concentrations. Ethanol crossover occurs when ethanol passes through the membrane and reacts with oxygen at the cathode to produce acetic acid, which is eventually delivered back to the anode (James and Pickup, 2010). The main approach to solve this problem is through modification of the membrane as the core of the DEFC. The rate of ethanol crossover depends on the ethanol concentration in the anode catalyst layer (CL). Thus, feeding a diluted ethanol solution may help prevent ethanol crossover, but this may result in specific energy losses in the DEFC system. Andreadis *et al*. (2006) developed a mathematical model to describe ethanol behavior and its influencing factors in the DEFC. The model showed that the crossover rate increased linearly with the inlet ethanol concentration up to the maximum value of 10.0 M. The parasitic current formation at the cathode depended on the ethanol crossover and was greater at low current density. Another factor was that increasing the porosity of the diffusion and catalyst layers also increased the ethanol crossover rate as well as parasitic formation. Kontou *et al*. (2007) done experiments using a Nafion 115-based MEA received same findings for the ethanol permeation rate at various ethanol concentrations. A mathematical model developed by Suresh and Jayanti (2011) to examine the effect of operating current density on ethanol crossover for various ethanol feed concentrations. Maab and Nunes (2010) have used modified (sulfoneated poly (ether ether ketone)) SPEEK membranes. They suggested two methods to prepare effective SPEEK membranes that may reduce the crossover problem. The first method is coating the SPEEK with a

carbon molecular sieves (CMS) layer, and the second is making SPEEK/PI (polyimide) blends. They compared the results of CMS-coated SPEEK and the SPEEK/PI blends, the SPEEK/PI blends have exhibited better performance. Wan and Chen (2009) prepared a composite anode containing a thin layer of Pt_{50}–Sn_{50} nanoparticles on Nafion membrane surface does suppress the ethanol crossover up to 17% and improve the performance up to 6% (average value) at 80°C. Battirola *et al*. reduced ethanol crossover by using doped-Nafion® 117 membranes with Pt and Pt-Ru nanoparticles. Rhee *et al*. (2003) studied the permeation of formic acid through Nafion 112 and Nafion 117 membranes at room temperature, the permeation of formic acid is higher through Nafion® 112 (50 μm) than through the thicker 180 μm Nafion® 117.

Crossover of BH_4^- can be solved by developing membrane electrolytes with high BH_4^- resistivity and cathode catalysts with high selectivity for electro-reduction of oxidant and high tolerance towards borohydride electro-oxidation (Ma *et al*., 2010). Raman and Shukla (2007) used Nafion 961 membrane to reduce borohydride crossover, from anodic to cathodic compartments of the cell, instead of Nafion 117. Li *et al*. (2003) developed a DBFC anode made of a Zr-Ni alloy, a cathode made of Pt/C, Nafion 117 as membrane and compared with Nafion 112 membrane, Nafion 117 membrane demonstrated a considerable resistance to borohydride crossover and resulted in acceptable cell performance. Suda (2002) mitigated the BH_4^- crossover problem by adopting a fuel cell structure using Nafion membrane as electrolyte to separate the fuel from the cathode. Ma *et al*. (2012) modified a cost-effective and eco-friendly chitosan membrane by phosphate or triphosphate salt, chitosan triphosphate (CsTP) membrane demonstrates lower BH_4^- crossover rate than chitosan phosphate (CsP) membrane.

2.2. Cost

The cost of fuel cell system must be reduced before they can be competitive with conventional technologies. Fuel cell costs can be broken into three areas: the material and component costs, labor (i.e. design, fabrication, and transport), and capital cost of the manufacturing equipment (Marcinkoski *et al*., 2011). Only labor and capital costs can be reduced through mass-manufacturing. Material and component costs, such as catalysts, membrane and bipolar plates are dependent on technological innovations and the market (Sun *et al*., 2011; Odeh *et al*., 2013). The manufacturers of fuel cells have to continue to collect subsidies from governments to scale these units up for commercial applications with limited success because of the challenges of cost, durability, robustness or reliability. One method of reducing costs is to develop Low cost, high-performance membranes, high-performance catalysts enabling ultra-low precious metal loading, and lower cost, lighter, corrosion-resistant bipolar plates to make fuel cell stacks competitive. As a result, research and development of fuel cells has been directed to solve the issues of materials, chemistry, water and hotspots (Houchins *et al*., 2012; DOE Annual merit review proceedings, 2013). Electrolyte membranes are a major cost component of Fuel Cell stacks at low production volumes. These membranes also impose limitations on fuel cell system operating conditions that add system complexity and cost. Reactant gas and fuel permeation through the membrane leads to decreased fuel cell performance, loss of efficiency, and reduced durability in both PEMFCs and DMFCs. To address these challenges, the U.S. Department of Energy (DOE) Fuel Cell Technologies Program, in the Office of Energy Efficiency and Renewable Energy, supports research and development aimed at improving ion exchange membranes for fuel cells (Houchins *et al*., 2012). Matos *et al*. (2015) performed electro-oxidation of formic acid on Pd-based catalysts supported on hybrid TiO_2-C materials prepared from different carbon origins by solvothermal and slurry synthesis, which will allow to reduce considerably the amount of expensive noble metal at the anode of DFAFC. Ma *et al*. (2012) prepared a cost-effective and eco-friendly chitosan membrane and modified by phosphate or triphosphate salt for DBFC and achieved a peak power density of 685 mW cm^{-2} at 60°C, which is over 50% higher than the power performance of a DBFC using commercial Nafion® materials. Ma and Sahai (2012) employed Chitosan, a cost-effective and eco-friendly material to prepare both electrode binder and polymer electrolyte and anode consisting of Ni-based composite electrocatalysts loaded on Ni foam substrate was developed and employed to reduce the cost and Chitosan membrane gave more than 50 % higher power performance than the commercial Nafion® membranes in DBFCs and costs less than 10% of the cost of Nafion®. Choudhury *et al*. (2012) developed a DBFC employing Na_2HPO_4-based ionically crosslinked CS hydrogel membrane

electrolytes (ICCSHMEs) to reduce the cost of fuel cell by replacing commercial Nafion® membrane. Baglio *et al*. (2010) investigated a low-cost fluorine-free proton conducting polymer electrolyte, consists of a sulfonated polystyrene grafted onto a polyethylene backbone for DMFC mini-stacks. Its performance is compared with Nafion 117 membrane, despite the lower performance, the fluorine-free membrane showed good characteristics for application in portable DMFCs especially with regard to the perspectives of significant cost reduction. Huang *et al*. (2014) provided a promising way for the decrease of noble metal loadings for DMFCs. Added magnesium oxide (MgO) nanoparticles as a sacrificial pore-former into the catalytic layer (CL) and micro-porous layer (MPL) in the anode of a membrane electrode assembly (MEA) leads to a significant increase in catalyst utilization and a decrease in charge-transfer resistance of the anodic reaction, which results in reduction of noble metal loading and performance improvement.

2.3. Durability and stability

One of the major concerns in the commercialization of Fuel Cells is the stability of the cell during long-term operation. Portable fuel cell systems may operate up to 2000 h. For the same weight and volume, fuel cells can achieve much longer lifetimes than the traditional Li-ion battery. The lifetime of a fuel cell system is primarily determined by its durability, which is often evaluated in terms of platinum catalyst degradation, carbon catalyst support corrosion, membrane chemical attack and ageing of specific components. Durability affects other design criteria such as efficiency and cost. Improvements in nafion-based membranes due to the addition of inorganic compounds (SiO_2, silanes, Zr, MoPha, etc.) and acidic-basic composites (e.g., polyaryl) decrease methanol crossover but do not reduce cost. Hydrocarbon membranes are cheaper and more technically effective for DMFCs than Nafion membranes. They have lower methanol crossover and higher conductivity and stability (Neburchilov *et al*., 2007). The durability of fuel cell systems has not been established. The degradation mechanisms and failure modes within the fuel cell components and the mitigation measures that could be taken to prevent failure need to be examined and tested. Contamination mechanisms in fuel cells due to air pollutants and fuel impurities need to be carefully addressed to resolve the fuel cell durability issue.

Peng *et al*. (2010) improved durability and more stable current output of a μDMFCs equipped with a water/air management device (WAMD). The system yielded a water removal rate of 5.1μl s^{-1} cm^{-2}, which is about 20 times much faster than the water generation rate of a μDMFC operated at 400 $mAcm^{-2}$. Jiang *et al*. (2005) carried out a 60 h life-time test of a direct ethanol fuel cell (DEFC) at a current density of 20 mA cm^{-2} (the beginning 38 h) and 40 mA cm^{-2} (the last 22 h). The home-made 50% Pt/C and 20% Pt–4% Sn/C were employed as the cathode and anode of a DEFC, respectively. Fifteen percent of the original maximum power density of the DEFC was lost after a 60 h life-time test. The agglomeration of the electrocatlaysts, the destruction of the anode PtSn/C catalyst, and the cathode flooded accelerated the degradation of the DEFC performance. However, in another experiment, they studied a 10 h lifetime test of DEFCs based on commercially available PtRu black catalyst to find a better MEA fabrication process in order to control the degradation problem. Their group concluded that the decal transfer method or delamination resulted in better cell performance than the brushing method of MEA fabrication because it made better contact between the catalyst layer and the electrolyte membrane, resulting in higher catalyst utilitzation. Their efforts may help increase the durability of DEFCs in the future. Hou *et al*. (2011) prepared a polymer electrolyte membrane for alkaline direct ethanol fuel cell (ADEFC) by dipping Nafion112 membrane into KOH solution for some time at room temperature. This single cell active ADEFC with Nafion112/KOH membrane delivered a peak power density of 58.87 mW/cm^2 at 90°C, meanwhile, it can stably run for at least 12 h above 0.2 V. On the other hand, Pt-free air breathing ADEFC with Nafion112/KOH can output a peak power density of 11.5 mW/cm^2 at 60°C, and the corresponding lifetime was as long as 473 h above 0.3 V. Hou *et al*. (2011) prepared KOH doped polybenzimidazole (PBI/KOH) membrane as polymer electrolyte membrane for alkaline direct alcohol fuel cell (ADAFC) and its durability is evaluated by means of ex situ and in situ tests. The results showed that the system could operate stably for 336 h above 0.3 V. Hong *et al*. (2010) designed a miniature air breathing compact direct formic acid fuel cell (DFAFC), with gold covered printed circuit board (PCB) as current collectors and back boards and this DFAFC showed long-term stability at constant

current density. Cai *et al*. (2012) developed a 10-cell DFAFC stack, which can stably operate for about 50 h by one fuelling with 1.5 L of 10 mol L^{-1} formic acid solution. Four refueling procedures can bring a discharge time of about 240 h for the DFAFC stack. Wu *et al*. (2013) demonstrated a passive, air-breathing 4-cell micro direct methanol fuel cell (μDMFC) stack featured by a fuel delivery structure for a long-term stable power supply. The stack is operated for 100 h and observed a 3% performance decrease. A key to commercialization of DBFC is to demonstrate its reliability and long-term operation. Li *et al*. (2003) showed that a DBFC using surface-treated Zr–Ni Laves phase AB_2 alloy as anode and Pt/C as cathode was able to operate stably for 29 h at 200 mA cm^{-2}. Ma *et al*. (2012) prepared a cost-effective and eco-friendly chitosan membrane and modified by phosphate or triphosphate salt for DBFC and received a stable performance over the test period of more than 100 h at discharge of 120 mA cm^{-2} at 30ºC. Choudhury *et al*. (2012) developed a DBFC employing Na_2HPO_4-based ionically crosslinked CS hydrogel membrane electrolytes (ICCSHMEs) and received a stable cell performance with a cell voltage loss of only 100 mV during an operation period of 100 h. Li *et al*. (2013) developed a DBFCs using Ni-Pd/C as the anode catalyst and polypyrrole-modified carbon-supported $Co(OH)_2$ [$Co(OH)_2$.PPy/BP] as the cathode catalyst to depress hydrogen evolution resulted in high performance stability. However, lifetime of fuel cells could be extended by controlling the flow conditions (i.e. humidity, flow rates and temperature) without any other alterations (i.e. materials or catalyst), and an optimized design can significantly reduce the impact of these flow conditions (Knights *et al*., 2004; Jang *et al*., 2008).

2.4. Size and weight

For portable applications, the size and weight of the fuel cell system should be comparable with the size and weight of the technology that it replaces, e.g., a battery. The presently high weight and volume of hydrogen and liquid fuels (methanol, ethanol, formic acid, Borohydride solution) storage is one of the main challenges for commercialization of fuel cell systems. Use of a portable hydrogen generating device (e.g., portable electrolysers) will solve the above issue. However, this increases the cost of the system. The size and weight of current fuel cell systems must be further reduced ,this applies not only to the fuel cell stack, but also to the ancillary components and major subsystems (i.e., fuel processor, compressor/expander, and sensors) making up the balance of power system.

Kim *et al*. (2008) investigated the possibility of the portable application of a direct borohydride fuel cell (DBFC), For weight reduction, carbon graphite is adopted as the bipolar plate material with this weight reduced by 4.2 times with 12% of performance degradation caused by insufficient contact between the end-plate and MEA from a lack of stacking force. For volume reduction Hong *et al*. (2011) designed a miniature air-breathing twin-cell stack consists of two face-to-face single cells with one shared fuel reservoir for direct formic acid fuel cell (DFAFC) applications.

2.5. Water management

Ineffective water management leads to liquid-phase water blockage and mass-transport-limited performance or decreased proton conductivity as a result of dehumidification of the ionomer. The portable fuel cells must be able to operate in environments where ambient temperatures fall below 0°C, a challenge for low-temperature fuel cells. R&D is needed to improve the designs of the gas diffusion layers, gas flow fields in bipolar plates, catalyst layers and membranes to enable effective water management and operation in subfreezing environments**.** Both low durability and reliability are caused by accumulated degradation of materials and catalyst due to water and heat issues. The degradation of materials and catalyst are mainly because of poor water management, fuel and oxidant starvation, corrosion and chemical reactions of cell components that cause dehydration or flooding. The dehydration can damage the membrane and flooding can facilitate corrosion of the electrodes, the catalyst layers, the gas diffusion media and the membrane (Schmittinger and Vahidi, 2008). Effective management of the water produced in low-temperature fuel cells is needed to alleviate flooding and/or drying out of the membrane over the full operating temperature range. So Water management is a very important parameter for the performance of a small portable fuel cell. The water level in a fuel cell affects the electrode kinetics, membrane properties, and transport of reactant. In the case of DMFC, methanol is oxidized at the anode producing hydrogen, which is transported through proton exchange membrane. Without water, the PEM will resist for the transport of hydrogen and hence each proton requires 2.5 water molecules to

diffuse through the membrane. This proton in turn combines with oxygen at the cathode and produces water. Too much water accumulation in the cathode leads to the poor performance not only due to the flooding resulting in unavailability of the catalyst layer for the reaction but also poor diffusion of oxygen toward cathode. To achieve good performance optimal water balance is required in the anode and cathode. Although the excess water in the cathode can be removed by active water control, this is difficult due to the space constraints as well as the requirement of part of the produced energy to run the pump. The present use of carbon support does not work at high power load due to high flooding and thereby difficulty in the oxygen transport. Tsujiguchi *et al*. (2013) investigated the effect of the flooding on the power generation characteristics of the DFAFC. A hydrophobic filter inserted to the cathode surface to inhibit the flooding, this hydrophobic filter decreased the cathode over-potential significantly and improved the performance. For DEFC Li *et al*. (2010) experimented with using a water trap connected to the exit of the cathode channel and filled with anhydrous $CaSO_4$ (Dryerite®) to collect the water effluent. Peng *et al*. (2010) designed and fabricated successfully an effective water/air management device (WAMD) for μDMFCs by SU-8 molding and selective surface modification processes. The system yielded a water removal rate of 5.1$\mu ls^{-1}cm^{-2}$, which is about 20 times much faster than the water generation rate of a μDMFC operated at 400 $mAcm^{-2}$. Deng *et al*. (2013) designed and fabricated a novel micro-direct methanol fuel cell (μ-DMFC) with a CNT-MEA compound structure using MEMS technology for water management. Water produced by the electrochemical reaction can be captured by CNT layer and transported outside to prevent flooding and humidify dry oxygen which due to capillary action of carbon nanotube. This results in improvement in the cell performance. Liu and Wang (2008) studied the effectiveness of an anode WML on water crossover in a DMFC. It was reported that the wettability of the anode WML is important in controlling the water crossover. Shaffer and Wang (2009) employed a one dimensional, two-phase model to investigate the importance of using an anode WML to decrease the water for MEAs using the high concentration solutions of methanol. Wu *et al*. (2013) proposed a multi-layered membrane, consisting of an ultra-thin reaction layer composed of well-dispersed PtRu catalysts, SiO_2 nanoparticles and Nafion ionomers sandwiched between two thin membranes for DMFCs operating with neat methanol. This membrane offers better water management for DMFCs operating with neat methanol and enables improvements in cell performance. Peled *et al*. (2003) and Blum *et al*. (2003) reported that the use of a highly hydrophobic cathode WML makes it possible to have water-neutral operating conditions for a DMFC with low methanol feed concentration. Xu *et al*. (2010) added two additional layers of MPL-coated carbon cloth at the cathode of the DMFC worked as the water management layer (WML). It lowered the water and methanol crossover and increased the fuel efficiency. Yang and Zhao (2009) investigated the water transport in a DMFC by incorporating both anode and cathode WML, simultaneously. It was reported that optimum design of the anode porous structure reduces the diffusion flux of water to the cathode, while optimum design in the cathode is more effective in the convective back-flow of water to the anode. Research is needed to investigate the effectiveness of the anode WML compared to the cathode WML, or vice versa. Jewet *et al*. (2007) proposed two additional gas diffusion layer (GDL) and with the addition of air filter to increase the hydraulic pressure at the cathode which eventually will drive water created from the reaction back across the membrane to the anode. The addition of air filter is to block small airborne particle, create heat insulation and reducing water evaporation and lower methanol crossover. Guo and Faghri (2009) also developed a DMFC with air filter that functions as a water proof layer for the fuel cell cathode as water management. They had specifically developed a DMFC system characterized in passive technology for methanol fuel delivery, water recirculation, air and thermal management. For a superior performance of a fuel cell, proper distribution of the reactants and water management is necessary.

2.6. Hydrogen evolution

The hydrogen evolution was one of the most critical problems to the performance improvement of the DBFC stack and commercial DBFC development. The stacking loss of the DBFC was mainly caused by hydrogen evolution, which resulted in an uneven fuel distribution between the cells of the stack. Higher initial concentrations of borohydride lead to faster rates of hydrogen evolution. This hydrogen evolution would decrease not only the DBFC performance but also fuel

utilization. A great deal of effort has been directed towards curtailing the main route to hydrogen evolution, namely, borohydride hydrolysis. One of the ways to overcome this limitation is to add some materials that are known for their inhibiting effect on hydrogen evolution to the BH_4^- solution. Another way is finding some anode catalysts on which BH_4^- can be completely electro-oxidized but no hydrolysis reaction occurs. On the other hand, more efforts should be made in optimization of flow field design and improvements of anode structure such as forming hydrophobic pore. Li *et al*. (2006) proposed two ways to reduce hydrogen evolution in DBFC, one is adding Pd, Ag and Au catalysts in the anode and another effective way is Coating a thin Nafion film on the catalyst surfaces. If the Nafion loading is too high, on the other hand, ingress of the fuel to the active sites is hindered; the optimal content was found, therefore, to be less than 25 wt. %. The hydrogen generation rate was also reduced by decreasing the temperature, which carried a penalty in terms of the cell performance. To depress hydrogen evolution Suda and co-workers employed Nickel based hydrogen storage alloys as the anode materials (Liu and Suda, 2008) and added Pd/C catalyst to FMH-Ni anode (Liu *et al*., 2008). Martins *et al*. (2007) proposed Thiuorea (TU) and tetraethyl ammonium hydroxide (TEAH) as inhibitors for the borohydride hydrolysis reaction. Celik *et al*. (2010) used thiourea (TU) as the additive in the sodium borohydride solution for minimizing the anodic hydrogen evolution on Pd, results in increase the performance of a direct borohydride fuel cell. Kim and co-workers (2008) tried to improve stack performance by decrease of hydrogen evolution influence through suitable anode shape design.

3. Portable fuel cell developing companies

Many companies and research groups work on developing different types of Portable Fuel Cell technologies to make them more advantageous than their competing technologies, i.e. batteries. Such fuel cells are especially crucial for the devices where high power density and long operation time are needed. Their application areas include consumer electronics, laptops, battery chargers, external power units and military applications. Lilliputian Systems received $5 million to help buy equipment for its Wilmington facility, which will produce USB charging systems, and Intel Capital took an equity stake in Lilliputian. Horizon Fuel Cell Technologies began shipments of the world's first miniaturized hydrogen fuel cells and refueling stations for use in model hobby radio controlled vehicles. The company also launched its new pocket-size fuel cell battery charger for the portable consumer electronics markets. Panasonic became an approved partner of SFC Energy, which includes the certification of Panasonic's Toughbook products for operation with SFC's fuel cells. Neah Power Systems announced that it will produce a hybrid fuel cell technology that recharges lithium ion batteries in consumer electronics. The Table 2 gives the list of portable fuel cell manufacturing companies across the globe.

4. Future targets for portable fuel cells

The U.S. Department of Energy has established targets for fuel cell cost, durability, power, energy and Mean time between failures for portable fuel cells commercialization.

Table 3 shows the DOE technical targets for portable fuel cell systems. The cost is based on production volumes of 50,000, 25,000, and 10,000 units per year for < 2 W, 10–50 W, and 100–250 W systems, respectively. The specific and volumetric energy densities of liquid methanol are 5.53 Wh g^{-1} and 4.35 Wh cm^{-3}, respectively, based on the LHV of 638.1 kJ mol^{-1}. If the electrical efficiency of a DMFC is 30%, then the effective specific and volumetric energy densities of methanol itself will be 1600 Wh kg^{-1} and 1300 Wh L^{-1}, respectively, which are 2.5 (1600/650) and 1.4 (1300/900) times those of the 2015 targets. Obviously, a system carrying more methanol will more easily meet those targets. For example, the energy density target of 900 Wh L^{-1} can be easily met when the volume of liquid methanol is around 70% of the total system volume (900/1300). Based on this fact, targets for the specific energy and energy density are met easily by carrying more liquid fuels. The specific power and the power density, however, are more crucial.

5. Conclusion

In this paper the challenges of DLFCs (Direct Liquid Fuel Cells), like fuel crossover, cost, durability, water management, weight and size are reviewed along with approaches being investigated to overcome these challenges. Progress in solving these technical challenges will certainly play a large role in commercialization of fuel cells. The

Table 2.
Major fuel cell system solutions development companies (Sharaf *et al*., 2014)

Country	#	Company	FC type(s)	Market(s)
United States	1	Motorola	DMFCs	Consumer electronics
	2	MTI Micro	DMFCs	Consumer electronics Battery chargers
	3	Neah Power	DMFCs	Consumer electronics Portable power generators Portable military equipment
	4	Protonex	PEMFCs SOFCs	Portable military equipment UAVs Battery chargers APUs Portable power generators EPS RAPS
	5	Ultra Electronics AMI	SOFCs	Consumer electronics APUs Battery chargers Portable military equipment Portable power generators
	6	UltraCell	RMFCs	Consumer electronics Portable power generators Portable military equipment
Japan	1	Canon	PEMFCs	Consumer electronics
	2	Hitachi	SOFCs DMFCs	Residential distributed CHP generationl Consumer electronics Portable power generators
	3	NEC	DMFCs	Consumer electronics
	4	Panasonic[a]	PEMFCs DMFCs	Residential distributed CHP generation Portable power generators Consumer electronics
	5	Sony	Microbial FCs DMFCs	Consumer electronics Battery chargers
	6	Toshiba	DMFCs PEMFCs PAFCs	Consumer electronics Battery chargers Residential distributed CHP generation EPS
Germany	1	Heliocentris	PEMFCs	Toys and educational kits RAPS EPS
	2	Schunk	PEMFCs	Battery chargers General-purpose stacks and systems
	3	SFC Energy	DMFCs	Battery chargers RAPS EPS Portable power generators Portable military equipment
	4	Siemens	DMFCs PEMFCs SOFCs	Consumer electronics Marine propulsion Industrial distributed CHP generation
United Kingdom	1	Intelligent Energy	PEMFCs	L-FCEVs LTVs EPS Residential and commercial distributed CHP generation Consumer electronics

(*Continued*)

Table 2.
Continued

Country	#	Company	FC type(s)	Market(s)
South Korea	1	LG[b]	DMFCs SOFCs	Consumer electronics Industrial and commercial distributed CHP generation
	2	Samsung	DMFCs PEMFCs SOFCs	Consumer electronics Portable power generators Portable military equipment Distributed power generation
Sweden	1	Cellkraft	PEMFCs	RAPS EPS Portable military equipment
	2	myFC	PEMFCs SOFCs	Consumer electronics Battery chargers
Taiwan	1	Antig	DMFCs	Consumer electronics Battery chargers Portable power generators
Denmark	1	Serenergy	PEMFCs RMFCs	EPS APUs Material handling L-FCEVs Battery chargers Portable power generators
France	1	BIC[c]	N/A	Consumer electronics Battery chargers
Singapore	1	Horizon	PEMFCs DMFCs	UAVs Consumer electronics Battery chargers Portable power generators Toys and educational kits RAPS EPS L-FCEVs

[a]And its subsidiary Sanyo.
[b]In June2012,LG acquired Rolls-Royce Fuel Cell Systems.
[c]On November 2011,BiC acquired Angstrom Power.

Table 3.
Fuel Cell Commercialization Targets (Fuel cell technologies office: multi-year research, development, and demonstration plan. US Department of Energy, 2012)

Market	Characteristics	Unit	Current Status	Future Target
< 2 W Micro Portable[a]	Specific Power	W-kg^{-1}	5	10
	Power Density	W-L^{-1}	7	13
	Specific energy	Wh-kg^{-1}	110	230
	Energy Density	Wh-L^{-1}	150	300
	Cost[b]	$-system^{-1}	150	70
	Durability[c]	h	1,500	5,000
	MTBF[d]	h	500	5,000
10–50 W Small Portable[a]	Specific Power	W-kg^{-1}	15	45
	Power Density	W-L^{-1}	20	55
	Specific energy	Wh-kg^{-1}	150	650
	Energy Density	Wh-L^{-1}	200	800
	Cost[e]	$-system^{-1}	15	7
	Durability[c]	h	1,500	5,000
	MTBF[d]	h	500	5,000

(*Continued*)

Table 3.
Continued

Market	Characteristics	Unit	Current Status	Future Target
100–250 W Medium Portable[a]	Specific Power	W-kg^{-1}	25	50
	Power Density	W-L^{-1}	30	70
	Specific energy	Wh-kg^{-1}	250	640
	Energy Density	Wh-L^{-1}	300	900
	Costf	$-system^{-1}	15	5
	Durability[c]	h	2,000	5,000
	MTBF[d]	h	500	5,000

importance of weight, volume, and lifetime in portable power applications provides a potential advantage to fuel cells with their high energy densities and the lack of a need for lengthy recharging cycles. Economically, it is reasonable to expect small-scale fuel cells for portable power applications to be the first to achieve widespread market penetration, likely in the very near future. To achieve that, different cost-effective materials have been recently explored as current collectors, membrane, and diffusion and catalyst layers both for the anode and cathode side. In this paper the list of portable fuel cells making companies across the globe and the targets for commercialization of fuel cells for portable power applications were also discussed.

References

Abdelkareem M.A., Nakagawa N., 2006. DMFC employing a porous plate for an efficient operation at high methanol concentrations. *Journal of Power Sources* **162**, Pp. 114–123.

Andreadis G., Song S., Tsiakaras P., 2006. Direct Ethanol Fuel Cell Anode Simulation Model. *Journal of Power Sources* **157(2)**, Pp. 657–665.

Andreadis G., Tsiakaras P., 2006. Ethanol Crossover and Direct Ethanol PEM Fuel Cell Performance Modeling and Experimental Validation. *Chem. Eng. Sci.* **61(22)**, Pp. 7497–7508.

Andreadis G.M., Podias A.K.M., Tsiakaras P.E., 2008. The Effect of the Parasitic Current on the Direct Ethanol PEM Fuel Cell Operation. *Journal of Power Sources* **181(2)**, Pp. 214–227.

Baglioa V., Stassi A., Modica E., Antonucci V., Aricò A.S., Caracinob P., Ballabio O., Colombo M., Kopnin E., 2010. Performance comparison of portable direct methanol fuel cell mini-stacks based on a low-cost fluorine-free polymer electrolyte and Nafion membrane. *Electrochimica Acta* **55**, Pp. 6022–6027.

Bauer F., Willert-Porada M., 2004. Microstructural characterization of Zr-phosphate–Nafion® membranes for direct methanol fuel cell (DMFC) applications. *Journal of Membrane Science* **233**, Pp. 141–149.

Bhat S.D., Sahu A.K., George C., Pitchumani S., Sridhar P., Chandrakumar N., Singh K.K., Krishna N., Shukla A.K., 2009. Mordenite-incorporated PVA-PSSA membranes as electrolytes for DMFCs. *J. Membr. Sci.* **340**, Pp. 783–83.

Blum A., Duvdevani T., Philosoph M., Rudoy N., Peled E., 2003. Water-neutral micro direct-methanol fuel cell (DMFC) for portable applications. *Journal of Power Sources* **117**, Pp. 22–25.

Cai W., Yan L., Li C., Liang L., Xing W., Liu C., 2012. Development of a 30 W class direct formic acid fuel cell stack with high stability and durability. *International Journal of Hydrogen Energy* **37**, Pp. 3425–3432.

Cassidy Houchins., Greg J. Kleen., Jacob S. Spendelow., John Kopasz., David Peterson., Nancy L. Garland., Donna Lee Ho., Jason Marcinkoski., Kathi Epping Martin., Reginald Tyler, Dimitrios C. Papageorgopoulos, 2012. U.S. DOE Progress Towards Developing Low-Cost, High Performance, Durable Polymer Electrolyte Membranes for Fuel Cell Applications. *Membranes* **2**, Pp. 855–878.

Cenk Celik., Fatma Gul Boyaci San., Halil Ibrahim Sarac., 2010. Improving the direct borohydride fuel cell performance with thiourea as the additive in the sodium borohydride solution. *International Journal of Hydrogen Energy* **35**, Pp. 8678–8682.

Cenk Celika., Fatma Gul Boyaci San., Halil Ibrahim Sarac., 2008. Effects of operation conditions on direct borohydride fuel cell performance. *Journal of Power Sources* **185**, Pp. 197–201.

Chien H.C., Tsai L.D., Huang C.P., Kang C.Y., Lin J.N., Chang F.C. 2013. Sulfonated graphene oxide/Nafion composite membranes for high-performance direct methanol fuel cells. *International Journal of Hydrogen Energy* **38**, Pp. 13792–13801.

Deng H., Zhang Y., Li Y., Zhang X., Liu X. 2013. A CNT-MEA compound structure of micro-direct methanol fuel cell for water management. *Microelectronic Engineering* **110**, Pp. 288–291.

DOE Annual merit review proceedings, 2013. In: http://www.hydrogen.energy.gov/annual_review13_proceedings.html

Fernández-Moreno J., Guelbenzu G., Martín A.J., Folgado M.A., Ferreira-Aparicio P., Chaparro A.M., 2013. A portable system powered with hydrogen and one single air-breathing PEM fuel cell. *Applied Energy* **109**, Pp. 60–66.

Fuel cell technologies office, 2012. multi-year research, development, and demonstration plan. US Department of Energy.

Gosalawit R., Chirachanchai S., Basile A., 2009. A Thermo and electrochemical characterization of sulfonated PEEK-WC membranes and Krytox-Si-Nafion composite membranes. *Desalination* **235**, Pp. 293–305.

Guo Z., Faghri A., 2009. Development of a 1W passive DMFC. International Communications in Heat and Mass Transfer 35, Pp. 225–39.

Hong P., Liao S., Zeng J., Huang X., 2010. Design, fabrication and performance evaluation of a miniature air breathing direct formic acid fuel cell based on printed circuit board technology. *Journal of Power Sources* **195**, Pp. 7332–7337.

Hong P., Liao S.J., Zeng J.H., Zhong Y.L., Liang Z.X., 2011. A miniature passive direct formic acid fuel cell based twin-cell stack with highly stable and reproducible long-term discharge performance. *Journal of Power Sources* **196**, Pp. 1107–1111.

Hou H., Wang S., Jin W., Jiang Q., Sun L., Jiang L., 2011. KOH modified Nafion 112 membrane for high performance alkaline direct ethanol fuel cell. *International Journal of Hydrogen Energy* **36**, Pp. 5104–5109.

Hou H.Y., Wang S., Jiang Q., Jin W., Jiang L., Sun G., 2011. Durability study of KOH doped polybenzimidazole membrane for air breathing alkaline direct ethanol fuel cell. *Journal of Power Sources* **196**, Pp. 3244–3248.

Huang Q., Jiang J., Chai J., Yuan T., Zhang H., Zou Z., Zhang X.G., Yang H., 2014. Construction of porous anode by sacrificial template for a passive direct methanol fuel cell. *Journal of Power Sources* **262**, Pp. 213–218.

Huang Y.F., Chuang L.C., Kannan A.M., Lin C.W., 2009. Proton conducting membranes with high selectivity from crosslinked poly (vinyl alcohol) and poly (vinyl pyrrolidone) for direct methanol fuel cell applications. *Journal of Power Sources* **186**, Pp. 22–28.

Ismail A.F., Othman N.H., Mustafa A., 2009. Sulfonated polyether ether ketone composite membrane using tungstosilicic acid supported on silica–aluminium oxide for direct methanol fuel cell (DMFC). *Journal of Membrane Science* **329**, Pp. 18–29.

James D.D., Pickup P.G., 2010. Effects of crossover on product yields measured for direct ethanol fuel cells. *Electrochimica Acta* **55**, Pp. 3824–3829.

Jang J.H., Chiu H.C., Yan W.M., Sun W.L., 2008. Effects of operating conditions on the performances of individual cell and stack of PEM fuel cell. *Journal of Power Sources* **180**, Pp. 476–483.

Jeong K.J., Miesse C.A., Choi J.H., Lee J., Han J., Yoon S.P., Nam S.W., Lim T.H., Lee T.G., 2007. Fuel crossover in direct formic acid fuel cells. *Journal of Power Sources* **168**, Pp. 119–125.

Jewett G., Guo Z., Faghri A., 2007. Water and air management systems for a passive direct methanol fuel cell. *Journal of Power Sources* **168**, Pp. 434–446.

Ma Jia, Nurul A. Choudhury., Yogeshwar Sahai., 2010. A comprehensive review of direct borohydride fuel cells. *Renewable and Sustainable Energy Reviews* **14**, Pp. 183–199.

Ma Jia, Yogeshwar Sahai., Rudolph G. Buchheit., 2012. Evaluation of multivalent phosphate cross-linked chitosan biopolymer membrane for direct borohydride fuel cells. *Journal of Power Sources* **202**, Pp. 18–27.

Jiang L., Sun G., Wang S., Wang G., Xin Q., Zhou Z., 2005. Electrode catalysts behaviour during direct ethanol fuel cell life-time test. *Electrochemistry Communication* **7**, 663-668.

Jochen A. Kerres., 2001. Development of ionomer membranes for fuel cells. *Journal of Membrane Science* **185**, Pp. 3–27.

Juan Matosa., Andrzej Borodzinski., Anna Mikolajczuk Zychora., Piotr Kedzierzawski., Bogusław Mierzwa., Karol Juchniewicz., Marta Mazurkiewicz., Juan C. Hernández-Garrido., 2015. Direct formic acid fuel cells on Pd catalysts supported on hybridTiO_2-C materials. *Applied Catalysis B: Environmental* **163**, Pp. 167–178.

Kamarudin M.Z.F., Kamarudin S.K., Masdar M.S., Daud W.R.W., 2013. Review: Direct ethanol fuel cells, *International Journal of Hydrogen Energy* **38**, Pp. 9438–9453.

Kamarudin S.K., Achmad F., Daud W.R.W., 2009. Overview on the application of direct methanol fuel cell (DMFC) for portable electronic devices, *International Journal of Hydrogen Energy* **34**, Pp. 6902–6916.

Kim C., Kim K.J., Ha M.Y., 2008. Investigation of the characteristics of a stacked direct borohydride fuel cell for portable applications. *Journal of Power Sources* **180(1)**, Pp. 114–121.

Kim C., Kim K.J., Ha M.Y., 2008. Performance enhancement of a direct borohydride fuel cell in practical running conditions. *Journal of Power Sources* **180(1)**, Pp. 154–161.

Klaus Tüber., Marco Zobel., Heribert Schmidt., Christopher Hebling., 2003. A polymer electrolyte membrane fuel cell system for powering portable computers. *Journal of Power Sources* **122**, Pp. 1–8.

Knights S.D., Colbow K.M., St-Pierre J., Wilkinson D.P., 2004. Aging mechanisms and lifetime of PEFC and DMFC. *Journal of Power Sources* **127**, Pp. 127–134.

Kontou S., Stergiopoulos V., Song S., Tsiakaras P., 2007. Ethanol/water mixture permeation through a Nafion® based membrane electrode assembly. *Journal of Power Sources* **171 (1)**, Pp. 1–7.

Li Y.S., Zhao T.S., Liang Z.X., 2009. Performance of alkaline electrolyte-membrane-based direct ethanol fuel cells. *Journal of Power Sources* **187**, Pp. 387–392.

Li Y.S., Zhao T.S., Yang W.W., 2010. Measurements of water uptake and transport properties anio-exchange membranes. *International Journal of Hydrogen Energy* **35**, Pp. 5656–5665.

Li Z.P., Liu B.H., Arai K., Suda S., 2003. A fuel cell development for using borohydrides as the fuel. *J. Electrochem. Soc*. **150**, Pp. A868–72.

Li Z.P., Liu B.H., Zhu J.K., Suda S., 2006. Depression of hydrogen evolution during operation of a direct borohydride fuel cell. *Journal of Power Sources* **163**, Pp. 555–559.

Li Z.P., Liu Z.X., Qin H.Y., Zhu K.N., Liu B.H., 2013. Performance degradation of a direct borohydride fuel cell. *Journal of Power Sources* **236**, Pp. 17-24.

Liliane C. Battirola., Jose F. Schneider., Iris C.L. Torriani., Germano Tremiliosi-Filho., Ubirajara P. Rodrigues-Filho., 2013. Improvement on direct ethanol fuel cell performance by using doped-Nafion® 117 membranes with Pt and Pt-Ru nanoparticles. *International Journal of Hydrogen Energy* **38**, Pp. 12060–12068.

Lin C.K., Kuo J.F., Chen C.Y., 2009. Preparation of nitrated sulfonated poly (ether ether ketone) membranes for reducing methanol permeability in direct methanol fuel cell applications. *Journal of Power Sources* **187**, Pp. 341–347.

Liu B.H., Li Z.P., Zhu J.K., Suda S., 2008. Influences of hydrogen evolution on the cell and stack performances of the direct borohydride fuel cell. *Journal of Power Sources* **183**, Pp. 151–156.

Liu B.H., Suda S., 2008. Hydrogen storage alloys as the anode materials of the direct borohydride fuel cell. *Journal of Alloys and Compounds* **454**, Pp. 280–285.

Liu F., Wang C.Y., 2008. Water and methanol crossover in direct methanol fuel cells-Effect of anode diffusion media. *Electrochimica Acta* **53**, Pp. 5517–5522.

Liu J.G., Zhao T.S., Liang Z.X., Chen R., 2006. Effect of membrane thickness on the performance and efficiency of passive direct methanol fuel cells. *Journal of Power Sources* **153**, Pp. 61–67.

Ma J., Sahai Y., 2012. Cost-effective Materials for Direct Borohydride Fuel Cells. *ECS Transactions*, **42 (1)**, Pp. 101-106.

Maab H., Nunes SP., 2010. Modified SPEEK membranes for direct ethanol fuel cell. *Journal of Power Sources* **195**, Pp. 4036–4042.

Maab H., Shishatskiy S., Nunes SP., 2009. Preparation and characterization of bilayer carbon/polymer membranes. *Journal of Membrane Science* **326**, Pp. 27–35.

Marcinkoski J., James BD., Kalinoski JA., Podolski W., Benjamin T., Kopasz J., 2011. Manufacturing process assumptions used in fuel cell system cost analyses. *Journal of Power Sources* **196**, Pp. 5282–92.

Martins J.I., Nunes M.C., Koch R., Martins L., Bazzaoui M., 2007. Electrochemical oxidation of borohydride on platinum electrodes: The influence of thiourea in direct fuel cells. *Electrochim. Acta* **52**, Pp. **6443–6449**.

Neburchilov V., Martin J., Wang H., Zhang J., 2007. A review of polymer electrolyte membranes for direct methanol fuel cells. *Journal of Power Sources* **169**, Pp. 221–238.

Choudhury A. Nurul, Jia Ma., Yogeshwar Sahai., 2012. High performance and eco-friendly chitosan hydrogel membrane electrolytes for direct borohydride fuel cells. *Journal of Power Sources* **210**, Pp. 358–365.

Odeh AO., Osifo P., Noemagus H., 2013. Chitosan: A low cost material for the production of membrane for use in PEMFC a review. *Energy Sources, Part A* **35**, Pp. 152–163.

Omar Z. Sharaf., Mehmet F. Orhan., 2014. An overview of fuel cell technology: Fundamentals and applications. *Renewable and Sustainable Energy Reviews* **32**, Pp. 810–853.

Park K.T., Jung U.Ho., Jeong S.U., Kim S.H., 2006. Influence of anode diffusion layer properties on performance of direct borohydride fuel cell. *Journal of Power Sources* **162**, Pp. 192–197.

Peled E., Blum A., Aharon A., Philosoph M., Lavi Y., 2003. Novel Approach to Recycling Water and Reducing Water Loss in DMFCs, Electrochem. *Solid-State Lett*. **6**, Pp. A268–A271.

Peng H.C., Chen P.H., Chen H.W., Chieng C.C., Yeh T.K., Pan C., Tseng F.G., 2010. Passive cathodic water/air management device for micro-direct methanol fuel cells. *Journal of Power Sources* **195**, Pp. 7349–7358.

Raman R.K., Shukla A.K., 2007. A Direct Borohydride/Hydrogen Peroxide Fuel Cell with Reduced Alkali Crossover. Fuel Cells **7(3)**, Pp. 225–231.

Rhee Y.W., Ha S.Y., Masel R.I., 2003, Crossover of formic acid through Nafion® membranes. *Journal of Power Sources* **117**, Pp. 35–38.

Schmittinger W., Vahidi A., 2008. A review of the main parameters influencing long term performance and durability of PEM fuel cells. *Journal of Power Sources* **180(1)**, Pp. 1–14.

Shaffer C.E., Wang C.Y., 2009. Role of hydrophobic anode MPL in controlling water crossover in DMFC. *Electrochimica Acta* **54**, Pp. 5761–5769.

Song S., Yi W., Peikang S., 2007. Thermodynamic and kinetic considerations for ethanol electrooxidation in direct ethanol fuel cells. *Chinese Journal of Catalysis* **28(9)**, Pp. 752–754.

Song S., Zhou W., Liang Z., Cai R., Sun G., Xin Q., Stergiopoulos V., Tsiakaras P., 2005. The effect of methanol and ethanol cross-over on the performance of PtRu/C-based anode DAFCs. *Appl. Catal. B Environ.* **55**, Pp. 65–72

Song S., Zhou W., Tian J., Cai R., Sun G., Xin Q., Kontou S., Tsiakaras P., 2005. Ethanol crossover phenomena and its influence on the performance of DEFC. *Journal of Power Sources* **145**, Pp. 266–271.

Suda S., 2002. Method for Generation of Hydrogen Gas, U.S. Pat. 6,358,488.

Sun Y., Delucchi M., Ogden J., 2011. The impact of widespread deployment of fuel cell vehicles on platinum demand and price. *International Journal of Hydrogen Energy* **36(17)**, Pp. 11116–11127.

Suresh N.S., Jayanti S., 2011. Cross-over and performance modeling of liquid-feed Polymer Electrolyte Membrane Direct Ethanol Fuel Cells. *International Journal of Hydrogen Energy* **36**, Pp. 14648–14658.

Takuya Tsujiguchi., Soshi Hirano., Takanori Iwakami., Nobuyoshi Nakagawa., 2013. The performance degradation of a passive direct formic acid fuel cell and its improvement by a hydrophobic filter. *Journal of Power Sources* **223**, Pp. 42-49.

Thiam H.S, Daud W.R.W., Kamarudin S.K, Mohammad A.B., Khadum A.A.H., Loh K.S, Majlan E.H., 2011. Overview on nanostructured membrane in fuel cell applications. *International Journal of Hydrogen Energy* **36**, 3187-205.

Thiam H.S., Daud W.R.W., Kamarudin S.K., Mohamad A.B., Kadhum A.A.H., Loh K.S., Majlan E.H., 2013. Performance of direct methanol fuel cell with a palladium–silica nanofibre/Nafion composite membrane. *Energy Conversion and Management* **75**, 718-726.

Tripathi B.P., Shahi V.K., 2009. Surface redox polymerized SPEEK–MO2–PANI (M =Si, Zr and Ti) composite polyelectrolyte membranes impervious to methanol. *Colloids and Surfaces A: Physicochemical and Engineering Aspects* **340**, 10-19.

Wan C.H., Chen C.L. 2009. Mitigating ethanol crossover in DEFC: a composite anode with a thin layer of Pt 50–Sn 50 nanoparticles directly deposited into Nafion® membrane surface. *International Journal of Hydrogen Energy* **34(23)**, Pp. 9515–9522.

Wan C.H., Lin M.T. 2013. Mitigating methanol crossover with self-assembled Pt 35–Ru 65 catalyst on Nafion surface. *Journal of Power Sources* **222**, Pp. 470–476.

Wang X., Hu J.M., Hsing I.M., 2004. Electrochemical investigation of formic acid electro-oxidation and its crossover through a Nafion® membrane. *Journal of Electroanalytical Chemistry* **562(1)**, Pp. 73–80.

Wu Q.X., Zhao T.S., Chen R., An L., 2013. A sandwich structured membrane for direct methanol fuel cells operating with neat methanol. *Applied Energy* **106**, Pp. 301–306.

Wu Z.L., Wang X.H., Teng F., Li X.Z., Wu X.M., Liu L.T., 2013. A long-term stable power supply μDMFC stack for wireless sensor node applications, *Journal of Physics: Conference Series* **476**.

Xu C., Faghri A., Li X., Ward T. 2010. Methanol and water crossover in a passive liquid-feed direct methanol fuel cell. *International Journal of Hydrogen Energy*, **35(4)**, Pp. 1769–1777.

Xu Q., Zhao T.S., Yang W.W., Chen R., 2011. A flow field enabling operating direct methanol fuel cells with highly concentrated methanol. *International Journal of Hydrogen Energy* **36**, Pp. 830–838.

Yang C.C., Lee Y.J., Yang J.M., 2009. Direct methanol fuel cell (DMFC) based on PVA/MMT composite polymer membranes. *Journal of Power Sources* **188**, Pp. 30–37.

Yang C.C., Lin C.T., Chiu S.J., 2008. Preparation of the PVA/HAP composite polymer membrane for alkaline DMFC application. *Desalination* **233**, Pp. 137–146.

Yang W.W., Zhao T.S., 2009. Numerical investigations of effect of membrane electrode assembly structure on water crossover in a liquid-feed direct methanol fuel cell. *Journal of Power Sources* **188**, Pp. 433–446.

Yu X.W., Peter G. Pickup., 2008. Recent advances in direct formic acid fuel cells (DFAFC). *Journal of Power Sources* **182**, Pp. 124–132.

Yuan T., Pu L., Huang Q., Zhang H., Li X., Yang, H., 2014. An effective methanol-blocking membrane modified with grapheneoxide nanosheets for passive direct methanol fuel cells. *Electrochimica Acta* **117**, Pp. 393–397.

Yuan W., Tang Y., Yang X.J., 2013. High-concentration operation of a passive air-breathing direct methanol fuel cell integrated with a porous methanol barrier. *Renewable Energy* **50**, Pp. 741–746.

Zhang H., Hsing I., 2007. Flexible graphite-based integrated anode plate for direct methanol fuel cells at high methanol feed concentration. Journal of Power Sources 167, Pp. 450–454.

Zhong S., Cui X., Fu T., Na H., 2008. Modification of sulfonated poly (ether ether ketone) proton exchange membrane for reducing methanol crossover. *Journal of Power Sources* **180**, Pp. 23–28.

Arab J Sci Eng (2018) 43:1225–1234
https://doi.org/10.1007/s13369-017-2813-7

RESEARCH ARTICLE - MECHANICAL ENGINEERING

Numerical Simulation and Experimental Comparison of Single, Double and Triple Serpentine Flow Channel Configuration on Performance of a PEM Fuel Cell

Venkateswarlu Velisala[1] · **G. Naga Srinivasulu**[1]

Received: 3 June 2017 / Accepted: 17 August 2017 / Published online: 24 August 2017

Abstract In this study, the effect of single (1-S), double (2-S) and triple (3-S) serpentine flow field configuration on the performance of PEM fuel cell (PEMFC) was investigated both numerically and experimentally. First, a complete 3-D PEMFC model was developed, and simulations were carried out to examine the effect of 1-S, 2-S and 3-S flow field configuration on the performance of PEMFC using commercial CFD code ANSYS FLUENT. Along with the cell performance, important parameters such as pressure distribution, mass fraction of hydrogen, oxygen, liquid water activity, current flux density distribution and the membrane water content have been presented. Next, an experimental study is carried out with a PEMFC by changing 1-S, 2-S and 3-S flow field configurations to verify the numerical predictions. Finally numerically and experimentally obtained performance curves have been compared, and 1-S flow channel fuel cell is found to exhibit the best electrochemical performance compared with the 2-S and 3-S flow channel fuel cells.

Keywords PEM fuel cell · CFD · Serpentine flow field · Current density · Membrane water content

1 Introduction

Fuel cell (FC) is an electrochemical device which transmutes the chemical energy directly into electrical energy. Depending on the type of electrolyte materials, FCs classified as polymer electrolyte membrane fuel cell (PEMFC), alkaline fuel cell (AFC), phosphoric acid fuel cell (PAFC), molten carbonate fuel cell (MCFC), and solid oxide fuel cell (SOFC).

The PEMFC utilizing a thin polymer film as the electrolyte can be considered as a reliable future power generating system, particularly for powering portable electronic devices, vehicular and residential power applications. This sort of fuel cell has numerous imperative points of interest, such as high efficiency, low operating temperature, clean, noiseless operation and quick start-up of the cell [1,2]. However, the performance and cost of the PEMFCs ought to be further optimized before these FCs gets to be focused in practical applications.

Bipolar plates (BPs) are a standout among the most important and viable components in the enhancement of performance of FCs. BPs supplies the reactants (H_2 and O_2), evacuates generated water, gathers generated current and gives support to the membrane electrode assembly (MEA) in FC. The pattern and configuration of channels significantly influence the adequacy of mass transport and additionally electrochemical reactions taking place in the FC. The ideal design of the channel dimension, pattern, orientation, and shape will prompt an enhanced and upgraded bipolar plate.

Modeling and simulation of FCs have achieved significance in recent years, as it annotates the transport phenomena and fundamentals of the processes which are taking place inside the system that may not be possible to conclude by experiments [3]. The performance of 3D PEMFC models has been articulated in detail, earlier in the literature. Berning et al. [4] and Nguyen et al. [5] presented 3D models to analyze the transport phenomena in the PEMFC with serpentine flow channels based on CFD approach. Li et al. [6] proposed a methodology to design flow fields for better water removal and also carried out experimental studies with different sizes of flow fields. Jeon et al. [7] and Wang et al. [8]developed a 3D CFD PEMFC model with different serpentine flow

✉ Venkateswarlu Velisala
2venkee@gmail.com

[1] Department of Mechanical Engineering, National Institute of Technology Warangal, Warangal, Telangana, India

field designs to examine the electrochemical reaction, transport phenomena and performance of the cell. Jang et al. [9] developed a 3D numerical PEMFC model with conventional flow fields to study the effect of the flow field design on the reactants consumption, water management, and the cell performance. Carcadea et al. [10] proposed a 3D PEMFC model with the help of CFD analysis for practical implementation on optimizing design and performance parameters. Yan et al. [11] developed three-dimensional PEMFC models to investigate the performance with different Flow channel designs such as parallel flow field, Z-type flow field, and serpentine flow field. Basu et al. [12] developed a two phase model to study flow maldistribution in parallel type gas channels of a PEM fuel cell. Akbari and Rismanchi[13] presented a 3-D CFD PEMFC model and analyzed for flow field configuration as well as contact resistance on PEMFC performance. Chang and Wu [14] experimentally studied the effect of three-pass serpentine, parallel-serpentine flow fields and various flow channel depths on miniature PEMFC. Lakshminarayanan [15] investigated the performance of single pass PEMFC with different flow channel designs numerically. Muthukumar et al. [16] numerically investigated the effect of increase in the number of serpentine passes in cathode flow channel on the PEMFC performance using commercial software package. Khazaee and Ghazikhani studied, the performance of a 25 cm^2 active PEMFC both numerically [17] and experimentally [18] using different flow channel geometry.

From the literature, it was observed that most the numerical [16,17,19–21] and experimental [18,20,22,23] works carried on serpentine channels with right angle corners for small active areas of the cell (25 cm^2). In this work, 49 cm^2 active area PEM fuel cell with 1-S, 2-S and 3-S flow fields with round corner has been developed using the commercial CFD code (ANSYS FLUENT) to study the performance. This round corner helped in reducing the pressure drop in flow channels which results in cell performance improvement. Along with cell performance, key parameters such as variation of pressure in flow channels, mass fraction of reactants, liquid water activity in the cathode flow channel and water content in the membrane have been predicted numerically. In order to validate the numerical results, experimental work also carried out and validated the numerical data with experimental data. The validated numerical data will be useful in the design and development of practical PEMFC. With this 3-D PEMFC model, it is possible to visualize the physical and electrochemical processes taking place during operation of FCs which is not possible with experiments.

2 Model Development

The present model of PEMFC was completed in three steps. The first step was modeling of individual parts such as current collectors, gas diffusion layer (GDL) of anode and cathode, membrane (PEM), the catalyst layer (CL) of anode and cathode done by SOLIDWORKS 2010. These parts have been assembled to get the complete fuel cell assembly, and geometric dimensions of these components are given in Table 1. The exploded view of the PEMFC with proposed serpentine flow fields is shown in Fig. 1. Then for some modifications, this assembly was exported to ANSYS DESIGN MODELER. With 'Fill' command the voids of the channels were filled with fluid. Next step is the creating high-quality mesh which was done by ANSYS WORKBENCH MESH. The computational domain was divided into 23 million elements for double serpentine PEMFC is shown in Fig. 2. As the accuracy of the solution strongly depends on mesh refinement, grid independency was tested. The current generated was simulated with the refined and regular meshes and noticed 0.05% variation in the results. Therefore, a regular mesh was adapted for the present simulations to save computational time and space.

Table 1 Geometric dimensions of the PEMFC model

Part	Length (cm)	Width (cm)	Height (cm)
Gas diffusion layers (GDL)	7	7	0.042 [29]
Catalyst layer (CL)	7	7	0.006 [29]
Membrane	7	7	0.0175 [29]
Channels	7	0.1	0.5

The third step was the definition of boundary conditions with thermo-physical and operating parameters of PEMFC for solving the reaction kinetics. The developed model is assumed as 3-D, steady, isothermal and the gases at the inlet as perfect, the flow as laminar, the fluid as incompressible, the porous layers such as GDLs, CLs and the membrane (PEM) as isotropic and the thermo-physical properties as constant[24,25].

2.1 Equations

Fundamental conservation equations such as conservation of mass, momentum and charge were used to develop a mathematical model for PEMFC. Conservation of energy equation was not considered as the model was assumed as isothermal. The PEMFC was examined in four parts: flow channels, GDLs, CLs and the membrane.

2.2 Flow Channel

Continuity equation for mass transport in a flow channel is

$$\rho\,(u\cdot\nabla)\,u+\nabla p-\nabla\cdot\eta\left(\nabla u+(\nabla u)^{T}\right)=0 \quad (1)$$

$$\nabla\cdot(\rho u)=0 \quad (2)$$

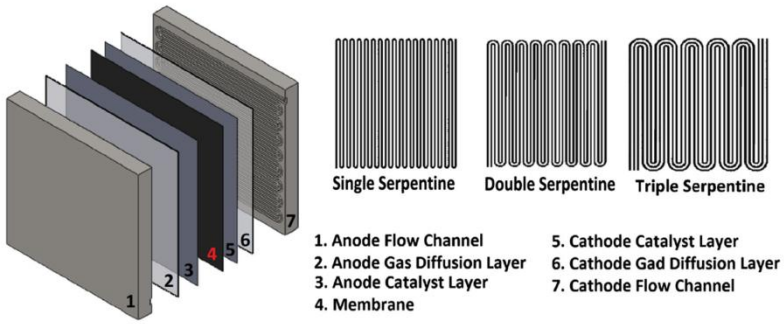

Fig. 1 Schematic diagram of PEMFC components

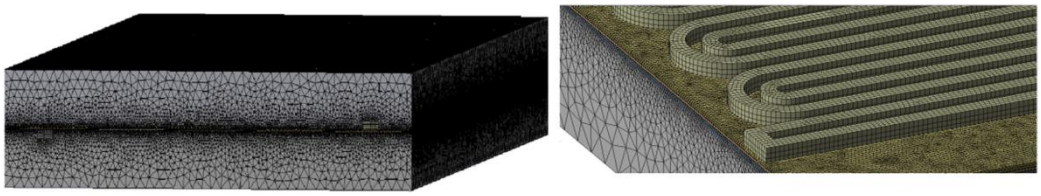

Fig. 2 Computational mesh of PEMFC

Maxwell-Stefan relation describes the mass transport of the species

$$\nabla \cdot \left[-\rho w_i \sum_j \left(D_{ij} \nabla x_j + (x_j - w_j) \frac{\nabla p}{p} \right) + \rho w_i u \right] = 0 \tag{3}$$

2.3 Gas Diffusion Layer

The phenomena taking place in the GDL may be explained by Darcy's law. Continuity equation with generation term

$$\rho (u \cdot \nabla) u + \nabla p - \nabla \cdot \eta \left(\nabla u + (\nabla u)^T \right) = -\frac{\eta}{k_p} u \tag{4}$$

A charge balance must be performed in the GDL

$$\nabla \cdot \left(k_s^{\text{eff}} \nabla \emptyset_s \right) = 0 \tag{5}$$

2.4 Catalyst Layer

A simplified Butler–Volmer equation is adapted to calculate local current density at the anode and cathode.

$$i_{\text{a}} = i_{\text{a}}^{ex} \left(\left(\frac{C_{\text{H}_2}}{C_{\text{H}_2}^{\text{ref}}} \right)^{0.5} \left[\frac{\alpha_{\text{a}} + \alpha_{\text{c}}}{RT} F \eta_{\text{a}} \right] \right) = 0 \tag{6}$$

$$i_{\text{c}} = i_{c}^{\text{ex}} \left(\left(\frac{C_{\text{O}_2}}{C_{\text{O}_2}^{\text{ref}}} \right)^{0.5} \left[\exp \left(-\frac{\alpha_{\text{c}} F \eta_{\text{c}}}{RT} \right) \right] \right) = 0 \tag{7}$$

2.5 Electrolyte

Charge balance of the electrolyte by neglecting crossover of gases

$$\nabla \cdot (k_e \nabla \emptyset_e) = 0 \tag{8}$$

Net water flux through the membrane

$$N_w = n_d M_{\text{H}_2\text{O}} \frac{i}{F} - \nabla \cdot (\rho D_w \nabla c_w) \tag{9}$$

The water diffusivity in the membrane

$$D_w = 1.3 \times 10^{-10} \exp \left[2416 \left(\frac{1}{303} - \frac{1}{T} \right) \right] \tag{10}$$

Water content inside the membrane is related to water vapor activity which affects the membrane protonic conductivity [26].

$$\lambda = 0.043 + 17.18a - 39.85a^2 + 36a^2 \quad if\, a < 1 \tag{11}$$

$$\lambda = 14 + 14(a - 1) \quad if\, a > 1 \tag{12}$$

$$a_{\text{a}} = \frac{C_{\text{H}_2\text{O},a}^{\text{MEM}} RT}{P_{\text{sat}}} \tag{13}$$

$$a_{\text{c}} = \frac{C_{\text{H}_2\text{O},c}^{\text{MEM}} RT}{P_{\text{sat}}} \tag{14}$$

$$a = \frac{a_{\text{a}} + a_c}{2} \tag{15}$$

Table 2 Key properties used in the PEMFC simulation

Parameter	Value
Reference concentration at anode	0.5 kmol/m^3 [29]
Reference concentration at cathode	1.0 kmol/m^3 [29]
Reference current density at anode	8000 A/m^2 [30]
Reference current density at cathode	200 A/m^2 [30]
Membrane equivalent weight	1100 kg/kmol [30]

Table 3 Operation conditions used in the PEMFC Simulation

Flow rate of H_2 at anode inlet (1-S, 2-S and 3-S)	2.05e−7 kg/s
Flow rate of O_2 at cathode inlet (1-S, 2-S and 3-S)	1.67e−6 kg/s
Operating pressure	1 bar
Operating temperature	323 K

3 Solver

A commercial solver called ANSYS FLUENT 15.0 with its built-in PEMFC add-on module (Fuel Cell and Electrolysis Model) has been used to solve the governing equations. For this model, 3-D, double precision and serial processing was opted. The operating pressure was 1 bar and the temperature was 323 K. Hydrogen and oxygen mass flow rates have been set as 2.05e−7 kg/s and 1.67e−6 kg/s, respectively, for three proposed PEMFC models. Key properties and operation parameters of the simulation model are given in Tables 2 and 3, respectively. The species concentration on the anode side of H_2, O_2, and H_2O were 0.8, 0, and 0.2, respectively. While, on the cathode side H_2, O_2, and H_2O were 0, 0.2 and 0.1, respectively. The open-circuit potential was fixed at 1.0 V. In order to solve reaction kinetics and to get pressure variation, H_2, O_2 fractions along the flow channel, anode voltage was kept as constant (0 V) and the cathode voltage was varied from 0.1 to 0.9 V. The simulations have been carried out in an Intel Xeon HP workstation with 32 GB RAM and 2.40 GHz CPU, running Windows 7 Operating System.

4 Description of the Experiments

4.1 The Fuel Cell Test Station and Fuel Cell

Numerical results may be assumed as realistic and correct if the numerical model is well-resolved and systematically validated with experimental results. For the purpose of comparing the present numerical results with the experimental data, experimental work was carried out to correlate the present numerical predictions with the experimental results. Before taking the readings, the FC was activated for about 2 hours to get better results. The experimental test was carried out under same operating conditions used in the simulation. The experimental work was conducted with a programmable SMART2 Fuel Cell Test system from WonATech (Korea) located at the Fuel Cell Laboratory at Centre for Sustainable Energy Studies, National Institute of Technology Warangal. All the dimensions of the flow field are same as used in the simulation and graphite is used for bipolar plate. N117 (Nafion) membrane with 0.4 mg Pt cm^{-2} for the anode and 0.6 mg Pt cm^{-2} for the cathode is used as MEA. A 0.042 mm thick carbon paper is used as GDL, and 0.06 mm thick catalyst layer is used on both sides of the membrane. The thickness of the membrane used is 0.0175 mm. The FFPs, current collectors and MEA used in the experiments are provided by Vinpro technologies (Fig. 3). A schematic drawing of the experimental setup is shown in Fig. 4. A single cell PEMFC was chosen in the study with an active area of 49 cm^2 along with proposed flow field plates depicted in Fig. 5.

5 Results and Discussion

Numerical and experimental investigation of proposed flow field configurations on PEM fuel cell performance has been completed. Numerically predicted pressure drop, the concentration distribution of hydrogen, oxygen, liquid water activity along the channel and the membrane water content for peak power performance of the three flow fields for PEMFC are shown in Figs. 6, 7, 8, 9, 10 and 11. Numerically and experimentally obtained polarization and performance curves of the proposed PEMFC models are shown in Fig. 12. PEMFC with single serpentine flow field gave a peak power performance at 0.5 V cell potential of current when the cell is operated at 1 bar pressure and 323 K temperature.

5.1 Pressure Drop

One of the key parameters which must be taken into account while designing the fuel cell is pressure drop which takes place in the flow channel. This pressure drop will help in deciding the type of blowers or compressors to be used to maintain sufficient pressure in the channel. This pressure drop also affects the electrochemistry of the fuel cell. Figure 6 shows the pressure drop in the cathode flow channel of three flow fields. The pressure drop is more at the inlet and decreasing gradually toward the outlet of the flow channel. Maximum pressure drops in 1-S, 2-S and 3-S flow field are 17.1Kpa, 9.2 Kpa and 1.6 Kpa, respectively. This drop in pressure is because of frictional and bending losses

5.2 Hydrogen and Oxygen Mass Fraction

Figures 7 and 8 show the hydrogen and oxygen mass fraction distribution along the anode and cathode flow channel at a

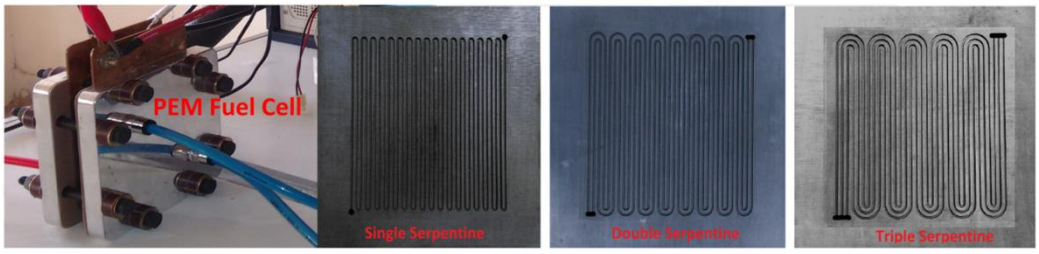

Fig. 3 Photograph of PEMFC with three flow field designs

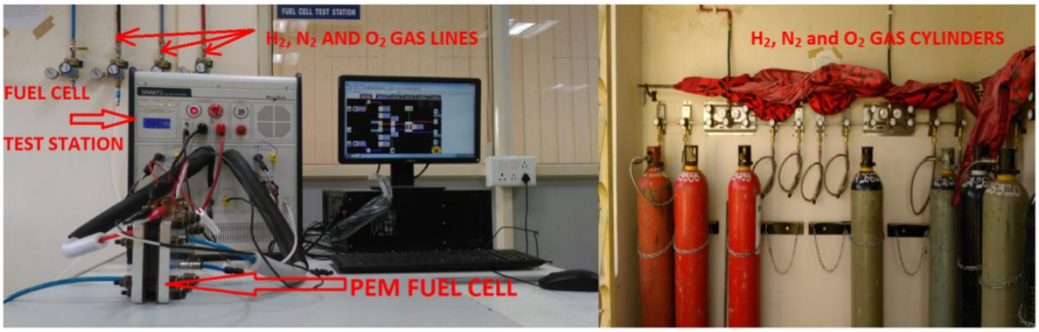

Fig. 4 Photograph of PEMFC test station with gas banks

cell potential of 0.5 V, respectively. Both H_2 and O_2 concentrations are more at the inlet and reduces gradually toward the outlet of the anode and cathode channels. The reduction of the species concentration in the channels is due to consumption of reactants in the reaction. It is also observed that species concentration distribution is more uniform in single serpentine flow channel as compared to the other two flow channels which has a positive effect on PEMFC output.

5.3 Current Flux Density Distribution

Figure 9 shows the current flux density distribution over the cathode catalyst layer at a cell potential of 0.5 V. It is observed that, the current flux density distribution is same in all three models. Current density values are less on the exit side of the anode and cathode compared with middle region of the cathode catalyst layer, because of less availability of hydrogen and oxygen at the exit side of anode and cathode channels. It is also observed that, the current density values are slightly higher for the 1-S flow field model than 2-S and 3-S flow field models.

5.4 Membrane Water Content Distribution

Figure 10 shows the membrane water content distribution at cell potential of 0.5 V. It is observed that, the water content in the membrane is more in the 1-S flow field model than 2-S and 3-S flow field models. A certain amount of water is essential to keep the membrane hydrated, and it improves the proton conductivity through the membrane, which influences the more cell output power. Water content distribution in the membrane and its value is good enough to conduct the protons from anode to cathode.

5.5 Liquid Water Activity in the Cathode Channel

Figure 11 shows the liquid water activity in the cathode channels at 0.5 V cell potential. The water produced on the cathode side is due to oxygen reduction reaction (ORR). A certain amount of water is required for efficient fuel cell run, and the excess water must be removed from the cell otherwise flooding takes place which reduces the fuel cell performance. It is observed that, the liquid water activity is less at the entry

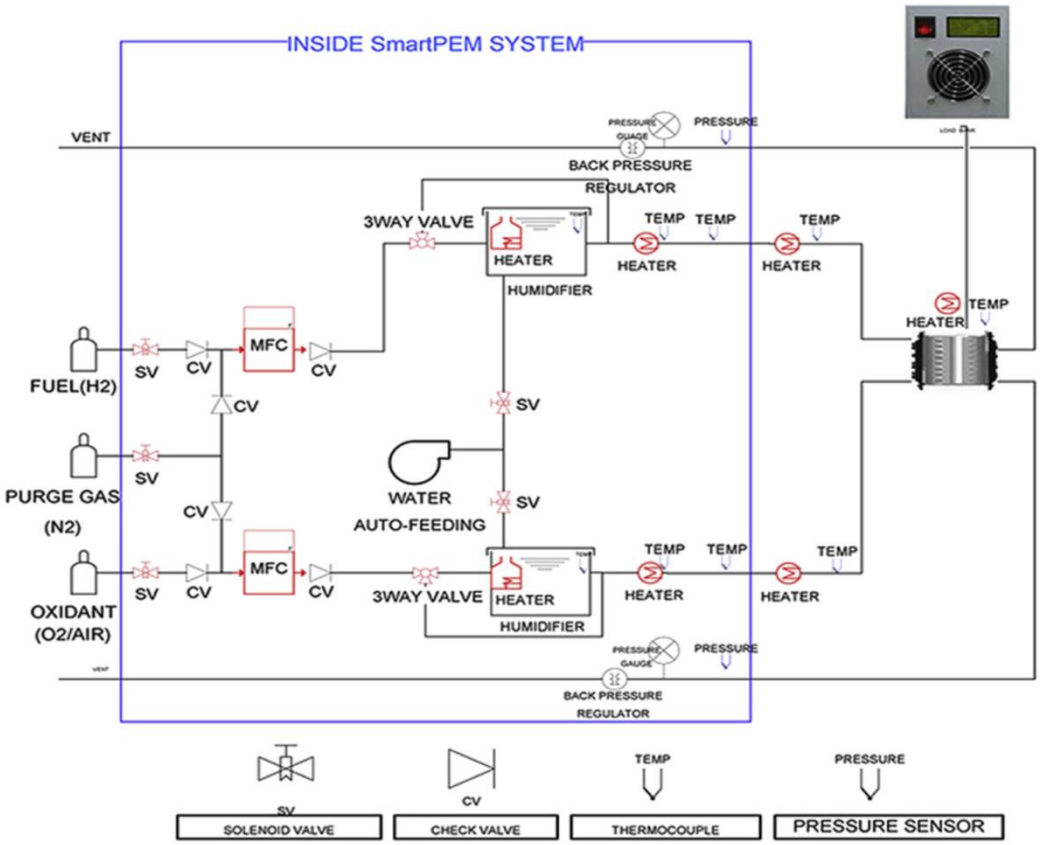

Fig. 5 Schematic of experimental setup

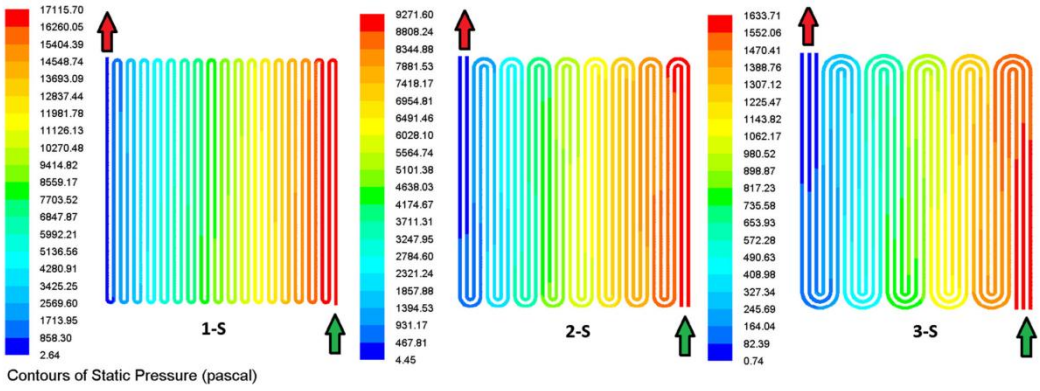

Fig. 6 Pressure (Pa) variation along cathode channel at 0.5 V

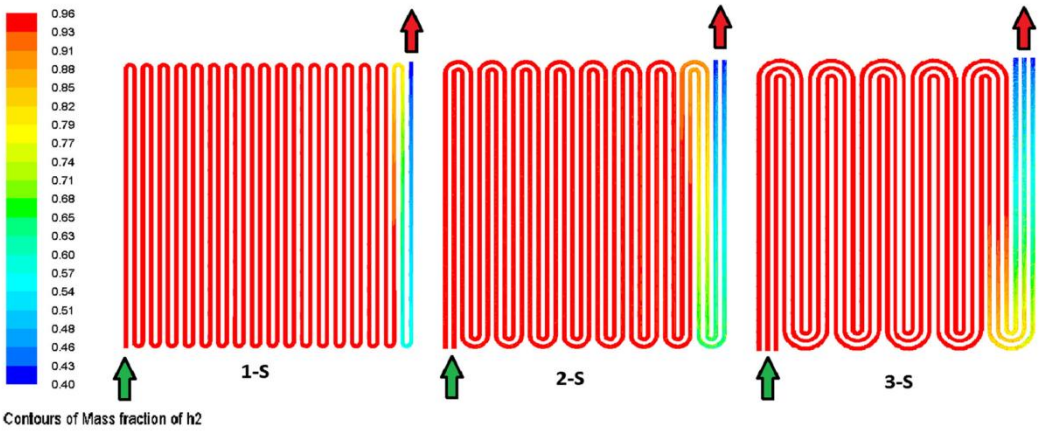

Fig. 7 Hydrogen mass fraction distribution at 0.5 V

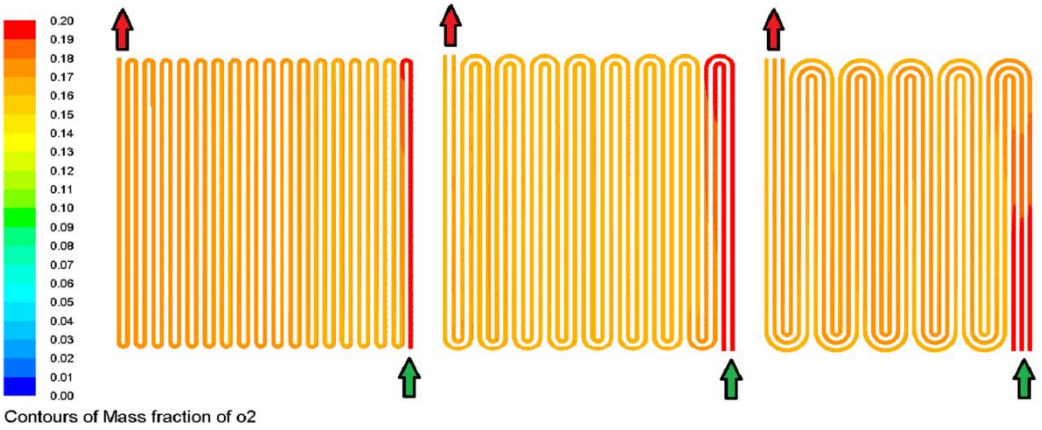

Fig. 8 Oxygen mass fraction distribution at 0.5 V

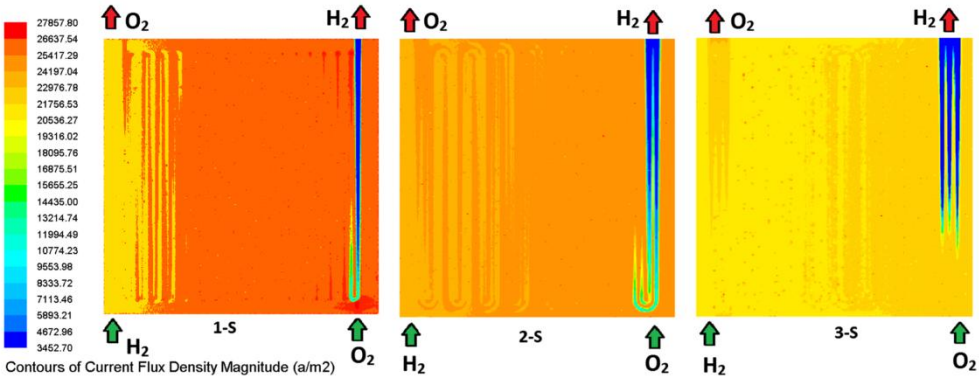

Fig. 9 Current flux density magnitude over cathode catalyst layer at 0.5 V

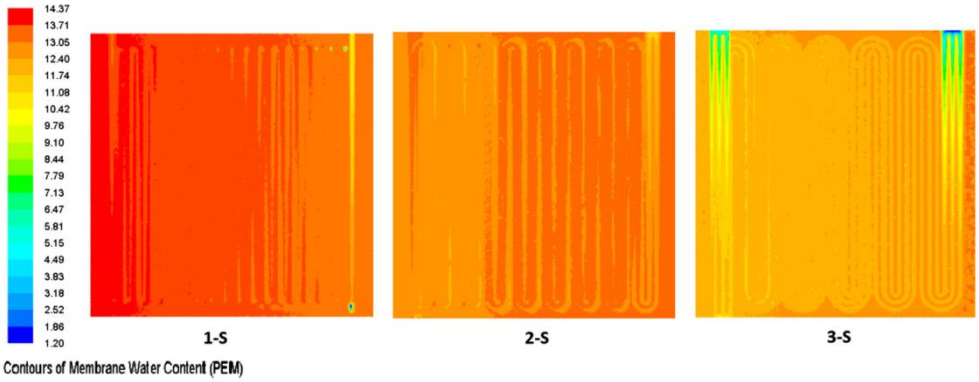

Fig. 10 Membrane water content at 0.5 V

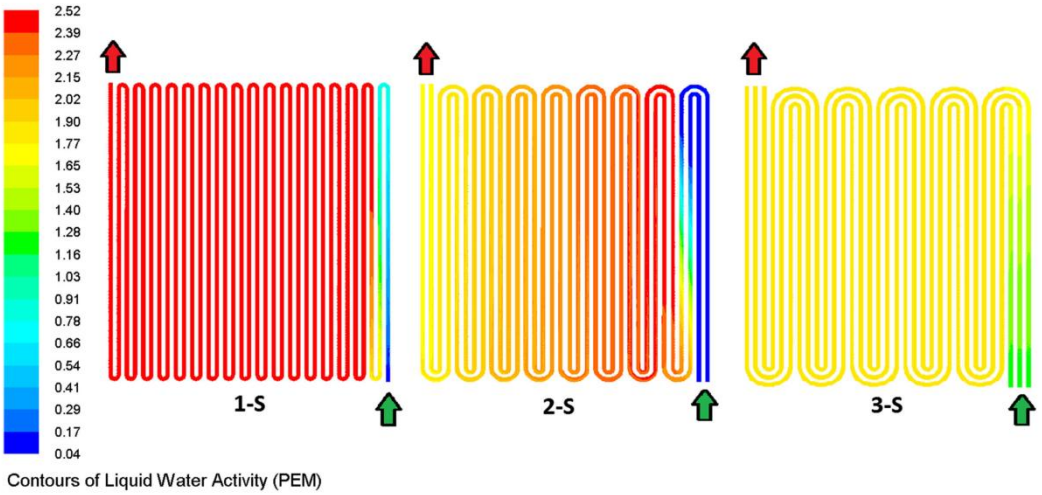

Fig. 11 Liquid water activity in the cathode channel at 0.5 V

Table 4 Pressure drops at the operating cell voltage of 0.5 V

Type of flow field	ΔP (Pa)	V_{in} (m/s)	W_{Cell} (W)	W_P (W)	W_{Net} (W)
Single serpentine	17115	8.49	0.38	0.016	0.364
Double serpentine	9271	4.32	0.34	0.006	0.334
Triple serpentine	1533	2.54	0.305	0.0004	0.3046

and it is increased gradually toward the exit of the cathode flow channels and water production rate is more at higher current densities. It is also observed that the water removal rate is better in single serpentine channel, than the double and triple serpentine channels due to higher velocities (shown in Table 4). Higher velocities help in faster water removal from the cell and improve cell performance. Similar results can be observed in the numerical work of Yan et al. [11], Basu et al. [12] and experimental work of Iranzo et al. [27] on PEMFC.

5.6 Pressure Drop Losses

The losses in pressure drop associated with power density are used to analyze the three flow field configurations.

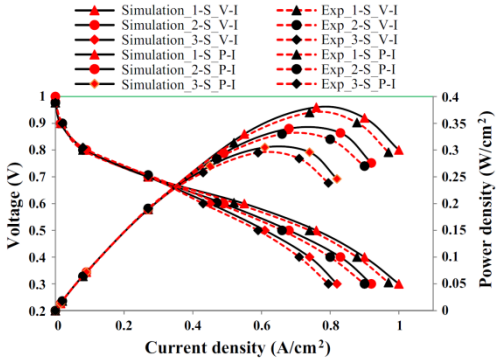

Fig. 12 Comparison of numerical and experimental results

$$W_{\text{net}} = W_{\text{cell}} - W_p \tag{16}$$

$$W_{\text{cell}} = i * V_{\text{cell}} \tag{17}$$

$$W_p = \frac{\Delta P * A_{\text{cha}} * V}{A_{\text{total}}} \tag{18}$$

Where, W_{net} is net power density, W_{cell} is cell power density, W_p is pressure drop loss in the cathode, ΔP is total pressure drop in the cathode channel, A_{cha} is the cross-sectional area at cathode channel inlet, V is the velocity of cathode fuel at the inlet of cathode channel, and A_{total} is the active area of the cell. Calculations on the pressure drop loss and output power of the three proposed flow fields at 0.5 V are given in Table 4. The result shows that as the number of flow passes increase, the pressure drop losses are decreased. It also reveals that, the flow field designs with more flow passes might decrease the pressure drop losses in a PEM fuel cell system. Because of small flow channel cross-sectional areas and low reactant inlet velocities the pressure drop losses are negligible in PEMFCs when compared with cell output power, W_{cell}[28].

The performance of the PEMFC with 1-S, 2-S and 3-S flow fields is shown in Fig. 12. It is observed that the numerical results are in good agreement with the experimental results and the effect of channel design on the cell performance is negligible at lower current densities but at higher current densities the effect of channel design is significant. It is also observed that the performance of the PEMFC with 1-S is better than PEMFCs with 2-S and 3-S. The decrease in number of flow channel passes will increase the reactant inlet velocities, which improves the liquid water removal from the channel and porous layers. Due to this more oxygen transports to the cathode catalyst layer to participate in the electrochemical reactions and accordingly, the cell performance improves. This might be the reason for PEMFC with 1-S to perform better than PEMFCs with 2-S and 3-S. The peak powers of proposed designs are given in Table 5.

Table 5 Peak power of three flow field designs

Flow field type	Peak powe (simulation)	Peak power (experimental)	% deviation b/w Exp and Sim data
Single serpentine	0.38 (18.62)	0.37 (18.13)	2.71
Double serpentine	0.34 (16.66)	0.33 (16.17)	3.03
Triple serpentine	0.305 (14.95)	0.295 (14.45)	3.39

6 Conclusion

A complete 3-D model of PEMFC having active area 49 cm^2 (7 cm × 7 cm) was developed. A CFD study was completed to examine the effect of single, double and triple serpentine flow fields on PEMFC performance. Simulations were carried out to get a polarization curve, the concentration profile of each species and pressure distribution. The numerically obtained polarization curves of three different flow channel designs were compared with experimentally obtained polarization curves of same flow field designs and they show good agreement.

The predictions show that when the cell was operated at more than 0.7 V, the effect of channel design on the cell performance was negligible, but when the cell was operated at less than 0.7 V, then the channel design effect becomes significant. The decrease in number of flow channel passes will increase the inlet reactant velocities, which improves the water removal from the cell. Due to this the more oxygen transports to the cathode reaction sites to participate in the electrochemical reactions and accordingly, the cell performance increases. Lastly, the investigations shows that a decrease in the number of flow channel passes increases the cell performance to a maximum while the total pressure drop in the cell continues to increase for a 49 cm^2 active area PEMFC for a given inlet reactant flow rates. Further, our investigations may concentrate on larger active area fuel cells and different operating parameters for improvement of PEMFC performance.

Acknowledgements The authors gratefully acknowledge the financial support provided by TEQIP-II/ CoE - Centre for Sustainable Energy Studies, National Institute of Technology Warangal (NITW).

References

1. Veziroglu, T.N.; Şahin, S.: 21st century's energy: hydrogen energy system. Energy Convers. Manag. **49**(7), 1820–1831 (2008)
2. Hossain, M.; Islam, S.Z.; Pollard, P.: Investigation of species transport in a gas diffusion layer of a polymer electrolyte membrane fuel cell through two-phase modelling. Renew. Energy **51**, 404–418 (2013)
3. Caglayan, D.G.; Sezgin, B.; Devrim, Y.Y.Y.; Eroglu, I.: Three-dimensional modeling of a high temperature polymer electrolyte

membrane fuel cell at different operation temperatures. Int. J. Hydrogen Energy **41**(23), 1–11 (2016)
4. Berning, T.; Lu, D.M.; Djilali, N.: Three-dimensional computational analysis of transport phenomena in a PEM fuel cell. J. Power Sources **106**(1), 284–294 (2002)
5. Nguyen, P.T.; Berning, T.; Djilali, N.: Computational model of a PEM fuel cell with serpentine gas flow channels. J. Power Sources **130**(1–2), 149–157 (2004)
6. Li, X.; Sabir, I.; Park, J.: A flow channel design procedure for PEM fuel cells with effective water removal. J. Power Sources **163**, 933–942 (2007)
7. Jeon, D.H.; Greenway, S.; Shimpalee, S.; Van Zee, J.W.: The effect of serpentine flow-field designs on PEM fuel cell performance. Int. J. Hydrogen Energy **33**(3), 1052–1066 (2008)
8. Wang, X.D.; Duan, Y.Y.; Yan, W.M.; Peng, X.F.: Local transport phenomena and cell performance of PEM fuel cells with various serpentine flow field designs. J. Power Sources **175**(1), 397–407 (2008)
9. Jang, J.-H.; Yan, W.-M.; Li, H.-Y.; Tsai, W.-C.: Three-dimensional numerical study on cell performance and transport phenomena of PEM fuel cells with conventional flow fields. Int. J. Hydrogen Energy **33**(1), 156–164 (2008)
10. Carcadea, E.; Ene, H.; Ingham, D.B.; Lazar, R.; Ma, L.; Pourkashanian, M.; Stefanescu, I.: A computational fluid dynamics analysis of a PEM fuel cell system for power generation. Int. J. Numer. Methods Heat Fluid Flow **17**(3), 302–312 (2007)
11. Yan, W.-M.; Li, H.-Y.; Tsai, W.-C.: Three-dimensional analysis of PEMFCs with different flow channel designs. J. Electrochem. Soc. **153**(10), A1984 (2006)
12. Basu, S.; Li, J.; Wang, C.Y.: Two-phase flow and maldistribution in gas channels of a polymer electrolyte fuel cell. J. Power Sources **187**(2), 431–443 (2009)
13. Akbari, M.H.; Rismanchi, B.: Numerical investigation of flow field configuration and contact resistance for PEM fuel cell performance. Renew. Energy **33**(8), 1775–1783 (2008)
14. Chang, D.H.; Wu, S.Y.: The effects of channel depth on the performance of miniature proton exchange membrane fuel cells with serpentine-type flow fields. Int. J. Hydrogen Energy **40**(35), 11659–11667 (2015)
15. Lakshminarayanan, V.; Karthikeyan, P.; Muthukumar, M.; Senthil Kumar, A.P.; Kavin, B.; Kavyaraj, A.: Numerical investigation of performance studies on single pass PEM fuel cell with various flow channel design. Appl. Mech. Mater. **592–594**, 1672–1676 (2014)
16. Muthukumar, M.; Karthikeyan, P.; Lakshminarayanan, V.; Senthil Kumar, A.P.; Vairavel, M.; Girimurugan, R.: Performance studies on PEM fuel cell with 2, 3 and 4 pass serpentine flow field designs. Appl. Mech. Mater. **592–594**, 1728–1732 (2014)
17. Khazaee, I.; Ghazikhani, M.: Three-dimensional modeling and development of the new geometry PEM fuel cell. Arab. J. Sci. Eng. **38**(6), 1551–1564 (2013)
18. Khazaee, I.; Ghazikhani, M.: Experimental characterization and correlation of a triangular channel geometry PEM fuel cell at different operating conditions. Arab. J. Sci. Eng. **38**(9), 2521–2531 (2013)
19. Chi, P.-H.; Weng, F.-B.; Su, A.; Chan, S.-H.: Numerical modeling of proton exchange membrane fuel cell with considering thermal and relative humidity effects on the cell performance. J. Fuel Cell Sci. Technol. **3**(3), 292 (2006)
20. Zenyuk, I.V.; Taspinar, R.; Kalidindi, A.R.; Kumbur, E.C.; Litster, S.: Computational and experimental analysis of water transport at component interfaces in polymer electrolyte fuel cells. J. Electrochem. Soc. **161**(11), F3091–F3103 (2014)
21. Wang, L.P.; Zhang, L.H.; Jiang, J.P.: Optimization of channel dimensions in the flow-field for PEMFC. Appl. Mech. Mater. **44–47**, 2404–2408 (2010)
22. Ozen, D.N.; Timurkutluk, B.; Altinisik, K.: Effects of operation temperature and reactant gas humidity levels on performance of PEM fuel cells. Renew. Sustain. Energy Rev. **59**, 1298–1306 (2016)
23. Kahveci, E.E.; Taymaz, I.: An experimental study of response surface methodology to optimise the operating parameters on PEM fuel cell. Int. J. Veh. Des. **71**(1), 321–334 (2016)
24. Wang, X.-D.D.; Duan, Y.-Y.Y.; Yan, W.-M.M.; Weng, F.-B.B.: Effects of flow channel geometry on cell performance for PEM fuel cells with parallel and interdigitated flow fields. Electrochim. Acta J. **53**(1), 5334–5343 (2008)
25. Zhang, Z.; Li, : Parametric study of the porous cathode in the PEM fuel cell. Int. J. Energy Res. **33**, 52–61 (2009)
26. Salva, J.A.; Iranzo, A.; Rosa, F.; Tapia, E.: Validation of cell voltage and water content in a PEM (polymer electrolyte membrane) fuel cell model using neutron imaging for different operating conditions. Energy **101**, 100–112 (2016)
27. Iranzo, A.; Boillat, P.; Biesdorf, J.; Tapia, E.; Salva, A.; Guerra, J.: Liquid water preferential accumulation in channels of PEM fuel cells with multiple serpentine flow fields. Int. J. Hydrogen Energy **39**(28), 15687–15695 (2014)
28. Li, Y.-S.; Han, Y.; Zhan, J.-M.: Uniformity analysis in different flow-field configurations of proton exchange membrane fuel cell. J. Fuel Cell Sci. Technol. **10**(3), 31003 (2013)
29. Iranzo, A.; Muñoz, M.; Rosa, F.; Pino, J.: Numerical model for the performance prediction of a PEM fuel cell. Model results and experimental validation. Int. J. Hydrogen Energy **35**(20), 11533–11550 (2010)
30. Han, Y.; Zhan, J.M.: The impact of channel assembled angle on proton exchange membrane fuel cell performance. J. Power Sources **195**(19), 6586–6597 (2010)

INTERNATIONAL JOURNAL OF AMBIENT ENERGY, 2018
https://doi.org/10.1080/01430750.2018.1456959

Taylor & Francis
Taylor & Francis Group

Computational fluid dynamics study of 3-pass serpentine flow field configuration on proton exchange membrane fuel cell performance

Venkateswarlu Velisala and G. Naga Srinivasulu

Department of Mechanical Engineering, National Institute of Technology Warangal, Telangana, India

ABSTRACT

A 3-D PEM fuel cell model with 3-pass serpentine flow field was developed to analyse the performance of the fuel cell. Simulations were carried out in the commercial ANSYS FLUENT 15.0 software with species concentration on the anode side as H_2 – 0.8, O_2 – 0, H_2O – 0.2 and on the cathode side H_2 – 0, O_2 – 0.2, and H_2O – 0.1. Along with the performance of the cell, key parameters like pressure drop, hydrogen mass fraction, oxygen mass fraction, liquid water activity and the membrane water content have been analysed. The results showed that when the cell was operated at a lower voltage of 0.4 V, i.e. a higher current density, hydrogen and oxygen consumption rates are high as well as water production rate. Finally, the proposed fuel cell model performance characteristics are compared with the available experimental data that shows good agreement.

ARTICLE HISTORY
Received 21 July 2017
Accepted 15 March 2018

KEYWORDS
PEM fuel cell; 3-pass serpentine flow field; current density; membrane water content; cell performance

1. Introduction

The ever increasing energy demand, emission-free energy generation, and other ecological issues have encouraged many researchers to look for advanced efficient energy conversion technologies (Beicha and Zaamouche 2013). Within such perspective fuel cell systems may be considered as a good alternative due to practical merits such as the high-energy density, superb dynamic response, low hostility to the environment, and lightweight as well as easy and fast recharging via a replacement or a refilled fuel cartridge (Velisala et al. 2015). Fuel cells are classified based on the type of electrolyte materials (Larminie and Dicks 2001). The commonly available fuel cell technologies include polymer electrolyte membrane (PEMFC), alkaline, phosphoric acid, molten carbonate, and solid oxide based fuel cells.

PEM fuel cells have numerous distinctive characteristics as compared with other fuel cell types, such as moderately low operating temperatures (around 80°C), high power density, quick start, faster response, and high modularity makes them as the most encouraging contender for future power generating devices in applications such as automotive, distributed power generation and compact electronic devices (Boettner et al. 2002; Mehrpooya et al. 2015). Designing and building prototypes of fuel cell are laborious and expensive (Hosseinzadeh 2012). The alternative is modelling the fuel cell system for simulation, this can permit the assessment of the fuel cell performance, lowering the cost and time along the design stage and tests (Corrêa et al. 2004). Berning et al. (2002) developed a complete 3-D fuel cell model taking into account computational liquid elements approach to study the transport phenomena in the fuel cell. Barreras et al. (2005) conducted both numerical and experimental studies to analyse the flow distribution in a 50 cm^2 area flow field of a PEM fuel cell. With these studies they concluded that non-homogeneous flow distribution in the flow channels causes a low performance of the fuel cell. Lum and McGuirk (2005) developed a steady-state, 3-D CFD model of polymer electrolyte membrane (PEMFC) to carry out parametric studies and validated his model with the work of Shimpalee et al. (1999). Carcadea et al. (2007) presented a 3-D CFD model to study fluid flow in channels, species transport in porous layers, water management, and current generated. This model has some limitations in understanding the complex physical and chemical processes happening inside the cell. Jang et al. (2008) also developed a 3-D numerical PEMFC model with conventional flow field designs to investigate performance and transport phenomena of the fuel cell. They found that serpentine flow field performance is better than the Z-type and parallel flow fields. Wang et al. (2009) developed 3-D PEM fuel cell models with single and triple serpentine flow fields to study the effect of the sub-rib convection on the performance at various channel aspect ratios. Change in the channel aspect ratio has a minimal effect on the performance of single serpentine flow field and a significant effect on the performance of triple serpentine flow field. Suresh et al. (2011) developed a new serpentine flow field with enhanced cross-flow for PEMFC applications and carried out both numerical and experimental studies. They have reduced the pressure drops and achieved uniform distribution of flow. Guo et al. (2014) developed a 3-D simulation model with bio-inspired flow field designs and investigated the performance of fuel cell both numerically and experimentally. They concluded that the bio-inspired designs considerably increase the cell performance by 20–25% compared to the conventional designs. Khazaee and Sabadbafan (2016) numerically investigated the effect of increasing the number of serpentine channels

CONTACT Venkateswarlu Velisala 2venkee@gmail.com; venkee.vel@nitw.ac.in

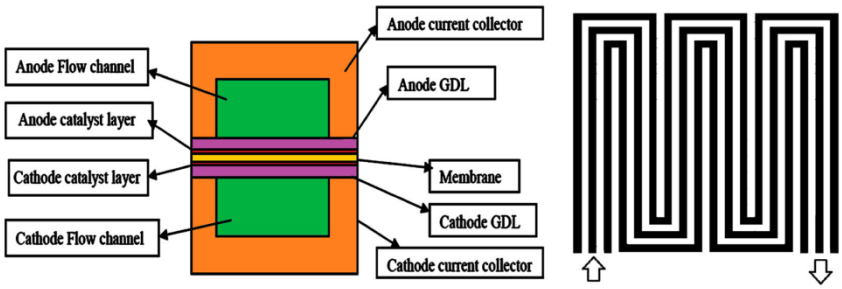

Figure 1. PEMFC assembly with 3-pass serpentine flow field.

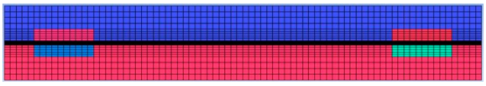

Figure 2. Computational mesh of PEMFC.

in the bipolar plates on fuel cell performance with rectangular, triangular and elliptical cross-section geometry. Caglayan et al. (2016) developed a 25 cm^2 active area numerical 3-D PEMFC model with single and triple-mixed serpentine flow channel and analysed the performance of the cell. They found that the triple-mixed serpentine flow channel is performing better than the single serpentine flow channel.

The pressure drop in the flow channel is an important consideration in the design of PEMFC as it will help in deciding the type of blowers or compressors to be used to maintain sufficient pressure in the channel. This pressure drop also influences the electrochemistry of the fuel cell. Most of the researchers have done work on serpentine flow channel with one pass. Recently, researchers started working on serpentine flow channels with multiple passes. In this work, a complete 3-D CFD model with serpentine flow channel having 3-pass has been developed and simulations have been carried out. Along with the performance of the fuel cell, key parameters such as pressure drop, hydrogen mass fraction, oxygen mass fraction, liquid water activity, and the membrane water content have been analysed. Using this model, it is possible to understand major physical and chemical processes occurring inside the cell which cannot be studied experimentally.

2. Model description

The whole computational domain is a 3-pass Serpentine channel, anode and cathode electrodes, catalyst layers, and membrane. All the components are modelled, assembled, and meshed in SolidWorks© CAD software and ICEM CFD as shown in Figures 1 and 2, respectively. The special add-on module for the fuel cell embedded in FLUENT solves the problem considering all the relevant equations. This software solves numerically the governing equations such as continuity, momentum, energy, species transport, and charge conservation by the finite volume method in the form of the SIMPLE algorithm and by the pressure correction method. The flow chart of the solution procedure is shown in Figure 3.

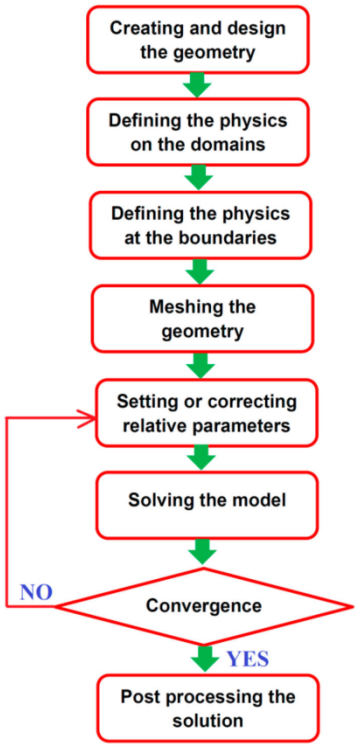

Figure 3. Flow chart of the numerical simulation.

2.1. Assumptions

(1) All the gases are ideal gases.
(2) The flow is steady, laminar, and incompressible.
(3) The system is isothermal (323 K).
(4) The product water is in liquid phase.
(5) The electrochemical reactions take place in the catalyst layers only.
(6) Porous structures like gas diffusion layers, catalyst layers and the membrane are isotropic.
(7) Neglect the gravity effect.

Table 1. Governing equations.

Continuity equation	$\frac{\partial(\rho u)}{\partial x}+\frac{\partial(\rho v)}{\partial y}+\frac{\partial(\rho w)}{\partial z}=\frac{\partial \rho}{\partial t}$
Momentum equation	$u\frac{\partial(\rho u)}{\partial x}+v\frac{\partial(\rho u)}{\partial y}+w\frac{\partial(\rho u)}{\partial z}=\frac{\partial \rho}{\partial x}+\frac{\partial}{\partial x}\left(\mu\frac{\partial u}{\partial x}+\frac{\partial}{\partial y}\left(\mu\frac{\partial u}{\partial y}\right)\right)+\frac{\partial}{\partial z}\left(\mu\frac{\partial u}{\partial z}\right)+S_{\mathrm{mom},x}$
Species transport equation	$u\frac{\partial(\rho y_i)}{\partial x}+v\frac{\partial(\rho y_i)}{\partial y}+w\frac{\partial(\rho y_i)}{\partial z}=\frac{\partial(j_{x,i})}{\partial x}+\frac{\partial(j_{y,i})}{\partial y}+\frac{\partial(j_{z,i})}{\partial z}+S_i$
Charge conservation	$\nabla.(\sigma_{\mathrm{sol}}\nabla\varphi_{\mathrm{sol}})+\mathrm{R}_{\mathrm{sol}}=0$
	$\nabla.(\sigma_{\mathrm{mem}}\nabla\varphi_{\mathrm{mem}})+R_{\mathrm{mem}}=0$

Table 2. Cell design parameters and transport properties (Guo et al. 2014).

Property	Value
Gas channel length	7 cm
Gas channel height	0.1 cm
Gas channel width	0.1 cm
Rib width	0.1 cm
Gas diffusion layer thickness	0.025 cm
Catalyst layer thickness	0.006 cm
PEM thickness	0.015 cm
Gas diffusion layer porosity	0.5
Catalyst layer porosity	0.5
PEM porosity	0.5
Oxygen diffusion coefficient	3e−5
Hydrogen diffusion coefficient	3e−5

The generated mesh file exported to fluent solver and boundary conditions shown in Table 1 have been applied before solution initialisation. Typical parameters used in this simulation are given in Tables 2 and 3. The pressure drop in channels, concentration distribution of H_2 and O_2 as well as current density distributions and membrane water content at the membrane/electrode interface were calculated numerically and presented.

Table 3. Key parameters for the simulations.

Cell operational temperature	323 K
Cell operating pressure	1 atm
Fuel	H_2
Oxidant	O_2
Fuel flow rate	2.05e−7 kg/s
Oxidant flow rate	1.67e−6 kg/s
Cell open circuit voltage	1.0 V

3. Results and discussion

A computational fluid dynamics study of 3-pass serpentine flow field PEMFC performance has been explored. Important parameters such as pressure drop, concentration distribution of hydrogen, oxygen, liquid water activity along the channel, and the membrane water content for peak power performance of the 3-pass serpentine flow field PEMFC are shown in Figures 4–8. The performance characteristics of the PEMFC are shown by the polarisation curve and performance curve in Figure 9.

Figure 4 shows the pressure drop in the anode and cathode flow channels respectively at 0.4 V cell potential. The pressure drop in the flow channel is an important consideration in the design of PEMFC as it will help in deciding the type of blowers or compressors to be used to maintain sufficient pressure in the channel. This pressure drop also influences the electrochemistry of the fuel cell. It is observed that pressure drops of 37.5 and 62.8 Pa occur in the anode and cathode flow channels respectively. These pressure drops are very less compared with single pass serpentine flow channels and these small pressure drops can be neglected as its impact on net cell output is very small. The reason for lower pressure drops in the proposed channels is because the given flow divided into three.

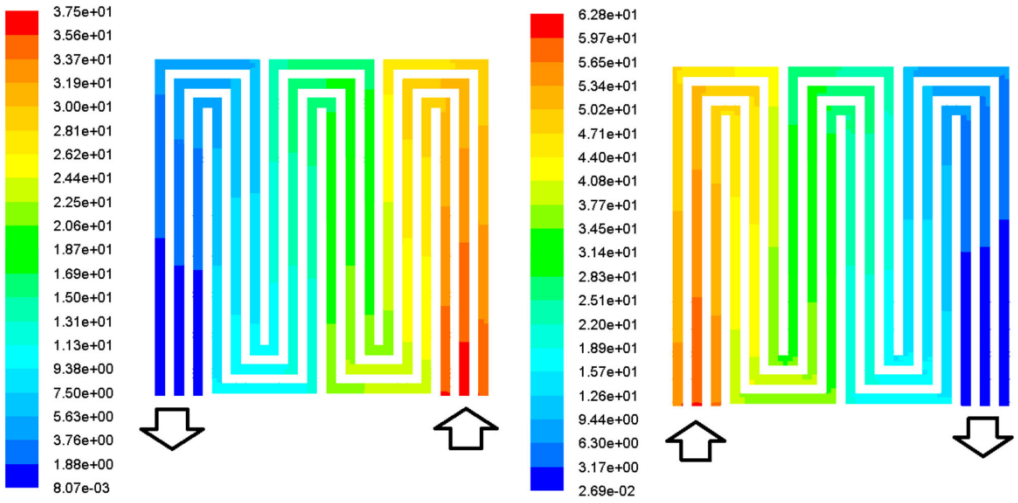

Figure 4. Contours of pressure drop (Pa) along the flow channel of the anode (left) and the cathode (right).

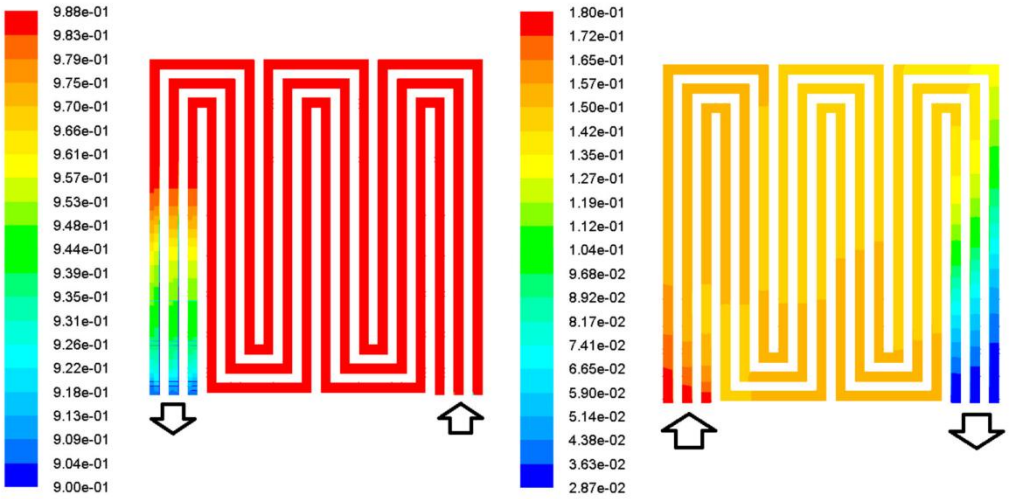

Figure 5. Contours of H_2 and O_2 mass fraction along the anode (left) and cathode (right) channel.

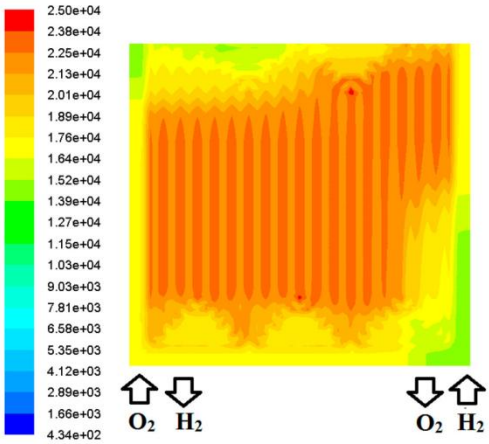

Figure 6. Current flux density distribution over the cathode catalyst layer at 0.4 V.

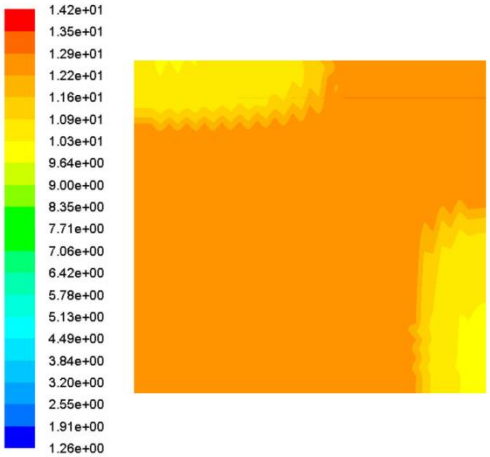

Figure 7. Membrane water content at 0.4 V.

Figure 5 shows the hydrogen and oxygen mass fraction distribution along the anode and cathode flow channel at a cell potential of 0.4 V. Both H_2 and O_2 concentrations are more at the inlet and gradually reduces towards the outlet of the channel. This reduction of species concentration in the channels is due the consumption of reactants in the reaction. The species concentrations are good enough till the last turn of the serpentine channels except the exit side of the channel. This can be improved with an increase in the flow of reactants so that reactants can uniformly distribute over the entire active area of the cell. It is observed that the rate of consumption of oxygen is more than hydrogen. Figure 6 shows the current flux density distribution over the cathode catalyst layer at a cell potential of 0.4 V. Uniform current density distribution over the cathode catalyst layer is observed except on the oxygen exit side which results in better performance of the fuel cell.

Figure 7 shows the membrane water content distribution at a cell potential of 0.4. Water content distribution in the membrane is similar to the current density distribution in Figure 6. Proton conductivity of the membrane depends on the water content inside the membrane. If the water content inside the membrane is very less than the required, then the membrane gets dried out and if the water content in the membrane is higher than the required then it causes flooding. Both membrane dry-out and flooding will affect cell performance negatively. This can be avoided if the distribution of water is uniform throughout the membrane.

Figure 7 shows the liquid water activity in the cathode channel at 0.4 V cell potential. Water is generated on the cathode side due to oxygen reduction reaction. Some amount of water is essential to keep the membrane hydrated, but excess water

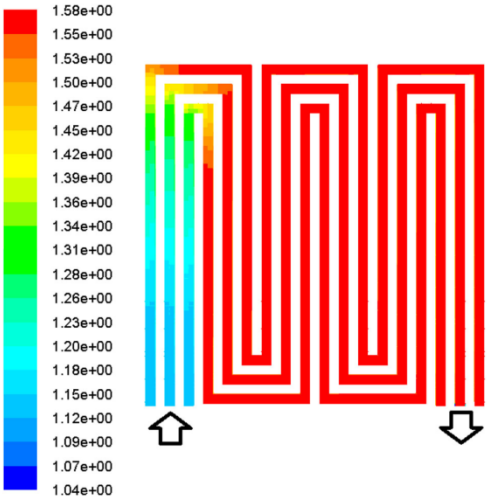

Figure 8. Liquid water activity in the cathode channel.

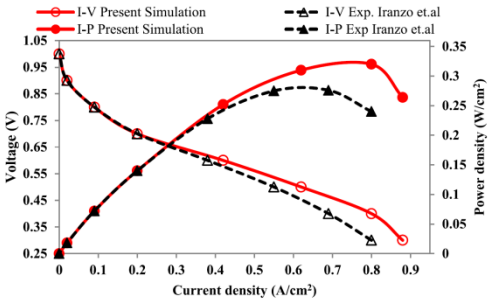

Figure 9. Polarisation and performance curve.

generated must be evacuated from the fuel cell. From Figure 7, it is observed that the liquid water activity is less at the inlet and it is increasing gradually towards the outlet of the cathode flow channel, i.e. the channel is able to remove the excess water from the cell effectively. Finally, the proposed model is validated by comparing with Figure 9 and shows the comparison of polarisation and performance curves of simulation data and the experimental data of Iranzo et al. (2010). The experimental data were taken from a 50 cm^2 active area single cell with serpentine flow field plate having five parallel channels and nine rows at 40°C. The membrane used is Nafion-117 membrane with catalyst loadings of 0.3 and 0.6 mg/cm^2 at anode and cathode electrodes respectively for the experiments. The simulation results slightly over predict the experimental results.

4. Conclusion

A computational fluid dynamics study on 3-pass serpentine flow field PEMFC was carried out and few key parameters such as the mass fraction of hydrogen, oxygen, liquid water activity, water content in the membrane and performance of the PEMFC have been explored. It is concluded that a maximum power density of 0.32 W/cm^2 was obtained at 0.4 V cell potential @ 0.8 A/cm^2 of current density. The simulation results of the proposed model are compared with the available experimental data which showed good agreement. The present study may be extended to examine the effect of the different key operating parameters like cell operating temperature, pressure, reactants humidity, and flow direction of reactants on PEM fuel cell performance.

Nomenclature

u	velocity in the x direction (m/s)
v	velocity in the y direction (m/s)
w	velocity in the z direction (m/s)
ρ	density of reactant gases (kg/m^3)
p	pressure
μ	viscosity (kg/sm^2)
S_{mom}	momentum sink term
T	temperature (K)
E	total energy
h	enthalpy
τ_{eff}	effective shear tensor
k_{eff}	effective conductivity
σ_{mem}	electrical conductivity of the membrane (S/m)
σ_{sol}	electrical conductivity of the electrode (S/m)
ϵ	porosity
α_{an}	anode charge transfer coefficient
A_{ca}	cathode charge transfer coefficient

Disclosure statement

No potential conflict of interest was reported by the authors.

Funding

The authors acknowledge the financial support provided by TEQIP-II/ CoE – Centre for Sustainable Energy Studies, National Institute of Technology, Warangal.

ORCID

Venkateswarlu Velisala http://orcid.org/0000-0002-7217-9965

References

Barreras, F., A. Lozano, L. Valiño, C. Marín, and A. Pascau. 2005. "Flow Distribution in a Bipolar Plate of a Proton Exchange Membrane Fuel Cell: Experiments and Numerical Simulation Studies." *Journal of Power Sources* 144 (1): 54–66.

Beicha, A., and R. Zaamouche. 2013. "Electrochemical Model for Proton Exchange Membrane Fuel Cells Systems." *Journal of Power Technology* 93 (1): 27–36.

Berning, T., D. M. Lu, and N. Djilali. 2002. "Three-dimensional Computational Analysis of Transport Phenomena in a PEM Fuel Cell." *Journal of Power Sources* 106 (1): 284–294.

Boettner, D. D., G. Paganelli, Y. G. Guezennec, G. Rizzoni, and M. J. Moran. 2002. "Proton Exchange Membrane Fuel Cell System Model for Automotive Vehicle Simulation and Control." *Journal of Energy Resources Technology* 124: 20.

Caglayan, D. G., B. Sezgin, Y. Y. Y. Devrim, and I. Eroglu. 2016. "Three-dimensional Modeling of a High Temperature Polymer Electrolyte Membrane Fuel Cell at Different Operation Temperatures." *International Journal of Hydrogen Energy* 41 (23): 1–11.

Carcadea, E., H. Ene, D. B. Ingham, R. Lazar, L. Ma, M. Pourkashanian, and I. Stefanescu. 2007. "A Computational Fluid Dynamics Analysis of a PEM Fuel Cell System for Power Generation." *International Journal of Numerical Methods for Heat& Fluid Flow* 17 (3): 302–312.

Corrêa, J. M., S. Member, F. A. Farret, L. N. Canha, M. G. Simões, and S. Member. 2004. "An Electrochemical-Based Fuel-Cell Model Suitable for Electrical Engineering Automation Approach." *IEEE Transactions on Industrial Electronics* 51 (5): 1103–1112.

Guo, N., M. C. Leu, and U. O. Koylu. 2014. "Bio-inspired Flow Field Designs for Polymer Electrolyte Membrane Fuel Cells." *International Journal of Hydrogen Energy* 39 (36): 21185–21195.

Hosseinzadeh, E. 2012. "Modeling and Design of Hybrid PEM Fuel Cell Systems for Lift Trucks," PhD Thesis, Technical University of Denmark.

Iranzo, A., M. Muñoz, E. López, J. Pino, and F. Rosa. 2010. "Experimental Fuel Cell Performance Analysis Under Different Operating Conditions and Bipolar Plate Designs." *International Journal of Hydrogen Energy* 35 (20): 11437–11447.

Jang, J.-H., W.-M. Yan, H.-Y. Li, and W.-C. Tsai. 2008. "Three-dimensional Numerical Study on Cell Performance and Transport Phenomena of PEM Fuel Cells with Conventional Flow Fields." *International Journal of Hydrogen Energy* 33 (1): 156–164.

Khazaee, I., and H. Sabadbafan. 2016. "Numerical Study of Changing the Geometry of the Flow Field of a PEM Fuel Cell." *Heat and Mass Transfer* 52 (5): 993–1003.

Larminie, J., and A. Dicks. 2001. *Fuel Cell Systems Explained*. 2nd ed. West Sussex: John Wiley & Sons.

Lum, K. W., and J. J. McGuirk. 2005. "Three-dimensional Model of a Complete Polymer Electrolyte Membrane Fuel Cell – Model Formulation, Validation and Parametric Studies." *Journal of Power Sources* 143 (1–2): 103–124.

Mehrpooya, M., G. Nouri, M. H. Eikani, N. Khandan, and A. Hajinezhad. 2015. "Effects of Membrane Electrode Assembly Fabrication Parameters on the Proton Exchange Membrane Fuel Cell Performance." *International Journal of Ambient Energy* 33 (1): 639–644.

Shimpalee, S., S. Dutta, W. K. Lee, and J. W. Van Zee. 1999. "Effect of Humidity on PEM Fuel Cell Performance: Part II-Numerical Simulation." *Asme-Publications-Htd* 364: 367–374.

Suresh, P. V., S. Jayanti, A. P. Deshpande, and P. Haridoss. 2011. "An Improved Serpentine Flow Field with Enhanced Cross-Flow for Fuel Cell Applications." *International Journal of Hydrogen Energy* 36 (10): 6067–6072.

Velisala, V., G. N. Srinivasulu, B. Srinivasa, and K. V. K. Rao. 2015. "Review on Challenges of Direct Liquid Fuel Cells for Portable Application." *World Journal of Engineering* 12 (6): 591–606.

Wang, X.-D., Y.-Y. Duan, W.-M. Yan, D.-J. Lee, A. Su, and P.-H. Chi. 2009. "Channel Aspect Ratio Effect for Serpentine Proton Exchange Membrane Fuel Cell: Role of sub-rib Convection." *Journal of Power Sources* 193 (2): 684–690.